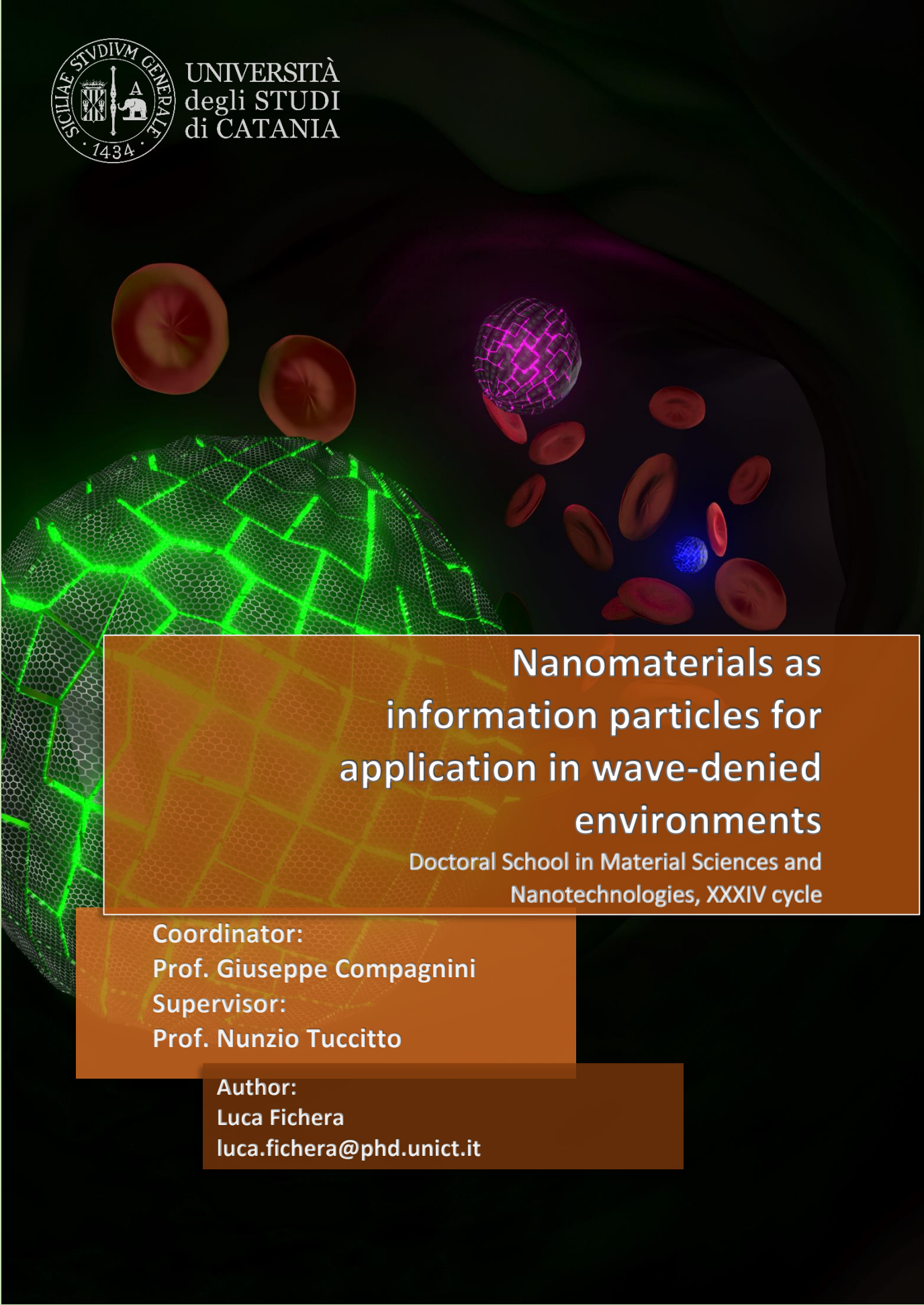




UNIVERSITÀ  
degli STUDI  
di CATANIA



# Nanomaterials as information particles for application in wave-denied environments

Doctoral School in Material Sciences and  
Nanotechnologies, XXXIV cycle

**Coordinator:**  
Prof. Giuseppe Compagnini  
**Supervisor:**  
Prof. Nunzio Tuccitto

**Author:**  
Luca Fichera  
[luca.fichera@phd.unict.it](mailto:luca.fichera@phd.unict.it)



## **Abstract**

*"Aware of its responsibilities and confident in its role, communication is a social expression, a value placed at the service of someone or something outside oneself: it is not enough to pronounce, write or draw in order to communicate; communication happens when it arrives, when the expression is comprehensible and becomes common knowledge for the construction of a discussion, a knowledge, a culture." This is a romantic definition of the word communication. Communication is embedded in nature and can be defined as behavioral, chemical or verbal. We, humans, have been using communication since time out of mind, mainly for the purpose of transferring information or a request to another living being. Nowadays, there are many different communication mediums that are widely used in all their forms, and technology has provided us with multiple platforms that allow us to connect two or more individuals in any place and at any time, request information or transfer a command to a device. In this perceived perfection, there are, however, several unresolved problems deriving from the type of carrier used to transfer the information. Typically, communication media use wired and wireless networks as channels through which data to be transmitted propagates to reach the destination, but there are several contexts in which these two channels cannot be used, e.g. due to engineering difficulties, or because of the impossibility caused by damage caused by electromagnetic radiation or its excessive attenuation. The aim of this PhD project is to propose molecular communication as an alternative communication medium, applicable in wave-denied contexts, to connect intelligent devices implanted in biological systems. This innovative bio-inspired communication method consists in using particles (e.g. chemicals, nanoparticles, proteins, pheromones, etc.) as a vector for the message to be transmitted, just as nature has been doing for millions of years. The development of this project has mainly touched on three areas of*

*molecular communication: the choice of the information particle in which to encode the information to be transmitted, the development of innovative modulation methods to make molecular communication reliable in particular environments that are difficult to control from the outside, and the exploitation of the characteristics of the communication channel to the advantage of the modulation methods themselves as a further optimization method.*

## **Abstract**

*“Consapevole delle proprie responsabilità e forte del proprio ruolo, la comunicazione è un’espressione sociale, un mettere un valore al servizio di qualcuno o qualcosa fuori da sé: non basta pronunciare, scrivere o disegnare per comunicare; la comunicazione avviene quando arriva, quando l’espressione è compresa e diventa patrimonio comune per la costruzione di una discussione, di un sapere, di una cultura.” È questa una romantica definizione della parola comunicazione. La comunicazione è insita nella natura e può essere definita come comportamentale, chimica o verbale. Noi umani da sempre ci avvaliamo della comunicazione, soprattutto dedita allo scopo di trasferire una informazione oppure una richiesta ad un altro essere vivente. Ad oggi i mezzi di comunicazione son tanti ed ampiamente utilizzati in tutte le loro forme, d’altronde la tecnologia ci ha messo a disposizione molteplici piattaforme che consentono di mettere in contatto due o più individui in qualsiasi luogo ed in qualsiasi momento, richiedere una informazione oppure trasferire un comando ad un dispositivo. In questa presunta perfezione, sono presenti però alcuni problemi irrisolti che derivano proprio dal tipo di vettore utilizzato per il trasferimento dell’informazione: tipicamente i mezzi di comunicazione utilizzano reti cablate e reti wireless come canali nel quale il dato da trasmettere si propaga per raggiungere il destinatario, ma sono diversi i contesti nel quale questi due canali non sono utilizzabili, vedi per difficoltà di tipo ingegneristico, vedi per impossibilità causata da danni provocati dalla radiazione elettromagnetica o comunque eccessiva attenuazione della stessa. Con questo progetto di dottorato, si vuol proporre la comunicazione molecolare come mezzo alternativo di comunicazione, applicabile in contesti “wave-denied”, per collegare dispositivi intelligenti impiantati nei sistemi biologici. Questo innovativo metodo di comunicazione bioispirato consiste nello sfruttare particelle (ad esempio chemicals, nanoparticelle, proteine, feromoni etc.) come*

*vettore per il messaggio da trasmettere, esattamente come la natura fa da milioni di anni. Lo sviluppo di questo progetto ha toccato principalmente tre ambiti della comunicazione molecolare: la scelta della information particle nel quale codificare l'informazione da trasmettere, lo sviluppo di innovativi metodi di modulazione per rendere affidabile la comunicazione molecolare in ambienti particolari e poco controllabili dall'esterno, sfruttare le caratteristiche del canale di comunicazione a vantaggio dei metodi di modulazione stessi come ulteriore metodo di ottimizzazione.*

v

|

# Summary

List of figures .....	x
Preface .....	1
Chapter 1 .....	6
Introduction .....	6
1.1 Artificial Molecular Communication .....	13
1.2 Propagation Schemes for Artificial Molecular Communication.....	16
1.3 Modulation Schemes for Artificial Molecular Communication.....	19
1.4 Conclusion and research project objectives .....	22
Chapter 2 .....	27
Nanoparticles as suitable messengers for molecular communication .....	27
2.1 Application of Nanoparticles in molecular communication.....	29
2.2 Carbon-Based Nanoparticles as information nanoparticles .....	34
Chapter 3 .....	38
Carbon Quantum Dots from Lemon Waste Enable Communication Among Biodevices .....	38
3.1 Materials and Methods .....	40
3.1.1 CQDs Synthesis.....	40
3.1.2 Characterization Methods.....	41
3.1.3 Molecular Communication Platform.....	43
3.2 Results and Discussions.....	44
3.2.1 CQDs Characterization .....	44
3.2.2 Molecular Communication Experiment .....	51



3.3 Conclusions.....	56
Chapter 4 .....	57
Self-assembled carbon nanoparticles as messengers for artificial chemical communication .....	57
4.1 Materials and Methods .....	59
4.1.1 Self assembled Carbon Nanoparticles Synthesis.....	59
4.1.2 Characterization methods.....	61
4.1.3 Molecular Communication Prototype.....	61
4.2 Results And discussion .....	62
4.2.1 CQDs characterization.....	62
4.2.3 Molecular Communication Approach .....	68
4.4 Conclusions.....	72
Chapter 5 .....	73
Reactive nanomessengers for artificial chemical communication.....	73
5.1 Materials and methods .....	75
5.2 Result and Discussions .....	78
5.2.1 Theoretical and simulative approach.....	78
5.2.2 Nanomessengers characterization.....	86
5.2.3 Artificial molecular communication platform.....	90
5.3 Conclusions.....	92
Chapter 6 .....	94
Fluorescent nanoparticle-based Internet of things .....	94
6.1 Materials and methods .....	96
6.2 Results and Discussions.....	97

6.2.1 The model.....	97
6.2.2 The experiment .....	105
6.3 Conclusions.....	114
Chapter 7 .....	116
Graphene Quantum Dots enable digital communication through biological fluid .....	116
7.1 Materials and methods .....	123
7.2 Results and discussion.....	124
7.2.1 The Model .....	124
7.2.2 The experiment .....	133
7.3 Conclusions.....	140
Chapter 8 .....	142
Fluorescent nanoparticles for secure communication among implantable medical devices .....	142
8.1 Preliminary Results.....	144
Chapter 9 .....	150
Final conclusions and future perspective.....	150
9.1 Ongoing works.....	154
9.1.1 Information particles.....	154
9.1.2 Innovative receivers .....	155
9.1.3 New modulation methods .....	155
References .....	157



## List of Figures

- Figure 1 - Molecular communication in nature: some sex pheromones used by insects..... 12
- Figure 2 – 3D representation of our typical Molecular Communication prototype. Starting from the right the components are: MCU unit to control the pump, a programmable syringe pump, the TX is a loop injector, the communication channel is a capillary tube a various length, the receiver is an optical detector of information particles. .... 26
- Figure 3 - Representation of the interactive communication process between two Janus gated nanodevices. This figure has been reproduced from ref. 60 with permission from Springer Nature, copyright 2017. .... 30
- Figure 4 - Pt-Based Janus micromotors moving in presence of H<sub>2</sub>O<sub>2</sub>. (A) Trajectories of half-coated Pt-based Janus particles in water at different fuel concentrations. (B) Scanning electron microscopy (SEM) image and associated motion mechanism of Pt-coated spherical silica microparticle. (C) SEM image of Pt sphere dimers and schematic depicting their synthesis. (D) Three sequential images of Pt Janus microparticles in motion overlaid with their corresponding angles and trajectories. (E) Schematic of the different motility scenarios in mesoporous silica Pt-based Janus particles. (F) Scheme of multilayer hollow Pt Janus microparticles. (G) SEM image (left) and optical image (right) of Pt shell. (H) Directional inversion on translational motion of Pt motors in presence of organic fuels (ethanol) and H<sub>2</sub>O<sub>2</sub>, and their corresponding motion mechanisms. This figure has been reproduced from ref. 48. .... 32
- Figure 5 - Measured received susceptibility time signal for a specific bit sequence obtained by using magnetic nanoparticles. This figure has been reproduced from ref. 65..... 33
- Figure 6 - a) Steps of hydrothermal synthesis of N-Doped Carbon Quantum Dots. Firstly the decomposition at 250°C, neutralization with NaOH, dialysis and centrifugation to remove smaller molecules and bigger residual. Finally the usable Carbon Quantum Dots. b) Typical fluorescent map of N-Doped Carbon Quantum Dots prepared via Hydrothermal Decomposition. .... 37

Figure 7 - (a) $5 \times 5 \mu\text{m}^2$ AFM image of Lemon-PEI CDs deposited onto silicon substrate (z scale: $0-20^\circ$ ); its histogram analysis of Lemon-PEI CDs' height obtained by several sections, three of which are represented in the inset; (b) $5 \times 5 \mu\text{m}^2$ AFM image of Lemon-only CDs deposited onto silicon substrate (z scale: $0-20^\circ$ ); its histogram analysis of height of lemon-only CDs obtained by several sections, three of which are represented in the inset. ....	45
Figure 8 - (a) FT-IR spectra and (b) UV-vis spectra of an aqueous suspension of lemon-PEI CDs. ....	46
Figure 9 - (a,d) Overlay of fluorescence spectra of aqueous suspensions of lemon-PEI CDs and lemon-only CDs, respectively, acquired at several excitation wavelengths as reported in the labels; (b,e) excitation-emission maps of aqueous suspensions of lemon-PEI CDs and lemon-only CDs, respectively; (c,f) photos depicting the qualitative appearance of the aqueous suspensions of lemon-PEI and lemon-only CDs. ....	48
Figure 10 - (a) Intensity of fluorescence peak as a function of the dilution of an aqueous suspension of lemon-PEI CDs ( $\lambda_{\text{ex}} = 340 \text{ nm}$ , $\lambda_{\text{em}} = 470 \text{ nm}$ ); (b) intensity of fluorescence peak as a function of the dilution of an aqueous suspension of lemon-only CDs ( $\lambda_{\text{ex}} = 330 \text{ nm}$ , $\lambda_{\text{em}} = 440 \text{ nm}$ ). ....	50
Figure 11 - Schematic representation in false color of the transversal diffusion following concentration gradients; (a) map of simulated molecular messenger concentration distribution with lower diffusion coefficient (b) and with higher diffusion coefficient. ....	53
Figure 12 - DOSY spectrum of lemon-PEI CDs dispersed in deuterium oxide ( $\text{D}_2\text{O}$ ). Diffusion coefficient values, $D$ , are reported on the y-axis. ....	54
Figure 13 - (a) Simulated message corresponding to "ECO" word in binary coding (simplified ASCII), obtained by modelling a capillary $0.40 \text{ mm}$ in radius and $200 \text{ mm}$ in length and setting the RMS velocity of the flow to $5.7 \text{ mm/s}$ and the pulse of information particles to a volume of $20 \mu\text{L}$ ; experimentally, transmission of the word "ECO" was performed by using (b) lemon-only and (c) lemon-PEI carbon dots, respectively. ....	55
Figure 14 - (a) Synthetic pathway for the synthesis of NPs-Triazine; (b) Schematic of the supramolecular self-assembly of NPs- Triazine. ....	60
Figure 15 - DOSY titration of NPs-Triazine with NDI. ....	63

Figure 16 - AFM images of the (a) native NPs, (b) NPs-Triazine, and (c) NPs-Triazine@NDI. The height scale is 2 nm for all images. ....	64
Figure 17 - UV-vis spectrum of CDs.....	65
Figure 18 - Fluorescence maps of (a) native NPs, (b) NPs-Triazine, and (c) NPs-Triazine@NDI. ....	66
Figure 19 - (a) Intensity of fluorescence peak as a function of the concentration; not reticulated NPs (blue) $\lambda_{emi} = 480$ nm with $\lambda_{exc} = 400$ nm and reticulated NPs-Triazine@NDI (green) $\lambda_{emi} = 490$ nm with $\lambda_{exc} = 410$ nm. (b) Stern–Volmer plot of unreticulated NPs (blue) and NPs-Triazine@NDI (green).....	67
Figure 20 - Probability distribution function of the detection time for different sets of velocity and diffusion parameters related to the release of two consecutive 1-bit pulses. ....	69
Figure 21 - (a) Schematic of artificial chemical communication prototype. (b) Received signal of a 1-bit pulse transmitted using non-reticulated NPs (green line) and reticulated NPs-Triazine@NDI (red line) as molecular messengers. Travel distance of 1.0 m, transport velocity of 1 cm s <sup>-1</sup> , NPs concentration of 0.85 g ml <sup>-1</sup> , loop volume of 20 $\mu$ l. (c) Probability distribution function of the detection time calculated by eqn (9) with several values of diffusion parameter D and using $v = 1$ cm s <sup>-1</sup> , $d = 1$ m. ....	71
Figure 22 - 3D project of RSK modulation prototype. Notice the presence of T-junction to inject the modulant. ....	77
Figure 23 - (a) Detected simulated signal of bit-1 by a receiver placed at various distances; (b) detected simulated signal of sequence 1-0-1-0-1 transported by a flux of various velocities. Time unit is reported in simulation steps. ....	79
Figure 24 - (a) Trend of variable flow pressure during the simulation of communication procedure; (b) sequence of bit-1 released by the transmitter; (c) sequence of bit-1 detected by the receiver. Time unit is reported in simulation steps. ....	81
Figure 25 - Representation of reaction shift keying modulation. ....	83
Figure 26 - (a) Trend of variable flow pressure during the simulation of communication procedure; (b) sequence of bit-1 released by the transmitter (blue line: messenger, red line: reactant); (c) sequence of bit-1 detected by the absorbance detector placed at the receiver; (d) sequence of bit-1	

- detected by the fluorescence detector placed at the receiver. The decoded binary sequence is reported at the bottom. .... 86
- Figure 27 - (a) AFM phase image of nanoparticles deposited onto mica substrate (z scale: 0–201); (b) histogram analysis of nanoparticle height obtained by several sections of AFM height image (not-shown); (c) overlay of UV-vis spectra of aqueous solutions of carbon nanoparticles,  $\text{CuCl}_2$  and 1 : 1 mixture of both, respectively; (d) overlay of fluorescence spectra of aqueous solutions of carbon nanoparticles acquired at several excitation wavelengths as reported in the labels. .... 88
- Figure 28 - (a) Fluorescence intensity of carbon nanoparticles as a function of the quencher concentration; (b) Stern–Volmer plot. .... 89
- Figure 29 - (a) transport flow velocity trend during the communication time. (b) Absorbance and (c) fluorescence signals detected by the receiver when “1-0-0-0-1-0” sequence is released in a real-working chemical communication platform. First 1-bit was released at time  $t = 0$ . Subsequent pulses have been released with 200 s delay time among each other. Between (b) and (c), the decoded binary sequence according to RSK modulation is reported. .... 91
- Figure 30 - Schematic representation of a conceivable molecular-IoT architecture. .... 95
- Figure 31 - (a) False color maps of simulated molecular messenger concentration distribution inside the capillary pipe acquired at different flow velocities (from top to bottom:  $v_1 = 16.45 \text{ mm s}^{-1}$ ,  $v_2 = 21.94 \text{ mm s}^{-1}$ ,  $v_3 = 27.43 \text{ mm s}^{-1}$ ,  $v_4 = 32.91 \text{ mm s}^{-1}$ ;  $v_5 = 38.4 \text{ mm s}^{-1}$ ). (b) Actuators’ response placed at various distances as a function of time. .... 102
- Figure 32 - (a) Relative signal width as a function of transmitter receiver distance at various velocities. (b) Normalized peak intensity as a function of transmitter receiver distance at various velocities. (c) Signal intensity and width ( $\times 10$ ) detected as a function of time. (d) Time delay between successive pulses required to avoid their overlap as a function of the travel path calculated for 5 different flow velocities. .... 103
- Figure 33 - Fluorescence detector response when (a) a single pulse of fluorescent nanomessengers is released or two subsequent pulses are released with (b) 50 s, (c) 100 s, and (d) 200 s of delay time (velocities values in the legend). .... 107

Figure 34 - Optimization results. (a) 3D representation of absolute (green dots) and relative peak–valley (red dots) intensity as a function of fluid velocity and pulse delay. (b) 2D plot of the two-plane intersection curve, the blue line in (a), and the fit (green dotted curve). ..... 110

Figure 35 - Actuators’ response to the release of specific messengers’ sequence: 1. blue-CQDs, 2. cyan-CQDs, 3. green-CQDs, 4. blue-CQDs and cyan-CQDs, 5. green-CQDs, 6. all CQDs, 7. cyan-CQDs and green-CQDs. .... 111

Figure 36 - (a) Temperature controlling of actuator A. (b) pH controlling of actuator B. (c) Conductivity controlling of actuator C. Fluorescence responses of each actuator are also plotted. .... 113

---

Figure 37 - A schematic concept for in-vivo Molecular Communication. A micro-robot monitors the temperature of a tissue using a specific sensor. It communicates temperature level encoding information inside fluorescent information nanoparticles and releasing them in the blood flow. Another micro-robot detects the information nanoparticles using a fluorescent detector and decodes the information. It could then release medication if necessary..... 120

Figure 38 - A schematic representation of the prototypal molecular communication system. To be noticed the motor that scan the emission wavelength..... 122

Figure 39 - (a) The probability distribution obtained solving the Advection Diffusion Equation using 200 mm path length, 0.35 mm radius, 0.4 mm/s flow velocity, 1.2 mm<sup>2</sup>/s diffusion coefficient and 5 mm initial pulse width. (b) Simulated fluorescent spectra approximated to a Gaussian with  $\mu = 437$  and  $\sigma = 47$ . (c) 3D plot of the signal reached by the receiver if it is able to acquire the entire spectra for each  $\delta t$  interval. The red line traced on the surface represents the back and forth explored by the receiver if it can scan the wavelengths according to a  $\cos(\mu t)$  function. On the plane  $P(t)$  vs Time is shown the projection of the red line obtained by several scans representing the signal that the receiver detects by scanning..... 127

Figure 40 - (a) Signals obtained from simultaneously releasing of two information nanoparticles having distinct fluorescence spectra. (b)



- Fourier transformations of signals in (a).(c) Signals detected by the receiver when the same fluorescent information particle is released at different times. (d) Fourier transformations of signals in (c)..... 129
- Figure 41 - Experimental Fluorescent spectra of the three commercial QDs at 290 nm excitation wavelength..... 130
- Figure 42 - Detected signals of QDs by scanning receiver. From sx: B-QDs, C\_G-QDs mixture, G-QDs and B\_C\_G-QDs. In bottom of image, fourier transformation of the signals and respective binary encoding meaning according to Equation 18. .... 132
- Figure 43 - Learning-plot obtained by PCA from the 35 simulated signals. We observe 7 dense clusters consisting of 5 points each. The inset represents a zoom near the cluster of B\_C- QDs. "Reference" is the reference signal point compared to the other four that are out of phase of a  $\Delta T$  written in the figure itself. .... 133
- Figure 44 - (a) Experimental signals detected by scanning receiver. From Top to bottom: B-QDs, C-QDs, G-QDs, B\_G-QDs mix, B\_C\_G-QDs mix and respective binary encoding meaning according to equation 18. (b) Fit plot of experimental signals. In blue the points relative to the learning-plot previously obtained by the simulated signals. In orange the points relative to the experimental signals fitted on the learning dataset in Fig. 43. .... 136
- Figure 45 - (a) Transfer of the value  $p = 0.8$ , in reference to a temperature variation, using ASCII language in binary coding. (b) Transfer of the value  $p = 0.8$ , using a specific encoding method described in Table 1. It should be noted that the signals labeled with "check status" are not useful for the transfer of information but are used for a check of the state of operation of the communication. .... 138
- Figure 46 - False-color images resulting from the simulations; (a) concentration of information nanoparticles present in the tube at the initial simulation time ( $t=0$ ); (b) effect of flow velocity on the spatial distribution of information nanoparticles when subjected to laminar flow inside a narrow-diameter tube under zero-slip conditions at the walls; (c) spatial distribution of nanoparticles with low diffusion coefficient ( $3 \cdot 10^{-12} \text{ m}^2/\text{s}$ ) after traveling through the entire tube; (d) same simulation conditions but with diffusion coefficient 10 times higher. .... 146

Figure 47 -(a) Signal detected by a receiver placed at a distance of 200 mm from the release point as obtained from simulations. Colors are associated with different values of diffusion coefficient; (b) Relevant fluorescence signal at 200 mm distance acquired during MoCo experiments. Colors are associated with different viscosity values. ... 148

## Preface

*Artificial molecular communication emerged from the need to cover some particular areas of communication science, in which the possibility of using conventional communication systems is in some way impeded or undesirable. In this technology, the carriers that transport a baggage of information from one point to another and in which the information is encoded are particles called information particles. They are released into the communication channel by the interlocutor, and then reach the position of the listener. The advantages of using particles as information carriers are numerous and have piqued the curiosity of many scientists over the last decade. The fields of modulability of a chemical signal are almost infinite thanks to the extreme variety of existing species. In fact, it is enough to slightly modify a physical or chemical property of an information particle to obtain a profoundly different data. Just think of the chemistry of carbon, where it is enough to slightly modify a carbon chain, a bond angle, or the ambient temperature to obtain different physical and chemical properties. This provides a potential alphabet of infinite signals and therefore infinite letters. This seems to be a small advantage, but actually, the number of available signals is never enough. The scarce number of available signals is a very current problem in the world of telecommunications: one example is the war for available frequency bands, for each generation change, which telephone operators and TV broadcasters need in order to be able to transmit signals. A chemical signal suffers from an interference which is different from that of a signal transmitted by radiation; hence, the fields of application are also separated,*

*making the two methods of communication complementary and only rarely overlapping. A chemical signal is also secure, safe from external attack. A signal sent by electromagnetic radiation is detectable and therefore subject to manipulation. Knowing the decoding key, the transmitted message is unencrypted; therefore, an attacker could exploit it for less than legitimate purposes. To detect a message transferred by molecular communication, one must act directly on the communication channel, take the chemical species and only then, knowing the decoding key, obtain the information. Furthermore, in almost all the cases that will be analyzed in the development of this work, the decoding depends on the shape of the signal, and this makes it almost impossible to know the transmitted data especially if the unwanted detector is not directly positioned in the flow of the communication channel. Molecular communication is also perfectly compatible with the natural processes of biological systems; nature itself teaches us that it is possible to communicate by means of molecules: from a macroscopic point of view using pheromones, terpenes etc., from a micro and nanoscopic point of view using mRNA, ions etc. We know that nature is an almost perfect and extremely complicated machine, and if molecular communication is used in this complex system, then its use in 'simplified' systems can certainly be implemented. Until few years ago, analyzing the existing literature, molecular communication could be divided into two macro-areas: the first one analyses molecular communication in nature, with data dating back even to many decades ago. The second, into which this research project falls, concerns the use of molecular communication for the development of artificial communication networks. In this last area, everything is still very meagre, incomplete and there are only a few established and*

*usually basic models. The development of powerful IT tools which occurred thanks to the technological advancement, and the still scarce interest of large industrial realities have unbalanced research on molecular communication towards the modelling and theoretical approaches while little attention has been given to the experimental one. Most of the works in the literature concern propagation models within complex communication channels, mathematical and physical studies and only very few experimental apparatuses. The initial aim of this research project is bringing order in the theory-experiment combination and proposing an effective method for the study of the phenomena involved to those who wish to study the field of molecular communication in depth, offering some starting points for research in this field. Since it is not thinkable to enlarge this research towards all fields in which molecular communication could be applied, at least ideally, this study will be purely oriented towards artificial molecular communication in biological and biomedical contexts for networks between devices implanted in biological systems. This results in a number of basic fundamentals for the development of the entire research project. Firstly, the information particles, which must be chosen carefully to allow efficient signal transmission, make them modulable and not subject to environmental noise, and to maintain low cytotoxicity and easy disposal after use. The second point to consider is the communication channel which, in order to emulate the channels in which biological fluids flow, is approximated to capillary systems in which directional flows caused by pressure gradients are present. Having established these simple concepts, we have developed a complete and reliable protocol for the study of the phenomena involved in the process of artificial molecular communication, which is therefore intended to*

*be the basis on which researchers wishing to investigate the subject can rely. In fact, the proposed system is complete both in terms of model study of the phenomenon and in terms of experimental verification. We believe it is necessary to rely on computer tools to realize an idea, since in a short time information is obtained on the feasibility and on the phenomenon to be observed, and subsequent experiments are optimized by focusing only on those that are probably more effective. Computational models have been developed using well-known programming languages (e.g. Python®) and the source code has been made available to the scientific community, and professional Multiphysics simulation platforms (Comsol Multiphysics) have been used to solve some of the more complex problems. However, it is essential to spend most of the time on experimental analysis, which shows details that may go unnoticed by simulations. A highly modular prototype experimental platform was developed to verify the results obtained from the computational simulations. Developing it independently has helped to keep the costs of the equipment moderate, and to know very well its criticalities and potential to act on them. In addition, it is a modular prototype, where every single component is replaceable and the behaviour of the mechanical and electronic parts can be controlled 100% thanks to the presence of ad hoc programmed microcontrollers. A large part of the work will be devoted to the instrumental and computational part because it was developed from scratch, without any specific skills in electronics and computer science. However, its development stimulated the entire thesis work: the modelling, prototyping, tests and experiments themselves highlighted the real criticalities concerning artificial molecular communication in confined environments, which would not have*

*emerged based solely on theoretical studies. In fact, every single problem that will be addressed in each chapter will be the result of a careful observation of the experimental phenomena that gradually appeared. The properties of fluids under microfluidic conditions show specific patterns of signal transmission that have nothing to do with macrofluidic conditions. We have learnt to exploit these properties in favor of molecular communication to optimize the transmission process and significantly increase the baud rate of the communication channel by acting solely on the flow properties and not on the molecular messenger. The knowledge gained from studies of the synthesis processes and characterization of carbon-based nanoparticles will enable us to identify them as ideal candidates for artificial molecular communication systems for bio-applications. On the one hand, the simple and inexpensive methods of synthesis, which allow them to be produced in large volumes without great economic expense and environmental impact, and on the other hand, the peculiar fluorescent properties that characterize them, have allowed us to successfully test the prototype experimental platform and to obtain excellent results about signal modulation methods and optimization of the communication channel baud rate. A summary of all the activities carried out and the results achieved for each of them can be found in the last chapter of the work.*

# Chapter 1

## Introduction

Historically, human beings have always felt the need to be able to communicate with others so that they can be defined “social animal[s]” [Aristotele, IV cent. B.C.]. Communication between individuals is therefore a science in continuous evolution and continuous modification. Closely related to the science of communication it is undoubtedly the study of the means that allow communication: from natural means such as voice or gestures, to artificial ones. The search for systems that can put in communication two distant places has always been a fundamental objective to bring closer people who are physically far away. Hundreds of years ago, primitive methods were already being used to exchange information at a distance, such as light produced by fire, smoke signals or the propagation of sound through particular environmental geometries or through instruments capable of amplifying a sound, such as horns or drums. We must thank Antonio Meucci and Alexander Bell for the real revolution of communication systems because, during the second half of the 1800's, they invented a device able to transmit the voice by means of electrical impulses directly and in real time: the telephone. It was then during the '900 that the means of communication "at a distance" have become accessible to all and therefore an integral part of our lives. Today, we have a wide variety of methods that allow us to stay in touch with the whole world, to transmit information in real time at an impressive speed and reliability. Everyone has a smartphone in their pocket, always connected to the Internet using the 4G or 5G network,<sup>1</sup> ready to receive



notifications or show to the entire web photos of their pets. Technology cannot and must not stop, so we think about the next goals of the science of communication systems and the points on which to focus. If historically this science was the prerogative of those who specialized in the field of communication, given the complexity of today's communication systems, even this subject can be categorized as interdisciplinary and needs figures who can contribute to different aspects of the same. The position of material scientists in the field of communication systems seems to be marginal, but it is fundamental since their task is to engineer new materials or nanodevices to make communication more and more effective and smarter as in the case of the contribution of materials science in the miniaturization of devices, in their integration in the environment or in their implantation within biological systems. The word "nanotechnology" is in the 21st century a synonym for innovation, progress, and improvement of everyday life. How can the world of communication systems be related to that of nanotechnology from a future perspective?

---



*Scheme 1 - A typical communication scheme between wireless devices.*

---

To understand this, it is necessary to make a quick description of the two systems separately, through which it will come naturally

to understand the subsequent connection. A communication medium can be defined as any system capable of transferring information from one point to another. Schematically, the main components of a communication system are three and are described in scheme 1. The transmitter (TX) is a device that takes care of packaging the information, encodes it in a suitable way and releases it in the communication channel, that is the medium in which it must propagate to reach the second device, the receiver (RX), which takes care of collecting the packet that contains the information, decodes it, and makes it usable. Obviously, transmitter and receiver must use the same encoding and decoding language in order to make effective the transmission process. If it does not seem complex conceptually, even the simplest communication system can be subject to errors in the transmission of information, mainly due to the noise that the communication channel can insert in the signal.<sup>2-4</sup> The encoding of information is done through symbols: a symbol is a characteristic signal that corresponds to a specific piece of information.<sup>5</sup> Noise or loss of symbols during the transmission process can prove to be a problem for the receiver to correctly decode the transmitted message. The need to make the process of transmitting information robust and secure requires that the message be encoded in such a way as to be little affected by the problems of the communication channel. The signal modulation methods were born to solve the problems described above because they allow to adapt the signal containing the information to the type of environment through which the message must be transferred.<sup>6,7</sup> The term nanotechnology should be analyzed in more detail: 'nano' refers to the dimensional range of the material that constitutes the technology. A material is considered nano

when at least one of its dimensions falls within the range between 1nm and a few hundred nanometers.<sup>8</sup> Therefore, two-dimensional materials (e.g. Graphene), nanofibers or nanotubes (e.g. Carbon Nanotubes or glass fiber), nanoparticles (e.g. carbon quantum dots) can be defined as nanoscopic.<sup>9-11</sup> The properties of these materials are strongly related to their size, since they are characterized by a very high area/volume ratio and this allows to enhance features that are not present in the macroscopic form of the material.<sup>12</sup> On the other hand, the term technology refers to functional materials, i.e. materials capable of performing a function by exploiting their physical and chemical properties. Nanotechnology is a well-established reality and finds application in many fields: from food to construction, in the textile sector, in the field of clean energy, in electronics and in the medical field.<sup>13-16</sup> Scientific progress has made it possible to greatly refine the methods of preparation of nanotechnological materials, so much so that we are now talking about nanodevices, consisting of large functional molecules, organic supramolecular aggregates, or organic/inorganic hybrids, perfectly engineered and capable of performing complex functions despite their small size.<sup>17</sup> Further expanding of the functionality of these nanodevices is of significant interest as it would allow the creation of systems able to perform very complex tasks autonomously. The connection between communication systems and nanotechnologies exactly occurs in this context of nanodevice evolution. Rather than making the single nanodevice more and more complex, causing an inevitable increase in size, as well as great difficulty in integration, we could think of making several nanodevices specialized in specific tasks communicate with each other, in order to create an interconnected and intelligent network. This is not a new

approach, but it is closely related to the concept of Internet of Things (IOT). The International Telecommunication Union (ITU) defines the Internet of Things as "a global infrastructure for the Information Society, enabling advanced services by interconnecting (physical and virtual) things based on, existing and evolving, interoperable information and communication technologies" (ITU 2012). Some communication methods of which we are aware are perfectly suited to this purpose. There are some years of wireless communication protocols designed specifically for the IOT applied to home automation, called ZIGBEE and MQTT,<sup>18,19</sup> based on the transfer of small packets of data directly between a device and the other or relying on a server. They are protocols designed to use a bandwidth as little as possible and to keep energy consumption as low as possible. Since a large number of communication methods and protocols already exist, the question might be: where can we look for new communication methods, alternative to those that already exist? Exchanging information via a wired medium requires a physical or visual contact between one device and another, such as a copper cable or more modern fiber optic cable. In many ways it is the most secure and stable system to ensure high bandwidth, minimize noise and maximize compatibility between systems. In nanoscopic optics, however, it is very complicated to connect independent nanodevices, especially if placed at a high distance, through a physical connection. A wireless communication method is better suited to networks consisting of several interconnected devices, both for practical engineering issues and for the possible expandability. However, there are conditions in which even wireless interconnection is not applicable or desirable. For example, environments where the attenuation of electromagnetic

radiation is much more pronounced than in normal air, such as in liquid media, especially if saline,<sup>20</sup> or where electromagnetic disturbances are high and increase noise considerably. Other limiting conditions may be underground environments, such as caves or tunnels, where thick walls act as a screen and information disperses rapidly. There are also situations in which the use of electromagnetic radiation is not recommended, for example in environments where there are wave-sensitive measurement methods, or even more so if we are talking about installations within biological systems. It is known in fact that the continuous exposure of tissues to radiation, including radio waves, causes problems such as local temperature increase of the exposed area, undesirable chemical reactions can be triggered and over time undesirable diseases can arise.<sup>21</sup> In the literature it is known that it is possible to build nanodevices equipped with emitting antennas or radiation receptors for the triggering of processes, such as drug release, or for monitoring, thus sensor purposes.<sup>22</sup> Since we are approaching an era in which the human-computer interaction is increasingly strong, the development of communication system that can meet the needs dictated by these situations is therefore essential, and artificial systems implanted in the human body will gradually become more complex, more advanced and more intelligent. Following the evolution of communication systems in the last decade, it is possible to find a very interesting concept of information transfer universally called *Molecular Communication* (MoCo). If the term may seem futuristic, it is actually the oldest method of communication ever used by nature. Nature, as a perfect and efficient machine, needs an equally efficient system for transferring information.

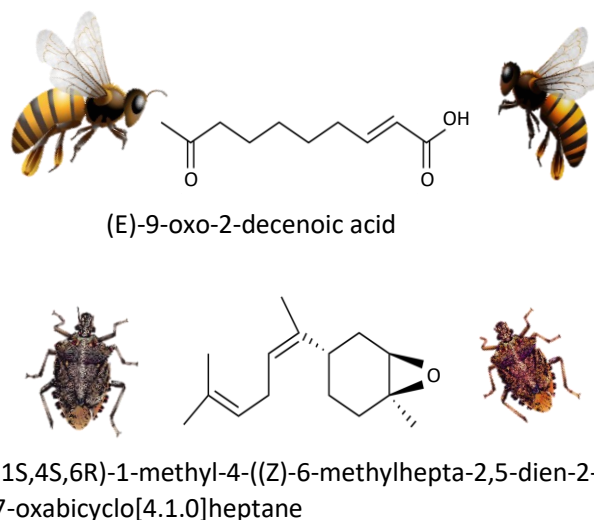


*Figure 1 - Molecular communication in nature: some sex pheromones used by insects.*

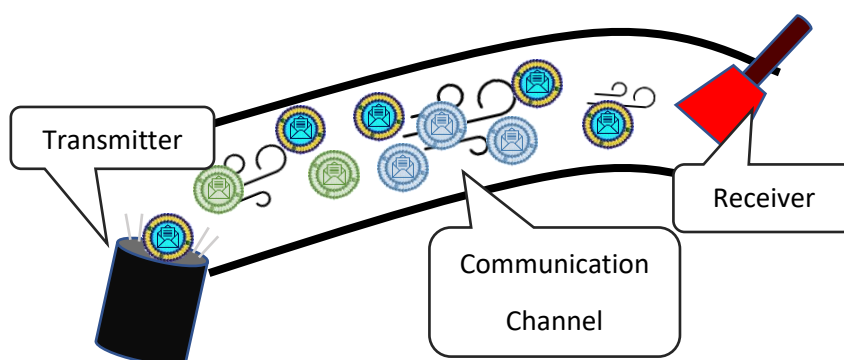
---

The examples that can be made are endless and extremely different from each other: the ability of RNA to transfer information from one part of the organism to another is a known and very fascinating mechanism. Even macroscopically, many examples of molecular communication can be made in nature: many animals send information encoded in molecules, such as pheromones, releasing them into the air, waiting to be received by other members of the same species.<sup>23</sup> Over the past decade, scientists have started to ask the question of how we might emulate nature and integrate its communication system effectively. The community that studies it today is very large and interdisciplinary: engineers, chemists, physicists, biologists and physicians actively participate in research in the field and also the

literature is very rich and articulate. From an applicative point of view, Molecular Communication is only in its beginning and many problems must be solved before it can be really applied. Before analyzing the achievements on which the writing of this thesis and the research project of the undersigned is based, the basic concepts of artificial molecular communication and the state of the art on the subject will be introduced.

### 1.1 Artificial Molecular Communication

Molecular communication (MoCo) is a method of transferring information from one point to another by encoding the message within chemical signals. Nature uses chemical signals to transfer information, both intracellularly and intercellularly, thus covering nanometer and micrometer distances.<sup>24</sup>



*Scheme 2 - A simplified scheme of a MoCo system in a closed environment.*

---

The possibility that some animal species possess to release pheromones in the air can be defined as a MoCo in the macroscale.<sup>25</sup> Analyzing these examples, if exploited in an appropriate way, the MoCo in artificial systems can be applied indiscriminately in all areas and at all distances. Obviously, each application requires a separate development since it is strongly dependent on the environment in which the chemical messenger propagates and on the nature of the same. To date, most of the works concerning MoCo are strongly oriented to the theorization and modeling of the transmitter - communication channel - receiver system. The transmitter (TX) releases several chemical messengers inside the communication channel, whose concentration is defined as  $C(t,x)$ , encoding in an appropriate way the message it intends to send. These messengers will propagate in the communication channel according to the laws that determine their movement in the environment, until they reach the receiver (RX), which then capture their presence and decode their content. About the propagation models of the chemical messenger in the communication channel and from the characteristics of the latter, it is possible to make some first classifications of the different MoCo systems. If the environment in which the chemical messenger propagates has no constraints and can move in all directions, the communication channel is defined as *open*, for example air or a large aqueous environment. The advantage of this kind of communication channel comes from its simplicity, from the fact that it is the environment itself the means of propagation of the chemical signal and being open it is possible to reach more receivers without constraints. The negative sides, however, concern the difficulty in predicting how the chemical messenger is actually propagated because all the



environmental and random factors come into play. In addition, the dispersion in all directions causing a reduction in signal strength is favored, as well as being subject to noise due to unanticipated interference that may cross the communication channel interposed between TX and RX. When the communication channel is a *closed* environment, such as a pipe, a capillary, or a guide defined by electromagnetic fields, the advantages and disadvantages defined by the *open* environment are reversed. Furthermore, it is easier to generate flow through a *closed* channel by applying pressure gradients to direct and speed the movement of the chemical messenger. Another method to classify the MoCo system concerns the physical size of the communication channel, we talk about microscale and nanoscale when the distance between TX and RX is in the range of micrometers or nanometers, respectively. The most widely used physical models to model chemical messenger transport in this size range are mostly based on Monte Carlo simulations.<sup>26</sup> If the communication channel has dimensions greater than millimeters it falls into the MoCo macroscale. The laws that are therefore applied to model larger communication channels use Fick's laws for diffusion and Navier Stockes equations to describe fluid dynamics.<sup>27</sup> Obviously, when trying to describe how the transport of a chemical messenger in a communication channel takes place, many factors must be taken into account simultaneously, such as viscosity, temperature, size of the communication channel, and self-diffusivity effects. Moreover, talking about chemicals, the possible interactions that are established by them and can modify the diffusive properties and the viscosity of the fluid, all chemical reactions that can introduce noise or lower the intensity of the signal, are not negligible.

## 1.2 Propagation Schemes for Artificial Molecular Communication

Several models of chemical messenger transport have been proposed for microscale MoCo. The simplest is the *free diffusion*,<sup>28–30</sup> in which particle motion is governed by *Brownian motions* and closely related to thermal energy.<sup>31,32</sup> This model does not require energy from outside to allow the motion since it exploits the thermal energy naturally present inside the communication channel. It is undoubtedly the simplest to apply, but also the most difficult to control and the slowest since the motions are purely random, i.e., the motion of each particle at time  $t_1$  is correlated with the motion at time  $t_1 - \Delta t$ . On the other hand, in biology we find many examples where *free diffusion* is exploited [see 1890, farsad], such as the neurotransmitter Acetylcholine released by nerve cells,<sup>33</sup> signaling by calcium ions or the transport of animal and plant pheromones.<sup>34,35</sup> In this model, it is critical to consider the parameters that affect the diffusion coefficient determined by the empirical *Stockes-Einstein equation* (Eq. 1).

---


$$D = \begin{cases} \frac{k_b T}{6\pi\eta R_h} & \text{if } S_m \gg S_{fluid} \\ \frac{k_b T}{4\pi\eta R_h} & \text{if } S_m \approx S_{fluid} \end{cases} \quad \text{Eq. 1}$$


---

$D$  is the diffusion coefficient,  $K_b = 1.38 \cdot 10^{-23}$  J/K is the Boltzmann constant,  $T$  the temperature,  $\eta$  the dynamic viscosity of the fluid. In macroscopic terms, the contribution of diffusion in the

dispersion of a chemical messenger pulse over time is described by *Fick's law* (Eq.2).

---

$$\frac{\delta C}{\delta t} = \nabla \cdot (D \nabla C) \quad \text{Eq. 2}$$

---

$C$  is the concentration function of position,  $t$  the time, and  $D$  the diffusion coefficient. A mathematical model for diffusion-based MoCo has been shown by *Pierobon M.* in ref.28. Given the problems, due to the slowness of the diffusion transport process, as well as to the difficulty to control it with extreme accuracy in an external environment, the literature is scarce in this sense and over the year the research has mainly focused on flow-assisted transport systems. In these systems, there is a natural dispersion by diffusion, as well as a transport caused by a flow generated by applying a gradient. The flow-based architecture becomes preferential especially in the MoCo macroscale due to the higher transmission speed of the chemical messenger. Flow generation results from the application of a gradient, or contribution of multiple gradients, of one or more properties of the communication channel. The most common is the pressure gradient, which generates flow in the lowest pressure direction. This is the same principle that is used for transporting fluids through pipes, flowing blood or generating wind in the environment and many natural MoCo processes are based on this: see hormonal communication through blood vessels such as insulin and glucagon. In ref <sup>36</sup> a mathematical model for MoCo through blood vessels, obtained by computational simulations, is

shown by signaling CD40 during the early stages of atherosclerosis.

---


$$\frac{\delta C}{\delta t} = \nabla \cdot (D\nabla C) - \nabla \cdot (vC) \quad \text{Eq. 3}$$


---

Compared to Eq. 2, Eq. 3 expresses the contribution of transport obtained by integrating the flow  $v$ , called the velocity field. This equation is called the Advection Diffusion equation and describes the dispersion, instant by instant, of a pulse of substance subject to a velocity field. By itself, the equation is relatively simple but requires accurate calculation of the velocity field by solving the Navier-Stokes differential equations.<sup>27</sup> In the case of transport inside a closed channel with a cylindrical cross section, the solution of the Navier-Stokes equations becomes decidedly simpler and appropriate for the purely prototypical study of long range MoCo. More complex examples of Flow-based exploitable for MoCo, in which the flow is not generated by pressure gradients, but by gradients of other types are present in the literature: electric and magnetic fields,<sup>37-39</sup> surface tension, electrons or light<sup>40-42</sup> can be exploited to direct the movement of the molecular messenger from TX to RX. In this regard, engineering the message-carrying species becomes a greater challenge to meet the requirements for both correctly encoding the information and being sensitive to the gradient present in the communication channel. By succeeding in this endeavor, numerous problems due to transport by simple gradient pressures such as laminar and turbulent flow would be solved, and analyzed in subsequent chapters. Finally, we define *active transport*, in

which the molecular messenger travels on board transporters such as molecular motors, bacteria, etc.<sup>43–46</sup> Modeling of this approach is much more complex and system-specific and currently only theorized given the difficulty of application in artificial media. We close this classification of chemical messenger propagation patterns with self-motion. It consists of self-movement by chemical propellers.<sup>47</sup> The implementation of a nano-propeller to a chemical messenger would allow its autonomous movement from the TX to the RX. The path would depend on the geometry of the propeller and other properties widely discussed in the literature.<sup>47–49</sup>

### 1.3 Modulation Schemes for Artificial Molecular Communication

The encoding and transmission of a message occurs as a series of sequential symbols, each in a time slot. The meaning of the symbol within the time slot depends on the modulation method chosen. To fully understand the need in MoCo to make use of signal modulation methods we must refer to the information theory, which finds as its progenitor the engineer and mathematician Claude Shannon,<sup>5</sup> and to the need to reduce communication errors and InterSymbol Interference (ISI) effects as much as possible.<sup>50,51</sup> The theory of information was born for the coding optimization of a message: it is the basis of compression systems, in which the number of symbols is reduced to the maximum, eliminating redundancies not necessary to the correct understanding of the message allowing to add targeted to increase the robustness of the transmission process. Signal

modulation consists of varying one or more signal properties in each timeslot. The symbols are then encoded according to these variations. To better understand these concepts, we must refer to the modulation systems in radio transmissions: the carrier of the information is a train of electromagnetic waves in the radio frequency. The modulation is obtained by varying the amplitude, frequency, polarity and phase for each timeslot. In MoCo the carrier of the information are small particles and therefore it is not possible to define the modulation as a wave but exploiting the intrinsic properties of the particles. Two extremely simple modulation schemes are proposed for diffusion-based and flow-based communication channels. Modulation systems by particle type, molecular shift keying (MSK),<sup>52</sup> whose symbol is discriminated by an intensive property of the particle, such as structure, size, shape or optical property. This type of systems has the advantage of being poorly subjected to channel noise, ISI and it is potentially possible to send more particle packets in short timeslots simultaneously and therefore more complex information in less time. On the other hand, the transmitter requires many particles for encoding, which experimentally means separate reservoirs containing the particles and multiple actuators handling the release. Moreover, the receiver must be specific in decoding as it has to distinguish the different particles from each other. Modulation systems by particle number, Concentration Shift Keying (CSK), in which symbols are discriminated by particle concentration in the timeslot.<sup>53</sup> The logic of this modulation method requires establishing concentration thresholds to correctly distinguish the meaning of each symbol.

---


$$S(t) = \begin{cases} 0 & \text{if } C(t) < C_1 \\ 1 & \text{if } C_1 < C(t) < C_2 \\ \dots & \dots \\ n & \text{if } C_n < C(t) < C_{n+1} \end{cases} \quad \text{Eq. 4}$$


---

Eq.4 shows the CSK logic for a communication system with  $n$  symbols.  $S(t)$  is the encoded symbol at time  $t$ ,  $C(t)$  is the particle concentration in the time slot while  $C_x$ , with  $x$  ranging from  $1$  to  $n+1$ , represents the threshold values to distinguish one symbol from the other. The advantages of this modulation method lie in its simplicity: it is sufficient a single type of particle and a single method of detection of the same because the information resides in the concentration. The limit, however, comes from a high probability of error, it is known in fact that more the thresholds are, higher is the risk of ISI.<sup>50</sup> It is therefore not advisable to use a large number of symbols and the transmission of information is slower. In the case where the symbols of a communication system are only two and the encoding is done in binary system, then the method of modulation by concentration is called On Off Keying (OOK).<sup>54</sup>

---

$$S(t) = \begin{cases} 0 & \text{if } C(t) < C_{threshold} \\ 1 & \text{if } C(t) > C_{threshold} \end{cases} \quad \text{Eq. 5}$$


---

The logic is described in Eq. 5, in which a single threshold can be defined. By combining several modulation methods, it is possible to build an advanced MoCo system capable of transferring many

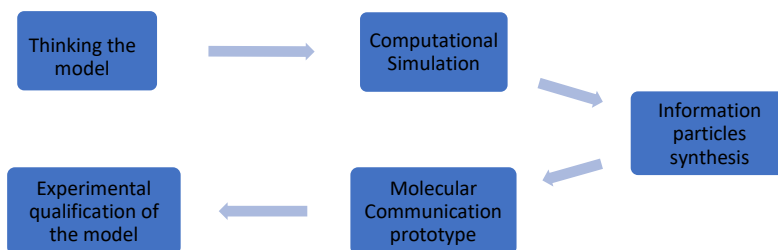
symbols and therefore rapidly transmitting even long and complex messages. The limits of the modulation methods described above lies, however, in the constraint of time synchronization between TX and RX. The flow or dispersion rate by diffusion must be perfectly controlled in order to correctly integrate each symbol within the predetermined timeslot. Errors in synchronization cause a decoding error of the information. It is not possible to apply these modulation methods where the flow within the communication channel is not predictable or controllable (e.g. biological systems) where time-independent modulation is required. Later in this lecture, a useful modulation method will be proposed to overcome the limitation of non-synchrony between flow rate and timeslot.

### 1.4 Conclusion and research project objectives

In this introductory chapter, the importance that the concept of artificial molecular communication can assume in the development of a new communication protocol based on the signaling through properly engineered information particles has been introduced. Since MoCo is already present in nature it is necessary to understand how to exploit tools already available in biological systems effectively. Conventional communication methods are now well-established, effective and efficient and will hardly be supplanted, so the integration of MoCo should be addressed where the limitations of other communication systems cannot be overcome otherwise, as explained at the beginning of the chapter. In fact, the proposed target concerns biological systems, namely bioimplants, cybernetics and cybermedicine. The



main components to obtain a proper transfer of information by MoCo have already been exposed: transmitter, receiver and communication channel. Fundamental as well is the choice of information particles because it must be appropriated by the chosen modulation method, as well as it must be compatible with the environment in which it propagates. An important contribution comes from the use of nanoparticles, which we define as 'information nanoparticles', because they are extremely versatile and adaptable to various contexts involving MoCo. Therefore, a separate chapter will be dedicated. The goals of this research project are set in a specific context of MoCo, perfectly aligned with the Target. Assuming that the aim is to simulate information transmission through biological fluids, the communication channel model falls under the concept of flow-assisted long-range MoCo in a closed environment. The fluids through which the dispersion of the information particle will occur are in the liquid state and purely aqueous. The approach used to develop the various aspects of the research project similarly follows the same workflow, described in Scheme 3. A project cannot be developed without solid fundamentals on which to build it, so the first point concerns the design of the work based on chemical and physical principles already well described in the literature. Thanks to the progressive enhancement of computational tools, both hardware and software, the possibility to model the system studied before developing the experimental part is now exploited in many areas of research.



*Scheme 3 - The proposed workflow to develop a Molecular Communication project.*

---

In the case of MoCo, modeling the process of transport of information particles through the communication channel, on the condition of knowing the chemical and physical properties of the system, becomes of fundamental importance not only to minimize the number of experiments to be performed, with gains in terms of time and consumption of chemicals, but especially because a computational model also has a predictive function for the learning that transmitter and receiver must do. Consolidated the computational part it is necessary to engineer the information particle in order to adapt it to the ideated model. The search for a simple synthesis, economic and ecofriendly for the development of the molecular messenger is a priority, especially because, as we shall see, the consumption is high as well as related to the modulation method adopted. To date, there is no commercial, experimental platform to emulate the processes involved in MoCo. In addition, there are many situations that you want to recreate and therefore a prototype for MoCo must be extremely modular and customizable. With the support of the entire research group a prototype, based on the scheme in Fig. 2, which

is interchangeable in every part and thus able to adapt itself to each experiment faced, was therefore designed. The common parts to all experiments are the following: a programmable homemade syringe pump to ensure the flow, the communication channel is a capillary with variable length and diameter, the transmitter is a loop to ensure the exact amount of information particle injected into the circuit, the receiver consists of a transducer of a certain property of the flow (e.g. fluorescence) in an electrical-analog signal. The electrical signal is then converted to digital using a DAC. All this is managed using a computer and scripts adapted to the system. The qualification of the model, through an experimental approach, is fundamental to demonstrate its actual applicability. In all scenarios, the experimental prototype is adapted, and information transferred from transmitter to receiver is tested. This is a general explanation of the approach, but, chapter by chapter, the workflow followed will be described more in detail.

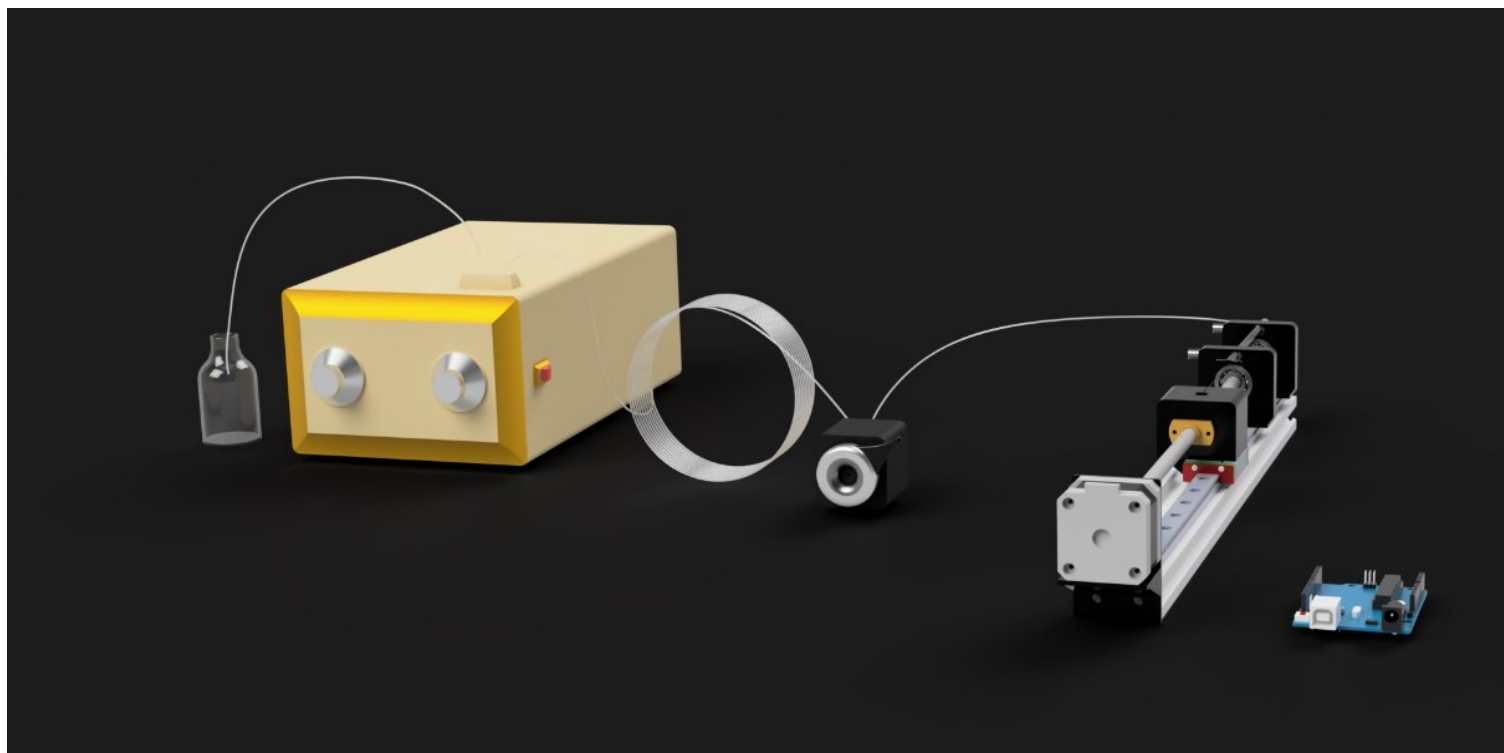


*Figure 2 – 3D representation of our typical Molecular Communication prototype. Starting from the right the components are: MCU unit to control the pump, a programmable syringe pump, the TX is a loop injector, the communication channel is a capillary tube a various length, the receiver is an optical detector of information particles.*

## Chapter 2

### Nanoparticles as suitable messengers for molecular communication

The choice of the correct information particle is a critical step in the development of an efficient system that exploits MoCo to transfer information between transmitter and receiver. The information particle must not only be suitable for the environment in which they propagate, both in terms of stability and toxicity, but they also must achieve an efficient transcoding in order to be tagged with the message and not lose part or all the information during transport. The parameter that most needs to be considered is specificity, but this goes hand in hand with sensitivity. For example, the use of highly specific systems, such as host-guest interaction or specially designed receptors, makes MoCo highly reliable because the detection of the information particle is characterized by very high sensitivity.<sup>55</sup> This effect is evident in the biological environment in the action of hormones or specific molecules that operate with high efficiency. It therefore falls into the case of MoSK modulation, i.e. monofunctional MoCo, in which the transferable information is single and uniform for each information particle. The use of the MoSK with the logic of an actuator (on-off) is the wisest choice. However, when a complex message must be encoded or the number of transferable information must be extended, it is no longer applicable without disproportionately increasing the number of information particles. The ideal procedure would be to encode articulated information using a single information particle. CSK modulation is well suited for sending binary messages using pulses of

## Nanoparticles as suitable messengers for molecular communication

information particles with known concentration. To recapitulate, an information particle must be designed *a priori* to be selective or non-specific to meet the application requirement. In any case, ideally, to be used successfully in MoCo, an information particle intended for use under physiological conditions must have several specifications:

- Easily synthesized
- Environmentally friendly
- Biocompatible
- Soluble/dispersible in aqueous fluids
- Easy to detect.

Finding already available information particles with all the characteristics listed above is not easy, but thanks to developments in recent years, it is possible to directly engineer a nano-system with the required characteristics. This is not a new approach, but there are now two decades of scientific literature from which it is possible to draw examples of the design and preparation of *ad hoc* developed nano-systems. In the case of MoCo and for the purpose of this research project, the focus will be on the application of nanoparticles as information particles. NPs are a massive class of materials that share common scale dimensions, which obviously fall within the nanoscale, between 1-100 nm. Since there exist a large amount of specialized texts about nanoparticles,<sup>11</sup> only a brief introduction will be made to focus on the application part dedicated to this work directly. NPs can be synthesized from organic or inorganic precursors and organic-inorganic hybrid systems can be obtained. Among the most common NPs are gold NPs (AuNPs), which are also widely used in biomedical phototherapy,<sup>56</sup> silicon NPs,<sup>57</sup> magnetic NPs<sup>58</sup> and

## Nanoparticles as suitable messengers for molecular communication

carbon NPs.<sup>59</sup> The great interest on nanoparticles comes from the properties dictated by their nanometric size. In fact, it is a transient size zone between a molecular system and a bulk and therefore the properties vary by changing the size only a bit. Some of the properties affected by size are electrical conductivity, radiation-matter interaction and some mechanical properties.<sup>60</sup> In addition to the intrinsic properties of NPs, it is possible to modify their structure or attach molecules, functional groups or other systems to their surface, thereby obtaining a wide range of useful properties. For this reason, NPs can be considered perfect candidates for use in MoCo.

### 2.1 Application of Nanoparticles in molecular communication

NPs have been extensively used in MoCo at both the macroscale and nanoscale, so an overview of the work that inspired this research project will be given here. In ref <sup>61,62</sup>, a nanoscale example of bifunctional communication between two Janus-NPs using two enzymatic processes and two molecular messengers was demonstrated. The Janus-NPs used were mesoporous Au-silica. The mesoporous silica part is filled with a molecular messenger and sealed with a cap. By an external stimulus, the cap opens and allows the release of the molecular messenger. The gold part is functionalized with biomolecules. Fig. 3 shows the communication process between them: on the first Janus-NP to glucose (messenger 1), which is transformed into gluconic acid on the second Janus- NP. This induces a local drop in pH, which induces the de-threading of the supramolecular b-CD:benzimidazole nanovalve and the release of N-acetyl-L-

## Nanoparticles as suitable messengers for molecular communication

cysteine (messenger 2), which is the feedback that finally induces the delivery of the reporter  $[\text{Ru}(\text{bpy})_3]_2$  from the first Janus-NP. This design can be considered as the basis of a Bio-IoT system, due not only to the possibility of receiving information from an external source, but also to the provision of feedback to the primary devices.

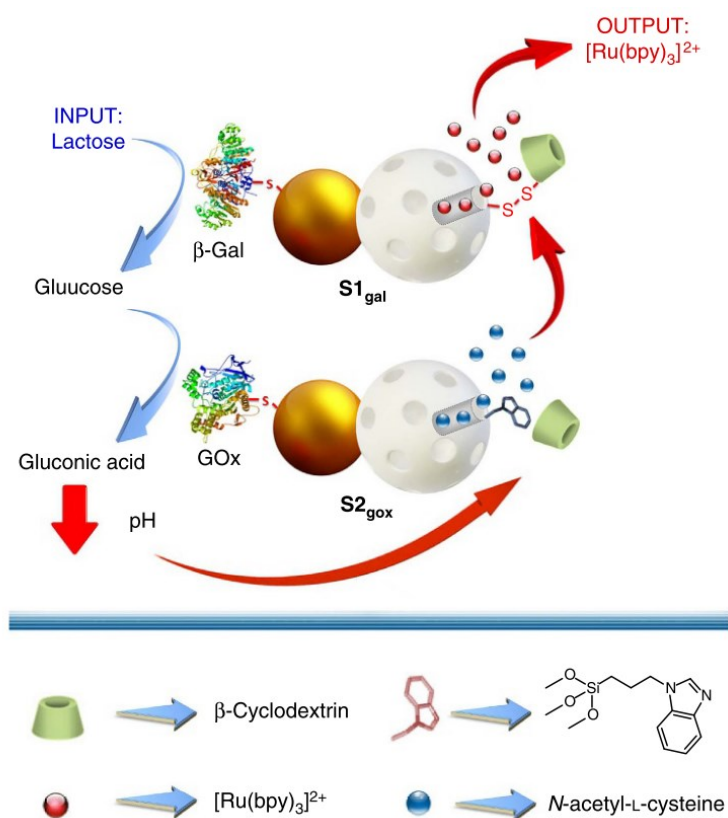


Figure 3 - Representation of the interactive communication process between two Janus gated nanodevices. This figure has been reproduced from ref. 60 with permission from Springer Nature, copyright 2017.



## Nanoparticles as suitable messengers for molecular communication

Even in the prototype that comes closest to the initial idea of MoCo in Bio-IoT systems, the *in vivo* release of a ruthenium-based bipyridine complex would be invasive. Furthermore, the preparation of Janus-NPs filled with molecular messengers requires the use of toxic reagents and there is also the problem of refilling the nanomachine after the release to ensure that the Janus-NPs are fully functional. Considering that the scientific community is working extensively on NPs, we expect that these limitations will be solved soon. A very promising class of NPs is self-propelled NPs. These consist in NPs which autonomously generate the boost that pulls them through a fluid, as a result of a chemical reaction (Fig. 4).<sup>48</sup> The most popular self-propelled NPs are Pt-coated and use the decomposition reaction of  $H_2O_2$  catalyzed by platinum to obtain the boost.<sup>63</sup> To precisely direct the motion along predetermined paths in the fluid a fine control of the geometry and the platinum-coated portion of the NP is required. There are currently many models in the literature describing self-propelled NPs and they have been actively studied more as catalytic motors or chemotaxis.<sup>64,65</sup> Currently, there are no real application examples of the use of self-propelled NPs in MoCo but, given their ability to carry molecular messengers or to encode within them the message to be transmitted, they can be used based on the active transport and self-transport models described above. The use of self-propelled NPs in MoCo requires a more refined control of the propagation direction of the information nanoparticles and the avoidance, as much as possible, of undesirable dispersions. Moreover, the application in the biological field is complex due to the formation of gas during propulsion, that could cause embolisms, and the continuous request of fuel.

## Nanoparticles as suitable messengers for molecular communication

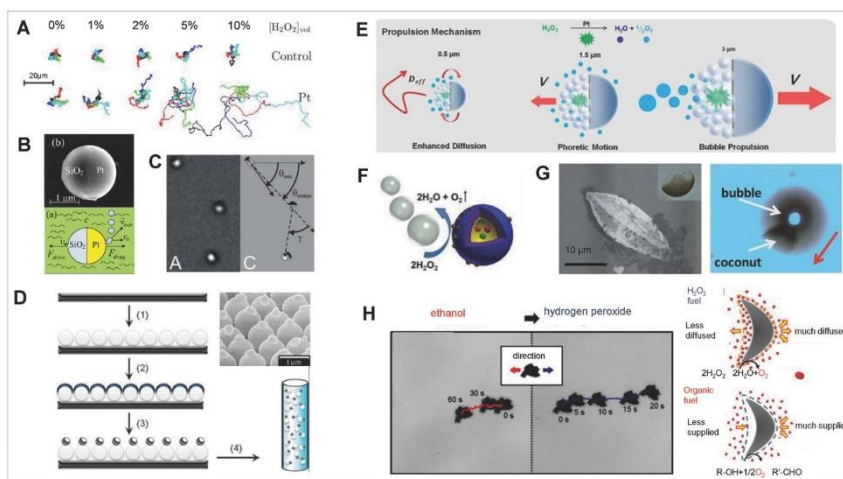


*Figure 4 - Pt-Based Janus micromotors moving in presence of H<sub>2</sub>O<sub>2</sub>. (A) Trajectories of half-coated Pt-based Janus particles in water at different fuel concentrations. (B) Scanning electron microscopy (SEM) image and associated motion mechanism of Pt-coated spherical silica microparticle. (C) SEM image of Pt sphere dimers and schematic depicting their synthesis. (D) Three sequential images of Pt Janus microparticles in motion overlaid with their corresponding angles and trajectories. (E) Schematic of the different motility scenarios in mesoporous silica Pt-based Janus particles. (F) Scheme of multilayer hollow Pt Janus microparticles. (G) SEM image (left) and optical image (right) of Pt shell. (H) Directional inversion on translational motion of Pt motors in presence of organic fuels (ethanol) and H<sub>2</sub>O<sub>2</sub>, and their corresponding motion mechanisms. This figure has been reproduced from ref. 48.*

An important feature that a suitable information NP should have been 'easy detectability'. Magnetic NPs would be perfect in this respect. In ref. 66 a MoCo platform was developed using a susceptometer coil as a receiver to detect the presence of moving magnetic material.

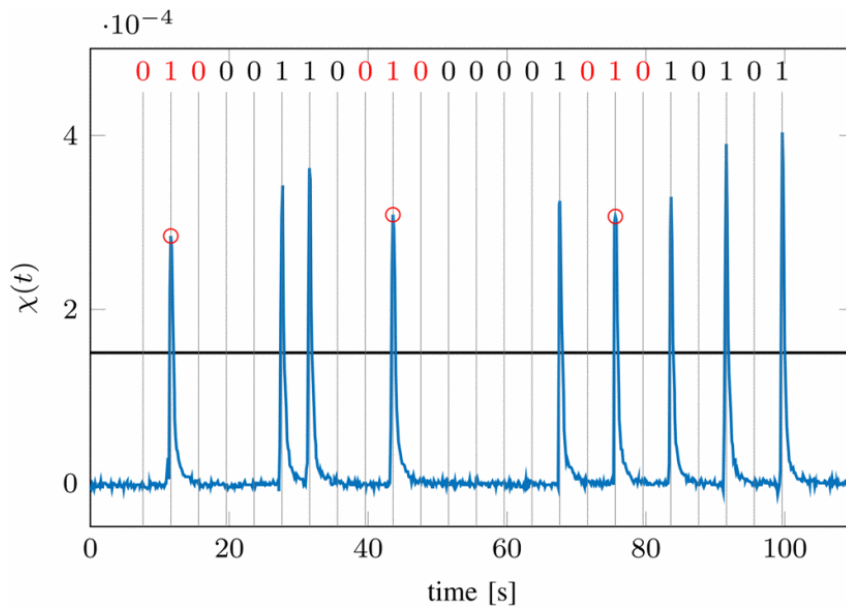


Figure 5 - Measured received susceptibility time signal for a specific bit sequence obtained by using magnetic nanoparticles. This figure has been reproduced from ref. 65

The modulation method used is the easier OOK (Fig. 5) but show the extremely quality of the transmission. The detection of magnetic NPs, however, requires extra care in the presence of complex chemical matrices, because of the interference of all moving charges like ions. Natural or artificial magnetic fields could also be sources of interferences and the sensing of low concentration magnetic materials could be compromised. Indeed, in the biomedical field, the detection of magnetic NPs is carried out with highly invasive techniques such as PET and MRI.

## 2.2 Carbon-Based Nanoparticles as information nanoparticles

A separate section is reserved to discuss carbon-based nanoparticles, since they represent the basis of the research project developed for this dissertation. In fact, as it will be described in the following chapters, their characteristics have made it possible to develop models and methods for artificial molecular communication in a simple and effective way. Specifically, the use of carbon-based Quantum dots (CQDs) or graphene-based Quantum dots (GQDs) with peculiar fluorescent properties have been proposed as non-specific information nanoparticles for MoCo in liquid media. The properties of CQDs can be modified in a multitude of ways, allowing specific physical and chemical modulation methods to be developed to obtain high information transfer efficiency. Since their first discovery in 2004,<sup>67</sup> due to their efficient luminescence properties, carbon nanoparticles are more promising than other carbon allotropes (nanodiamonds, graphenes, fullerenes, etc.) and conventional inorganic quantum dots for a wide variety of applications, including bioimaging, biosensing, chemical sensing, nanomaterial science, optoelectronic devices, photonics, solar cells, etc.<sup>68–72</sup> The hype resulting from the discovery of fluorescent carbon NPs has led to the development of a new generation of CQDs. The enthusiasm arising from the discovery of this class of particles derives from the effective simplicity of their preparation and versatility. Fluorescent carbon NPs are produced whenever a carbon source undergoes a carbonization process. The formation of these NPs in soot from candles, coffee grounds, milk or burnt hair has been confirmed.<sup>73–76</sup> In addition, coal, currently used as an energy source, can be a very rich source of CDs when it is in the

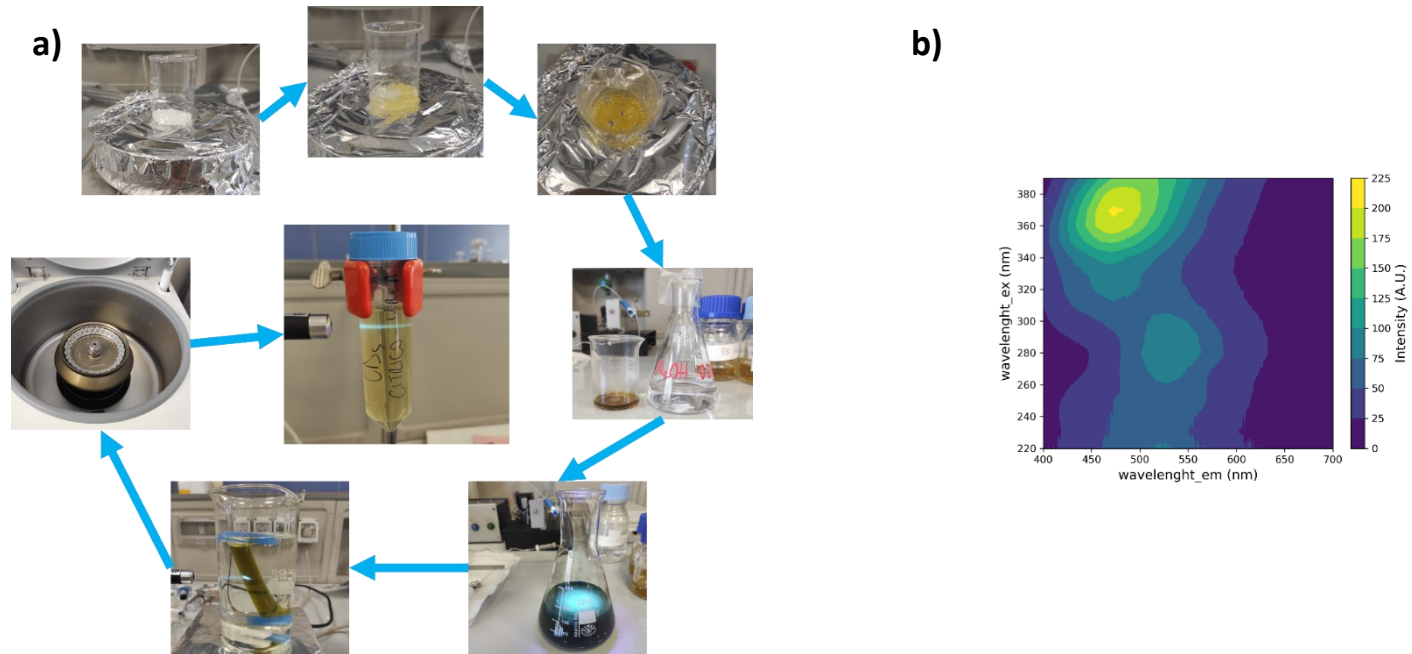
## Nanoparticles as suitable messengers for molecular communication

form of bituminous coke, coke or anthracite.<sup>77</sup> The potential of carbon-based QDs was immediately clear, so in the years following their discovery, the scientific community has not only produced a large amount of literature for their characterization and application, but it also proposed many synthesis techniques with different levels of sophistication, including laser ablation processes, pyrolysis, hydrothermal synthesis, microwave-assisted synthesis, and electrochemistry.<sup>78–82</sup> For use in MoCo, the ability to synthesize large quantities of fluorescent NPs from waste material makes it much more attractive and in line with *green chemistry* goals.<sup>80,83–85</sup> One of the best techniques for structural analysis of CQDs is atomic force microscopy (AFM). Since small quantities of CQDs can easily be deposited on flat substrates by drop casting, AFM provides excellent and reliable images with very small dimensional errors. The use of scanning electron microscopy (SEM) does not allow such a high resolution (in the nanometre range) to be obtained. In certain cases, it is possible to use very powerful microscopy techniques, such as transmission electron microscopy (TEM), but for the development of this project, it was not necessary to use it. Many TEM images of QCDs obtained by hydrothermal decomposition can be found in the literature. Structurally, these NPs appear as discs/spheres with diameters ranging from about 2 to 10 nm. The core has a structure graphene-like, while functional groups such as epoxy, carboxylic and carbonyl are present on the surface.<sup>86</sup> This structure makes them dispersible in aqueous solution if not chemically treated. Cell toxicity tests show a low degree of toxicity and good biocompatibility.<sup>87,88</sup> The use of carbon-based QDs in MoCo applications comes mainly from their unique fluorescence properties.<sup>89</sup> Indeed, most of these NPs have an absorption band

## Nanoparticles as suitable messengers for molecular communication

in the UV (between 200 and 400 nm) and a fluorescence band in the visible spectrum (between 400 and 600 nm). A high fluorescence yield is observed, making them detectable even at low concentrations. The mechanism of fluorescence is not perfectly known, with some theories attributing the effect to  $\pi$ - $\pi$  transitions within the graphene structures of the core, and others considering it a surface phenomenon due to the presence of trap sites, whereby passivation of the surface enables the above fluorescence phenomena to be triggered, resulting in an enhanced yield.<sup>90,91</sup> CDs are excellent information NPs because they allow the manipulation of many of the parameters necessary to optimize the communication process and excellent results have been obtained for the experimentation of new modulation methods. CQDs are known for their surface functionalization due to the presence of reactive groups such as epoxides and carboxyls.<sup>92</sup> Surface functionalization opens the door to a wide range of uses for CQDs. This property is important in MoCo because the surface functionalization of information nanoparticles makes the possibilities of experimenting with modulation methods, interaction effects with receivers and even improving integration and compatibility with the environment present in the communication channel.

## Nanoparticles as suitable messengers for molecular communication



## Chapter 3

### Carbon Quantum Dots from Lemon Waste Enable Communication Among Biodevices

We have shown that carbon-based information NPs (CNPs), more specifically carbon quantum dots (CQDs), are ideal candidates for application in MoCo.<sup>93</sup> As explained extensively in the previous chapter, the production of CQDs is simple and they are easily obtainable from various carbon sources. It is not necessary to start by using pure substances to decompose, but there are numerous examples in the literature of syntheses using raw biomass to produce carbon quantum dots (CQDs).<sup>94–98</sup> The synthesis that inspired the development of this work is based on a simple one-step hydrothermal synthesis using orange juice as the carbon source.<sup>99</sup> As a resident of Sicily, where the production and market of citrus fruits is one of the most prosperous, the idea of using citrus waste for the synthesis of high-value informational NPs for biomedical applications in the emerging technological field of MoCo would open the door to a new market and further enhance the products of this land. The motivation behind the use of citrus waste stems comes from its abundance: citrus is the most important fruit crop in terms of value worldwide. In 2016, the FAO (2017) estimated the world production of citrus fruits at about 124 million tonnes, with oranges accounting for about 67 million tonnes. Globally, about 41 million tonnes of citrus fruits are processed industrially each year, mainly to produce juice. However, the citrus industry considerably suffers during the post-harvest phase from rot and consequently the shelf life is reduced. The infection is caused by multiple fungal pathogens, including



## **Carbon Quantum Dots from Lemon Waste Enable Communication Among Biodevices**

Penicillium spp., Phytophthora spp., Alternaria spp., Colletotrichum spp. and Geothrichum spp.<sup>100,101</sup> The impact of these pathogens is reflected in the market - the aesthetic quality of rotten fruit severely limits its sales potential. Thus, post-harvest rots have a great impact on the citrus fruit market: since they reduce the shelf life of the fruit, they are a limiting factor for its transport over long distances and have an impact on storage and sales on the vendors' shelves. The unfortunate result is a huge amount of unsold products, thus a major waste problem and significant economic losses. Addressing this problem is crucial in today's society, which provides us with the tools and concepts to apply the circular economy, green economy, green chemistry which create a zero-waste society - based on the valorization of unsold products and waste. A more common example concerns the recovery of obsolete technology for the development of new technologies, which was unthinkable a few decades ago. The same reasoning can then be made for the development of nanotechnologies through the recovery of valuable precursors otherwise considered as waste. In fact, here we propose the transformation of a low-value waste (practically zero value) into a high-value nanotechnological resource in the field of biomedicine. Specifically, it will be presented how it is possible to obtain from the lemon juice derived from unsold lemons, excellent CQDs that can be successfully used in MoCo. The aim of this work is not to contribute to technical innovations in the field of MoCo, but to demonstrate the possibility of valorizing a waste raw material (lemons) in line with the concept of circular economy, giving it a second use through the preparation of highly fluorescent CQDs to be used in fields such as biomedicine.

### 3.1 Materials and Methods

#### 3.1.1 CQDs Synthesis

The synthesis of CQDs was conducted starting from 100 ml of pure lemon juice (called Lemon-only CQDs) or by adding to this 3.3 g of 50% branched polyethyleneimine (PEI) in water (Aldrich) (called Lemon-PEI CQDs) in a 400 ml crystalliser. It is known that PEI acts as a passivating species and allows better stabilisation of CQDs in solution and also has an enhanced effect on the fluorescence yield. The crystalliser was then placed on a heating plate at 175°C to trigger the decomposition process of the carbon precursors. As decomposition progressed, the colour of the solution changed from lemon-yellow to caramel. Once a more caramel-like consistency was achieved, the decomposition process was extended by adding three 33 ml aliquots of Milli-Q water, delayed 10 minutes maintaining the plate temperature at 175°C. A fourth 33 ml aliquot of Milli-Q water was added, spaced 10 minutes apart with the plate temperature at 175°C. A fourth 33 ml aliquot of water was finally added to stop the reaction and the resulting mixture was placed at room temperature to cool. However, the resulting solution is full of macroscopic carbonaceous residues and there are also several molecular forms that are not completely decomposed. The purification process of the CQDs thus obtained was carried out in three steps. The non-polar residues were removed by extraction with pure chloroform (Aldrich), in a separating funnel, so that the organic phase was separated from the aqueous phase by exploiting the immiscibility between the two phases. This process was repeated three times, replacing the waste chloroform with pure chloroform. The second

## **Carbon Quantum Dots from Lemon Waste Enable Communication Among Biodevices**

step consists of a dialysis purification process to remove the smallest water-soluble residues. Dialysis was performed by placing the CQDs solution inside a dialysis tube (Membra-Cel MC18 with a molecular weight cut-off of 14000 Daltons) and immersing it in a 400 ml beaker filled with Milli-Q water and keeping it under constant agitation. The water was replaced with fresh water three times (delayed 1 hour apart) and the discarded solution was observed to become increasingly clear. A final dialysis was carried out by keeping it stirred overnight. The last step was a cryocentrifugation for 1 hour and 50 minutes, at 6000 rpm and 3°C temperature to remove the suspension remaining in solution. Only the supernatant was collected and used for subsequent characterisation and MoCo experiments.

### **3.1.2 Characterization Methods**

Optical characterisation of the CQDs synthesised by the method described above was carried out using IR, UV and fluorescence spectroscopic techniques. IR analysis was performed using a Perkin-Elmer FT-IR spectrometer, UV-Vis analysis was performed using a Jasco V-750 spectrophotometer and fluorescence analysis using a Varian Cary Eclipse fluorescence spectrophotometer. Since it was not possible to determine the exact size dispersivity of the nanoparticles, the calculation of the fluorescence yield was estimated by comparison with sodium fluorescein dihydrate (Aldrich), used as a standard, by approximating the nanoparticle concentration on the basis of the following parameters, which were also partly obtained experimentally: an average NP diameter of 1.5 nm for Lemon-PEI CQDs, 1.8 nm for Lemon-only CQDs and

## Carbon Quantum Dots from Lemon Waste Enable Communication Among Biodevices

a density of 2.23 g/cm<sup>3</sup> (graphite density). Therefore, a molar mass for Lemon-PEI NPs of about 2376 g/mol and a molar mass for Lemon-only CQDs of about 4095 g/mol were estimated. The percentage fluorescence yield was calculated by considering the maximum fluorescence intensity of both CQDs and sodium fluorescein, normalised for the molar concentration according to Eq. 6.

---

$$\%_{\text{fluorescent yield}} = \frac{\frac{I_{Max\ CDS}}{M_{CDS}}}{\frac{I_{Max\ STD}}{M_{STD}}} \cdot 100 \quad \text{eq.6}$$

---

$I_{Max\ STD}$  is the maximum fluorescence intensity of the  $M_{STD}$  molar solution of sodium fluorescein,  $I_{Max\ CDS}$  is the maximum fluorescence intensity of the  $M_{CDS}$  molar solution – estimated according to the previous described procedure. The choice of concentration of the CQDs suspensions was made considering the quenching effects of the concentration well known in the literature. The concentration was therefore chosen based on the maximum fluorescence yield by developing Stern-Volmer Plots.<sup>102</sup> Atomic force microscopy (AFM) images were obtained using a multimodal Nanoscope IIIA apparatus from Digital Instruments (Santa Barbara, CA) used in air tapping mode on a silicon substrate. Budget Sensors' Tap 300G silicon probes, with a nominal resonant frequency of 300kHz, were used. NMR-DOSY information was collected using a Varian UNITY Inova 500 MHz spectrometer (1H at 499.88 MHz, 13C NMR at 125.7 MHz) equipped with a pulse field gradient module (Z axis) and a Varian tunable 5 mm inverse detection probe (ID-PFG). Simulations of the

## Carbon Quantum Dots from Lemon Waste Enable Communication Among Biodevices

transport process in MoCo were performed using Comsol Multiphysics© software and its two interfaces "Laminar Flow" and "Transport of Diluted Species".

### 3.1.3 Molecular Communication Platform

The prototype platform for carrying out the MoCo experiments was designed and manufactured in-house. The information transmitted by the information nanoparticles is done by fluorescence using an in-flow fluorometer (from Shimadzu) connected in analogue to a keythley 2611b used in voltmeter mode for analogue to digital conversion. The control centre consists of a standard PC digitally interfaced to the keythley. For greater control over data acquisition, *ad hoc* scripts were developed in python with the PyVisa libraries. The microfluidic system consists of a piston pump controlled by a stepper motor to ensure a constant flow rate and a Teflon tube connecting the transmitter and the receiver. The piston pump was designed in-house and manufactured using components purchased from RS Components and PETG-printed parts made on a 3D printer (Alfawise u30 pro). An aqueous fluid with a viscosity of 3.5 mPa·s was used as a carrier.

## 3.2 Results and Discussions

### 3.2.1 CQDs Characterization

The choice of preparing two types of CQDs, one using only lemon juice as carbon source (called Lemon-only CQDs) and the other adding polyethyleneimine (called Lemon-PEI CQDs), was made to demonstrate that, although it is known that the synthesis of CQDs in the presence of PEI has positive effects on the quality of the nanoparticles obtained, MoCo makes it possible to exploit those synthesized in the classical manner and to obtain correct information transfer. The positive factors that make Lemon-Pei better than those synthesized without the use of PEI are two: during the hydrothermal decomposition process, PEI acts as an additional source of nitrogen, which is known to act as a dopant in the carbonaceous core of CQDs, improving the quantum yield. In addition, its polymeric structure acts as a passivating agent that functionalizes the surface of CDs. The surface passivation effect also introduces emissive energy traps to promote the recombination of electron-carbon pairs resulting in a further increase in quantum yield.<sup>103–110</sup> The propagation of a molecular messenger in a fluid is strongly correlated to its fluid-dynamic properties, so that the study of the optical properties of QCDs is not enough, and an analysis of the structural properties and behavior when immersed in a fluid is also necessary. The dimensional investigation of CQDs is fundamental because it correlates with their dispersibility properties, and the structural investigation allows the fluid-CQDs and CQDs-CQDs interactions to be assessed. A synthesis that achieves low size-dispersion is attempted in order to minimize the effects of self-diffusivity and thus the broadening of the signal carried by the information

## Carbon Quantum Dots from Lemon Waste Enable Communication Among Biodevices

particles' dispersion in communication channel. It is known that the size dispersion of these nanoparticles depends on the chosen synthesis strategy.<sup>111–113</sup>

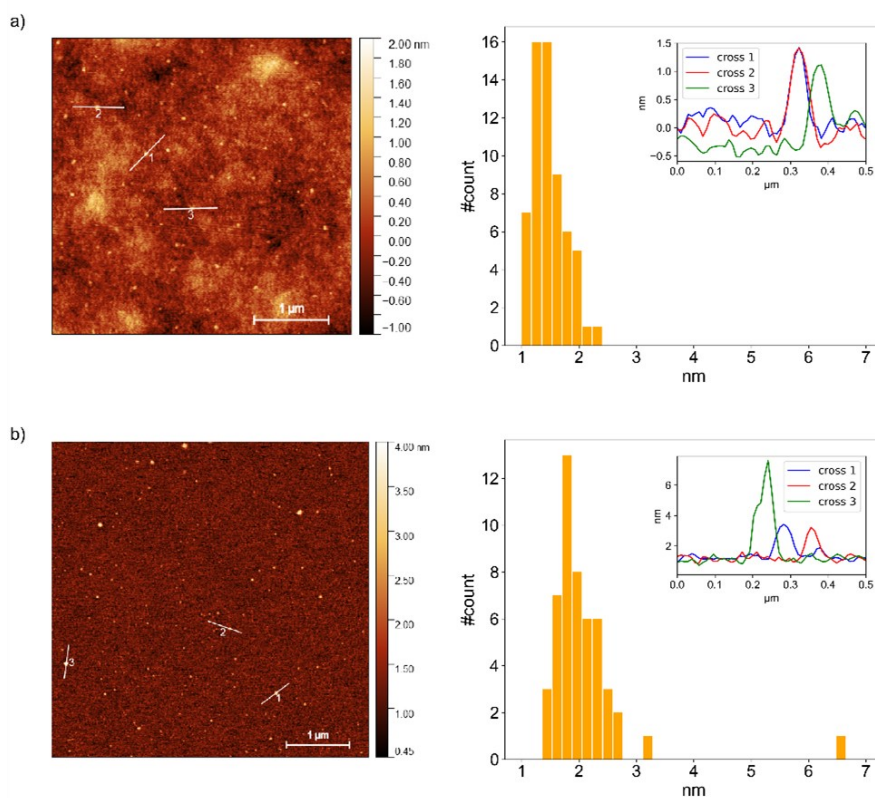


Figure 7 - (a)  $5 \times 5 \mu\text{m}^2$  AFM image of Lemon-PEI CDs deposited onto silicon substrate ( $z$  scale:  $0-20^\circ$ ); its histogram analysis of Lemon-PEI CDs' height obtained by several sections, three of which are represented in the inset; (b)  $5 \times 5 \mu\text{m}^2$  AFM image of Lemon-only CDs deposited onto silicon substrate ( $z$  scale:  $0-20^\circ$ ); its histogram analysis of height of lemon-only CDs obtained by several sections, three of which are represented in the inset.

## Carbon Quantum Dots from Lemon Waste Enable Communication Among Biodevices

The AFM characterization shown in Fig. 7a shows the typical Lemon-PEI CDs distribution obtained with the adopted synthesis strategy. A cross-sectional analysis was performed by observing the relative height of each NP in cross-sectional mode. The histogram shows a size dispersion of about  $\pm 0.5$  nm, centered around 1.5 nm. This dimensional uniformity was achieved by a very simple and economical synthesis strategy in terms of materials and solvents. The efficient synthesis results from the combination of the use of PEI in the carbonization step of the active components in lemon juice and the dialysis process.<sup>114</sup> For lemon-only CDs, a size dispersion of about  $\pm 0.5$  nm was obtained, but this time centered around 2 nm (Fig.7b).

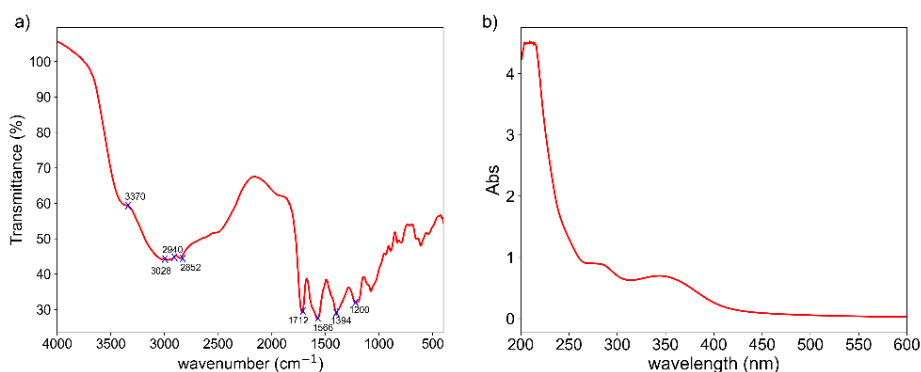


Figure 8 - (a) FT-IR spectra and (b) UV-vis spectra of an aqueous suspension of lemon-PEI CDs.

However, slightly larger particles greater than 3 nm were also detected, which were likely formed due to the absence of PEI acting as a capping agent. For a complete characterization of the NPs, an in-depth analysis of the optical properties was performed using IR, UV-Vis and fluorescence spectroscopy. Lemon-only CQDs



## Carbon Quantum Dots from Lemon Waste Enable Communication Among Biodevices

showed the typical properties of CQDs that can be synthesized from citric acid as a carbonaceous precursor. As they have been extensively described in the literature, the characterization will not be pursued here.<sup>115,116</sup> Lemon-PEI CQDs will be described in more detail. The FT-IR spectrum, shown in Fig. 8a, shows the characteristic absorption peaks for the stretching vibration of C=O at 1712 cm<sup>-1</sup>, C-N or C-O bonds at 1200 cm<sup>-1</sup>, N-H and O-H at 3370 and 3028 cm<sup>-1</sup> and C-H or O-H folding at 1394 cm<sup>-1</sup>. In addition, several peaks characteristic of PEI can be seen for Lemon-PEI CDs, such as 2940 and 2852 cm<sup>-1</sup> related to asymmetric and symmetric CH<sub>2</sub> stretching vibration and 1566 cm<sup>-1</sup> for N-H bonding.<sup>117</sup> Considering the peaks of the bonds where nitrogen is present, we can confirm N-doping and the PEI passivation. The UV-vis absorption spectrum (Fig.8b) shows absorption curves at 350 and 230 nm. In particular, the peak in the far UV is related to the  $\pi$ - $\pi^*$  transition of the aromatic systems in the graphene-structured core of the CQDs, while the peaks at low energies around 300 nm are related to the n- $\pi^*$  transition and the passivated surface.<sup>118,119</sup> Since our approach for designing the MoCo system uses a fluorescence receiver, it is the latter that needs further analysis. A high fluorescence yield has a fundamental impact on the efficiency and reliability of information transmission as higher intensities at the receiver improve the signal-to-noise ratio and reduce inter-symbol interference effects. It allows the use of lower concentrations of information nanoparticles, thus less consumption of chemicals with positive consequences on biological and environmental impact. Fig. 9a shows the fluorescence spectra (PL) of Lemon-PEI CDs when irradiated with excitation wavelengths in the range from 250 to 400 nm. The

## Carbon Quantum Dots from Lemon Waste Enable Communication Among Biodevices

strongest emission peak is centered at 470 nm upon excitation at 340 nm.

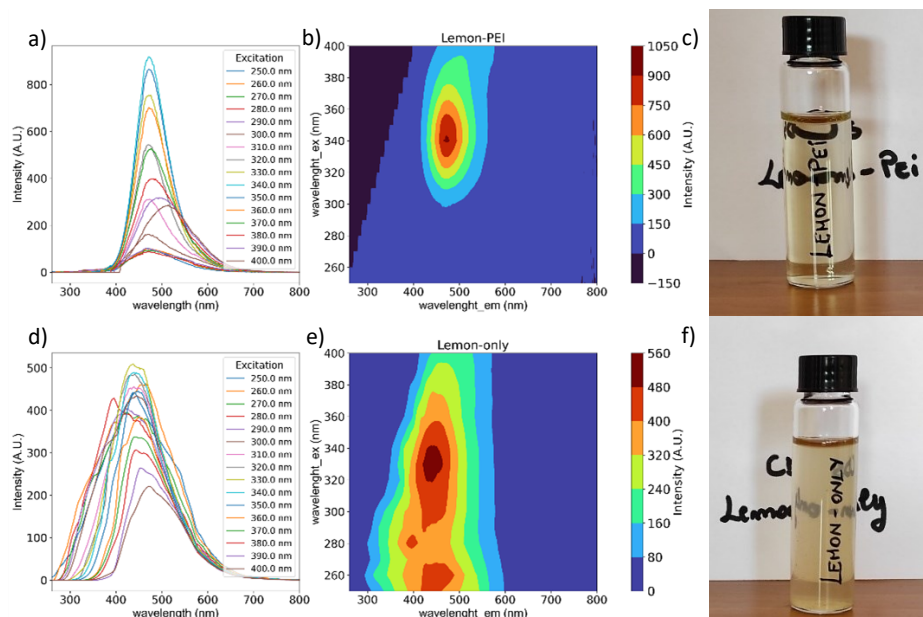


*Figure 9 - (a,d) Overlay of fluorescence spectra of aqueous suspensions of lemon-PEI CDs and lemon-only CDs, respectively, acquired at several excitation wavelengths as reported in the labels; (b,e) excitation–emission maps of aqueous suspensions of lemon-PEI CDs and lemon-only CDs, respectively; (c,f) photos depicting the qualitative appearance of the aqueous suspensions of lemon-PEI and lemon-only CDs.*

In order to define the fluorescence more precisely, the contour plot is shown in Fig. 9b and appears as a small patch in which the fluorescence falls within a relatively narrow window of emission wavelengths. This feature makes lemon-PEI CQDs easily distinguishable from interferers within the communication channel. Lemon-only CQDs show a broader fluorescence emission spectrum (Fig.9d) than PEI-treated CQDs, although with similar

## Carbon Quantum Dots from Lemon Waste Enable Communication Among Biodevices

intensity. The lemon-only CD solution appears *cloudier* due to the presence of suspended particulate matter, as shown in Fig.9f, which cannot be separated by cryocentrifugation (up to 15000 rpm) or filtration (0.2 mm pore size). CQDs are known to be affected by concentration-driven self-quenching processes [ref]. These can be described by the Stern-Volmer equation (eq.7).

---

$$I(c_{det}) = k(1 - e^{-\varepsilon c_{det} d}) \cdot \frac{1}{1 + K c_{det}} \quad \text{eq.7}$$

---

$\varepsilon$  is the molar extinction coefficient,  $d$  the optical path,  $K$  the Stern-Volmer constant,  $k$  is an instrumental correction parameter.<sup>120</sup> In order to experimentally determine the quenching profile of the synthesized CQDs, a series of fluorescence spectra was made from a highly concentrated solution towards progressive dilutions. The fluorescence maxima obtained were plotted as a function of dilution. As the quenching response is different for different substances, the starting concentration values are different. For Lemon-PEI CQDs, the starting suspension has a concentration of 5.40 g/L and successive dilutions are shown on the x-axis in Fig. 10a. The fluorescence trend follows the expected curve according to the eq.5. Upon closer examination of the obtained curve, the fluorescence in a first zone increases with dilution as the effects of self-quenching are reduced. When a maximum is reached, the effects of self-quenching disappear, and the fluorescence intensity gradually decreases. The maximum fluorescence intensity is obtained for the suspension diluted 1:4, corresponding to a concentration of 1.35 g/L. The same procedure

## Carbon Quantum Dots from Lemon Waste Enable Communication Among Biodevices

was carried out for Lemon-only CQDs, whose initial solution has a concentration of 7.55 g/L.

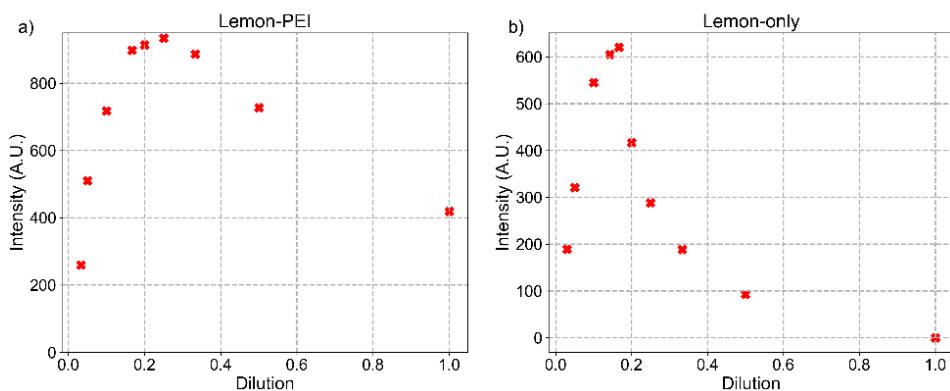


Figure 10 - (a) Intensity of fluorescence peak as a function of the dilution of an aqueous suspension of lemon-PEI CQDs ( $\lambda_{ex} = 340$  nm,  $\lambda_{em} = 470$  nm); (b) intensity of fluorescence peak as a function of the dilution of an aqueous suspension of lemon-only CQDs ( $\lambda_{ex} = 330$  nm,  $\lambda_{em} = 440$  nm).

The maximum fluorescence intensity was obtained for the 1:6 diluted suspension (Fig.10b), corresponding to 1.26 g/L. The calculation of the exact concentration allowed us to eliminate self-quenching effects and to be able to correctly determine the fluorescence yield. Sodium fluorescein was used as the standard because it is known to be an excellent fluorescent marker and its optical properties are well known in the literature.<sup>121</sup> No significant differences were obtained between the fluorescence yield of the Lemon-PEI and Lemon-only CQDs, at 5.2% and 6.3%, respectively. It should also be noted that the concentrations at which self-quenching effects are triggered for these nanoparticles are much higher than those used in a typical MoCo experiment.

### 3.2.2 Molecular Communication Experiment

An important insight required for the application of CQDs in MoCo concerns the study of physical properties governing diffusion and transport phenomena. The models of propagation of information particles within communication channels are at the basis of the development of systems that use chemical signals for the transfer of information. The applicable models are very variable and depend on the geometry of the channel, on the environment and on the type of propagation involved, whether flow-assisted or purely diffusive.<sup>122–124</sup> The idea of applying MoCo to biological systems requires a rigorous study of all possible scenarios which, at present, remain only partially theorized<sup>125,126</sup> and it is necessary to follow an experimental approach which is currently not very common. Generally, the theoretical study of dispersion processes starts from models related to the transport of matter within confined systems such as capillaries, where a continuous flow assists the movement of information particles. The equation involved in this case is the advection-diffusion equation (Eq. 8).

---

$$\frac{\partial C}{\partial t} = \nabla \cdot (D\nabla C) - \nabla \cdot (vC) \quad \text{eq. 8}$$

---

$C$  is the concentration of the pulse of information particles released into the communication channel,  $t$  the time,  $D$  the self-diffusivity coefficient of the substance and  $v$  the flow velocity of the transport fluid. Modelling the MoCo system as  $3D$ , we should consider the coefficient  $D$  and the velocity, not as vectors but as tensors and they strongly depend on the fluid-dynamic conditions

## Carbon Quantum Dots from Lemon Waste Enable Communication Among Biodevices

of the communication channel. The tensor  $\nu$  can be obtained by solving the Navier-Stokes equations in a relatively simple way if some approximations are considered.<sup>27</sup> For example, applying MoCo in biological environments, such as blood vessels, in a circular capillary with a diameter of less than a millimeter and velocities of the order of mm/s, the flow can be considered laminar,<sup>127</sup> so there is no mixing due to turbulent motions and the dispersion phenomena of information particles during transport depend exclusively on the shape of the laminar flow profile and the diffusion coefficient,<sup>128</sup> the contribution of which requires further investigation. Assuming that the diffusion coefficient is isotropic, it is possible to decompose it into two contributions of equal intensity: axial and transversal to the flow. The shape of the laminar flow makes the pulse of substance moving along the capillary like an "arrow". This is clearly visible in the simulations results shown in Fig. 11. The effect of the axial contribution on the dispersion is negligible compared to the dispersion effect of the laminar flow because we are considering high aspect ratio communication channels (long compared to the cross-sectional dimension). This implies instead that transverse diffusion has an incisive effect on the dispersion of the substance during transport.

## Carbon Quantum Dots from Lemon Waste Enable Communication Among Biodevices

---

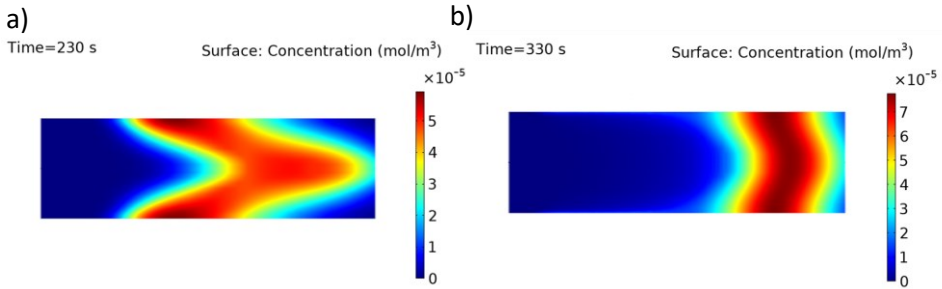


*Figure 11 - Schematic representation in false color of the transversal diffusion following concentration gradients; (a) map of simulated molecular messenger concentration distribution with lower diffusion coefficient (b) and with higher diffusion coefficient.*

---

Fig. 11b also shows the contribution of transverse diffusion: the substance pulse undergoes two concentration gradients that drive dispersion: i) in the front from the center towards the walls and ii) in the tail from the walls towards the center. As time passes and transport takes place, the laminar flow will tend to convert the information particles pulse to an arrowhead-like shape directed towards the detector, in contrast the transverse dispersion will tend to minimize it. The effect of high diffusion value is clearly visible in the simulation results shown in Fig. 6d and it has the effect to contrast the arrow-shape making the pulse compact. Thus, estimating the diffusion coefficient of CQDs is essential to design and optimize the configuration of the MoCo system.

---

$$D = \frac{k_B T}{6\pi\eta r_n} \quad \text{eq.9}$$


---

## Carbon Quantum Dots from Lemon Waste Enable Communication Among Biodevices

As a first approximation,  $D$  can be estimated using the Stokes-Einstein equation (eq.9), where  $k_B$  is the Boltzmann constant,  $T$  the temperature,  $\eta$  the fluid viscosity and  $r_n$  the radius of the nanoparticle, assuming that CQDs are spheres. A diffusion coefficient of  $1.5 \cdot 10^{-10} \text{ m}^2/\text{s}$  was estimated considering a temperature of 298.15 K, a viscosity of  $1 \text{ mPa} \cdot \text{s}$ , and an average nanoparticle radius of 1.5 nm. Experimentally, diffusion coefficient was calculated using DOSY (Diffusion Ordered Spectroscopy).

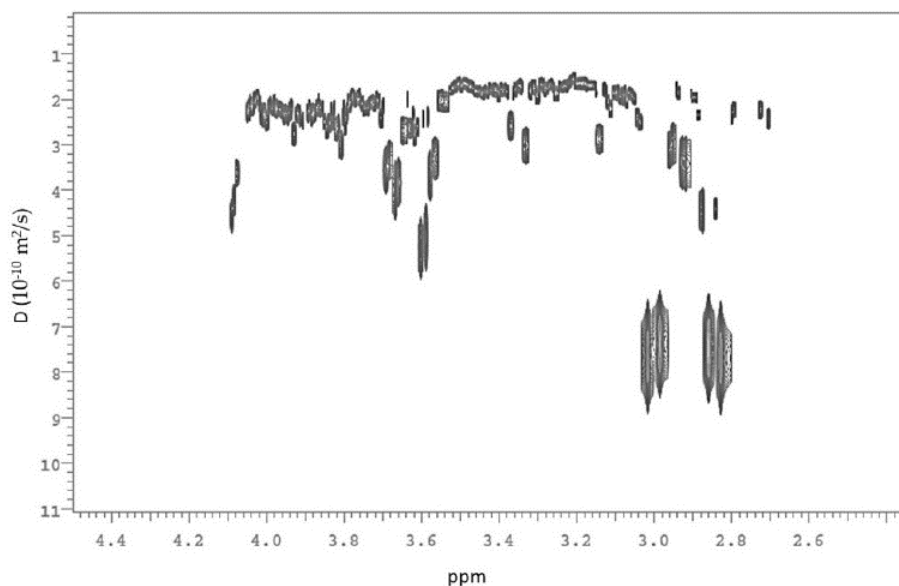


*Figure 12 - DOSY spectrum of lemon-PEI CDs dispersed in deuterium oxide (D<sub>2</sub>O). Diffusion coefficient values,  $D$ , are reported on the y-axis.*

The DOSY spectrum shown in Fig.12 was obtained using Lemon-PEI CQDs dispersed in deuterium oxide (D<sub>2</sub>O) at 27°C. This spectrum shows two groups of substances, exactly as expected:



## Carbon Quantum Dots from Lemon Waste Enable Communication Among Biodevices

one related to CQDs, whose experimental diffusion coefficient is between  $1.5$  and  $2 \cdot 10^{-10} \text{ m}^2/\text{s}$ , and a second one that can be related to the presence of molecular residues probably derived from PEI. Because of the lower hydrodynamic radius, the diffusion coefficient is experimentally higher (about  $8 \cdot 10^{-10} \text{ m}^2/\text{s}$ ). A similar diffusion coefficient was also obtained for lime-only CQDs. All this preliminary work is fundamental for the design, for the simulation, and for the experimental validation of a prototype system for MoCo in which the transfer of information takes place through microfluidic capillaries, in physiological solution, to mimic the blood vessels of the body, encoding the entire information, which must be transferred in the CQDs, obtained from the lemon juice waste.

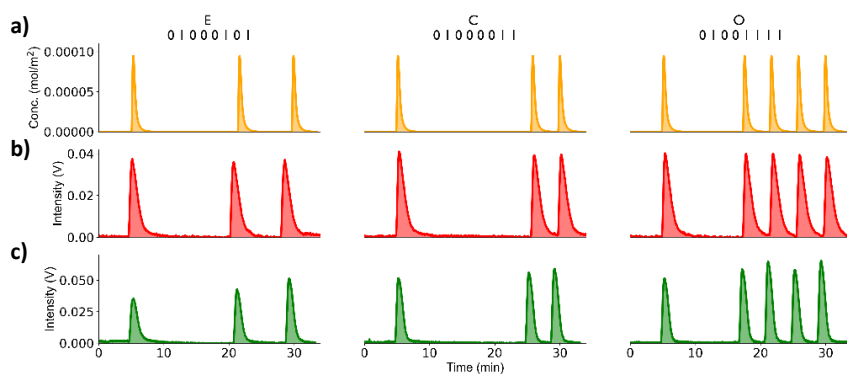


*Figure 13 - (a) Simulated message corresponding to "ECO" word in binary coding (simplified ASCII), obtained by modelling a capillary 0.40 mm in radius and 200 mm in length and setting the RMS velocity of the flow to 5.7 mm/s and the pulse of information particles to a volume of 20  $\mu\text{L}$ ; experimentally, transmission of the word "ECO" was performed by using (b) lemon-only and (c) lemon-PEI carbon dots, respectively.*

---

## Carbon Quantum Dots from Lemon Waste Enable Communication Among Biodevices

Following the classical design-simulation-experimentation procedure, Fig.13a shows the simulation of a message transfer by exploiting information particles and using the On-Off-keying (OOK) modulation method<sup>129</sup> in binary coding. The transmitted message corresponds to the word "ECO" encoded in simplified ASCII. Fig.13b-c show instead the results for the communication of the same message but obtained experimentally using the MoCo prototype previously described. Similar results were obtained with both types of CQDs, demonstrating that if the encoding is binary and the modulation is based on a simple On-Off concept, it is not necessary to obtain a high degree of refinement for the quality of the CQDs.

### 3.3 Conclusions

In both MoCo experiments a perfect transmission of the message has been obtained, according to the simulation previously carried out, both using Lemon-PEI and Lemon-Only CQDs demonstrating that simplifying the synthesis as much as possible and sacrificing part of the optical properties is not critical for this kind of experiments. Thus, easily synthesized, environmentally friendly, low-cost, biocompatible, soluble/dispersible (in aqueous fluids), and easy-to-detect CQDs prepared from lemon juice waste have the potential to be applied in emerging technological fields. MoCo is a new paradigm of bio-inspired communication where the transport of information occurs through information particles. So, a simple example of application that according to the green economy concept can open the way to potential biomedical applications of CQDs is showed here.

## Chapter 4

### Self-assembled carbon nanoparticles as messengers for artificial chemical communication

In the previous chapter, an example of how the use of CQDs synthesized in a simple, green and economical way is possible and of how it makes it possible to obtain a chemical with high added value from raw materials that are currently defined as waste has been given. This type of nanoparticle can be used successfully in MoCo, but to optimize the transmission process, it is necessary to work on the physical phenomenon of transport and, if necessary, on modulation methods, in order to obtain an acceptable baud rate. The phenomenon that most influences the baud rate is certainly ISI (intersymbol interference). The problem of overlapping signals, due to dispersion phenomena during transport, forces the distancing of information particle pulses in order to distinguish one symbol from the next.<sup>50</sup> Also in the last chapter it was explained that the dispersion of the substance during transport depends mainly on the velocity field due to the flow and the substance's typical self-diffusivity coefficient. In the case of communication channels that can be considered "microfluidic", with high aspect-ratio and low flow velocities, the contribution of transverse diffusion to the capillary predominates over longitudinal diffusion (see Fig. 11) and therefore the search for molecular messengers with a high diffusion coefficient is preferable in order to keep the substance pulse as compact as possible. If the diametrically opposite case is analyzed, i.e. a much wider communication channel (diameter in the order of millimeters) and high flow velocities (cm/second), the ideal

## Self-assembled carbon nanoparticles as messengers for artificial chemical communication

transport conditions are not met, more intense turbulent motions are triggered and longitudinal diffusion becomes predominant in signal broadening. Under these conditions, the search for the information particle is diverted towards species with a low diffusion coefficient and which can keep the signal compact even in the presence of turbulent motions. This part of the project therefore involves the synthesis, characterization and utilization of dynamic supramolecular aggregates of information nanoparticles to increase the average diffusion coefficient through the dynamic formation of clusters during transport. It has been demonstrated that the outer shell of CQDs is provided with functional groups suitable to be chemically modified in order to impart particular functionalities to the nanoparticles.<sup>86</sup> With the collaboration of a team of organic chemists, by appropriating chemical functionalization, a CQDs-based supramolecular aggregate equipped with diffusion coefficient suitable for information transfer by MoCo under the environmental conditions described above was synthesized.<sup>130</sup> Although the one-pot synthesis of CQDs<sup>84</sup> shows many interesting features as an eco-friendly and easy synthesis protocol, the covalent functionalization of the nanoparticle surface allows a greater control over their properties and therefore to tailor information particles for each context. The goal of this synthesis is to combine the simple one-pot synthesis of CQDs by carbonization of organic precursors, with covalent/non-covalent functionalization of the outer shell. Following, a supramolecular strategy can be used to obtain reversible ordered macrostructures tunable by physicochemical stimuli, which can also facilitate messenger degradation upon use. Examples regarding supramolecular aggregates of CQDs are very few, and mostly based on native

## Self-assembled carbon nanoparticles as messengers for artificial chemical communication

CQDs,<sup>116,131–134</sup> whose aggregation depends on electrostatic interactions,<sup>134</sup> host-guest recognition,<sup>135</sup> or hydrogen bonds<sup>116,131,132</sup>. The example reported here consists of CQDs covalently functionalized with triazine to obtain interacting arms via weak interactions. Naphthalene diimide (NDI) acts as a connector, bridging between the triazine arms of one nanoparticle and another to form an intermolecular network held together by hydrogen bonds. The subsequent formation of a 3D supramolecular structure of CQDs therefore occurs spontaneously and stably as soon as the NDI is added to the nanoparticles.<sup>136</sup>

### 4.1 Materials and Methods

#### 4.1.1 Self assembled Carbon Nanoparticles Synthesis

The preparation of the one-pot CQDs used for further functionalization can be divided into two main steps. In the first step, small quantities in grams of citric acid are weighed and placed in a beaker on a heating plate. The plate is heated up to a temperature of 200°C in order to activate the thermal degradation process that leads to the formation of CQDs; once an amber-coloured 'caramel' is obtained, it is cooled and then a 0.2 M NaOH solution is added until a pH of 8 - 8.5 is reached. At the end of this first step, a strongly fluorescent suspension is obtained which, however, in addition to containing our CQDs, also contains a series of by-products caused by thermal degradation. We then move on to the second step, which consists first, of a dialysis process and then, of a cryo-centrifugation process. These two steps allow us to obtain suspensions clean of the by-products formed during the synthesis and containing nanoparticles that are homogeneous

## Self-assembled carbon nanoparticles as messengers for artificial chemical communication

from a dimensional point of view. The result is a suspension that is visually much clearer than the previous one. The functionalization with triazine takes place in three steps. The entire description of the synthesis can be found in detail in ref. 130; here, only the most salient points will be described, as a more detailed focus will be made on the application in MoCo.

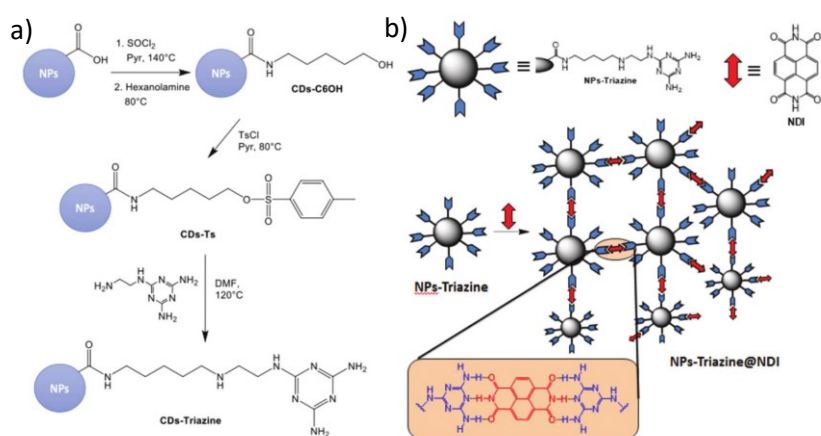


Figure 14 - (a) Synthetic pathway for the synthesis of NPs-Triazine; (b) Schematic of the supramolecular self-assembly of NPs-Triazine.

In Fig. 14a, the synthetic steps are shown schematically, which consist first of activating the carboxyl group by treating with pyridine in  $\text{SOCl}_2$  at  $140^\circ\text{C}$  overnight to convert the carboxyl group into acyl chloride. The addition of hexanolamine for condensation takes place after this activation process (step 1). The alcoholic group at the end of the chain is subsequently activated by treating the functionalized nanoparticles with tosyl chloride at  $80^\circ\text{C}$  overnight, thus inserting the tosyl group (step 2). The carbon in A of the tosyl group turns out to be reactive with the primary amine

## Self-assembled carbon nanoparticles as messengers for artificial chemical communication

of the triazine ethylenamine, a reaction conducted in DMF at 120°C for 48 hours (step 3). The supramolecular assembly is obtained by adding naphthalene diimide, which acts as a bridge to connect two triazine-functionalized nanoparticles (see fig 14b). Both native CQDs, triazine-functionalized nanoparticles (CQDs-Triazine) and supramolecular complexes with NDI (CQDs-Triazine@NDI) will be used for MoCo experiments.

### 4.1.2 Characterization methods

All intermediates obtained during the synthesis steps were characterized by <sup>1</sup>H NMR spectroscopy (Varian Unity inova 500MH), including the formation of the supramolecular complex. The diffusion coefficient was obtained by the DOSY technique with the aid of the NMR spectrophotometer. Optical characterization of the CQDs was carried out by UV-vis absorption spectroscopy (VALCO) and fluorescence spectroscopy (Agilent), obtaining fluorescence maps for different excitation wavelengths. Morphological characterization was carried out by Atomic Force Microscopy (Bruker).

### 4.1.3 Molecular Communication Prototype

The experimental molecular communication platform used is similar to the one described in chapter 3 and was used to verify the feasibility of our proposal in a phantom working environment. Summarizing the parts of which it is composed, described schematically in fig.21a, in a 20ul loop injector as transmitter,

## Self-assembled carbon nanoparticles as messengers for artificial chemical communication

we find a cylindrical tube simulating the transport channel, and a fluorescence flow detector as receiver and a peristaltic pump to ensure a constant flow of the transport solution, which acts as a liquid carrier. As we tried to simulate conditions far removed from microfluidic and laminar conditions, the capillary used has a diameter of 2mm, and the flow velocities provided by the peristaltic pump are of the order of cm/s. The analogue-digital converter for reading the voltage coming out of the fluorometer consists of an Xtralien X100 developer board and the data acquisition system is a PC assisted by scripts developed in Python.

### 4.2 Results And discussion

#### 4.2.1 CQDs characterization

An extensive analysis by NMR-DOSY technique was carried out to elucidate the effect of supramolecular assembly of CQDs-triazine in the presence of NDI.<sup>137-142</sup> Figure 15 shows the results of a titration of a nanoparticle solution with NDI. It is clear that the diffusion coefficient value saturates at  $1.42 \times 10^{-10}$  adding 5% of NDI, when in the absence of NDI it measures  $5.24 \times 10^{-10}$ . Adding only 5x10<sup>-4</sup>% of NDI, a value of  $1.80 \times 10^{-10}$  of D is obtained, in fact only a very small amount of NDI is requested to form the supramolecular aggregate.

---

$$\frac{V_a}{V_{a'}} = \left( \frac{D_{a'}}{D_a} \right)^{\frac{3}{2}} \quad \text{eq. 10}$$

---



## Self-assembled carbon nanoparticles as messengers for artificial chemical communication

Comparing the values of diffusion coefficient and taking Einstein's diffusion equation<sup>143</sup> into account, eq. 10 is derived. Where  $V_a$  and  $V_{a'}$  are the molar volumes of the particles and supramolecular structure if they are considered as spheres,  $D_a$  and  $D_{a'}$  are the respectively diffusion coefficient calculated by NMR-DOSY technique. Since the diffusion coefficient of the reticulated NPs decreases up to 5 times, we can estimate that the volume of supramolecular aggregation is more than one order of magnitude higher than that of the as-prepared NPs. This implies that after reticulation, a supramolecular aggregate composed of more than 10 nanoparticles is formed.

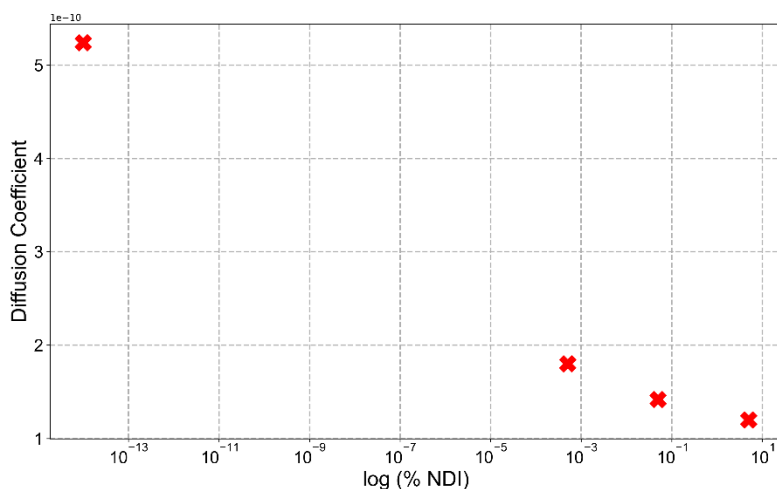
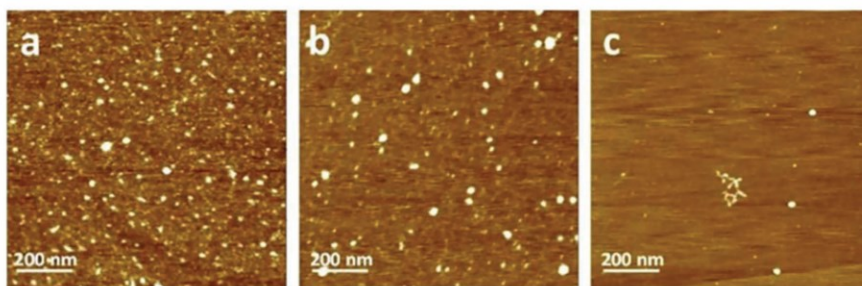


Figure 15 - DOSY titration of NPs-Triazine with NDI.

Once it was found that the supramolecular aggregate allowed the diffusion coefficient to be modulated and verified experimentally using the DOSY technique, a morphological study of these systems was carried out using Atomic Force Microscope. Samples were

## Self-assembled carbon nanoparticles as messengers for artificial chemical communication

prepared by drop casting on a flat silicon substrate from extremely dilute solutions to reduce flocculation effects and analyzed in tapping mode. Figure 16 shows the AFM images obtained from the sample containing native CQDs, CQDs-triazines and CQDs-triazines@NDI.



*Figure 16 - AFM images of the (a) native NPs, (b) NPs-Triazine, and (c) NPs-Triazine@NDI. The height scale is 2 nm for all images.*

---

The former (Fig. 16a) are characterized by an average diameter of 20nm and a height of about 2nm, so they look like a disk. Considering that the average height of a graphene layer is about 0.4nm, the native CQDs consist of a stack of about 5 layers. Fig. 16b shows the same type of analysis on the CQDs-triazines, where no significant differences are found with the non-functionalized ones, as evidence of the effective dispersion of the functionalized nanoparticles. By adding NDI, the formation of the supramolecular aggregate is instead clear (Fig. 16c). The study of optical properties is also essential to clarify the behavior of nanoparticles once they reach the optical receiver in a MoCo experiment and to program it accordingly. The UV-vis absorption spectrum of the CQDs (fig. 17) is characterized by two absorption bands at 220nm and 350nm

## Self-assembled carbon nanoparticles as messengers for artificial chemical communication

indicating  $\pi$ - $\pi^*$  and  $n$ - $\pi^*$  transitions, respectively. The small band at around 450nm is related to the surface functional groups. Since the optical receiver used in the molecular communication prototype consists of a flow fluorometer, it was necessary to characterize the fluorescence characteristics in more detail.

---

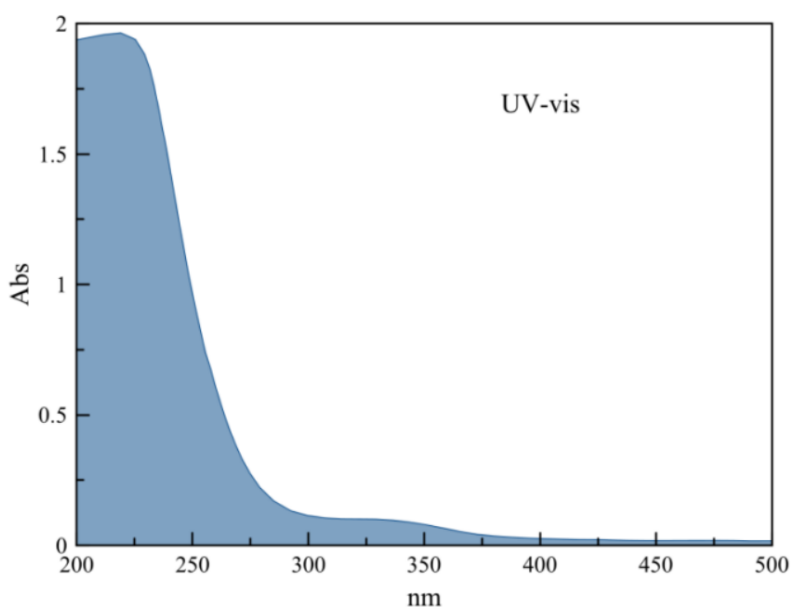


*Figure 17 - UV-vis spectrum of CDs.*

---

It is known that the fluorescence spectrum depends on the excitation wavelength of the light used to trigger the phenomenon.<sup>144</sup>

## Self-assembled carbon nanoparticles as messengers for artificial chemical communication

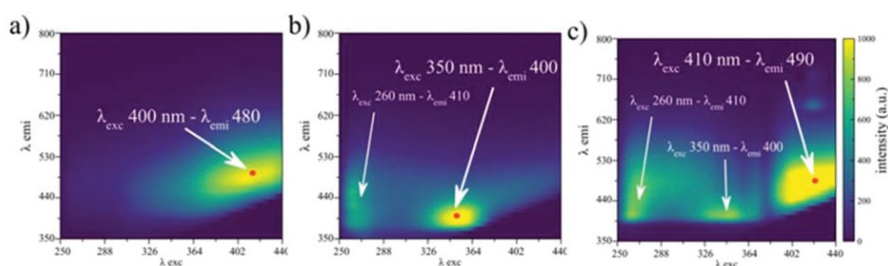


Figure 18 - Fluorescence maps of (a) native NPs, (b) NPs-Triazine, and (c) NPs-Triazine@NDI.

Figure 18 shows 2D fluorescence maps to get a clearer picture of where the different species used emit. The native CQDs show an emission maximum at  $\lambda_{emi} = 480$  nm when excited at  $\lambda_{exc} = 400$  nm (Fig. 18a). After cross-linking, the emission maximum of CQDs-Triazine@NDI (Fig. 18c) is slightly shifted by 10 nm ( $\lambda_{emi} = 490$  nm with  $\lambda_{exc} = 410$  nm). For the sake of completeness, fluorescence maps for CQDs-triazines are also shown, showing two fluorescence spots, one less intense and one more intense at  $\lambda_{emi} = 260$  nm with  $\lambda_{exc} = 410$  nm and  $\lambda_{emi} = 350$  nm with  $\lambda_{exc} = 410$  nm, respectively. Both native CQDs and those cross-linked by supramolecular interactions are subject to concentration self-quenching, as shown in Fig. 19a; supramolecular assembly has a strong influence on this phenomenon. In particular, the concentration at which the self-quenching effect starts to be observed (maximum level of fluorescence shown in Fig. 19a) is higher in the case of CQDs-Triazine@NDI than in the case of CQDs and the slope in the Stern-Volmer plot (fig. 19b) is 4 times lower once CQDs are self-assembled.

## Self-assembled carbon nanoparticles as messengers for artificial chemical communication

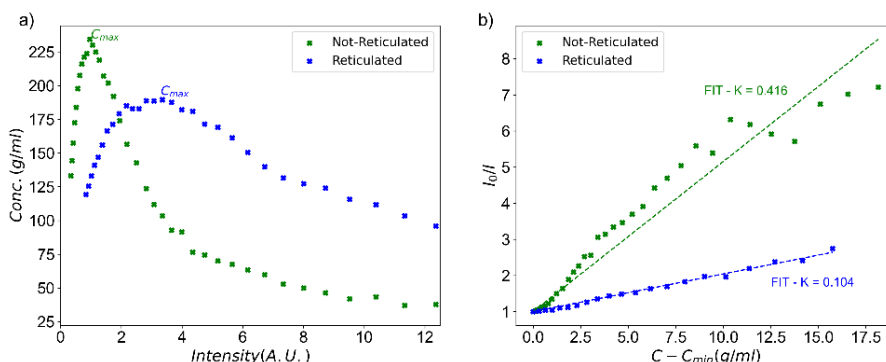


Figure 19 - (a) Intensity of fluorescence peak as a function of the concentration; not reticulated NPs (blue)  $\lambda_{emi} = 480$  nm with  $\lambda_{exc} = 400$  nm and reticulated NPs-Triazine@NDI (green)  $\lambda_{emi} = 490$  nm with  $\lambda_{exc} = 410$  nm. (b) Stern–Volmer plot of unreticulated NPs (blue) and NPs-Triazine@NDI (green).

Interestingly, the Stern-Volmer slope and the diffusion constant decrease after the cross-linking and are of the same magnitude. This confirms that the mobility of self-assembled CQDs is significantly reduced as the probability of self-quenching is related to the probability of interparticle collision, which, due to the reduction in the diffusion coefficient, is significantly hindered. Results on the characterization of supramolecular aggregates of CQDs show that they could potentially optimize the Inter-symbols Interferences (ISI) phenomenon under non-laminar flow conditions. Reiterating the fact that ISI is one of the major problems limiting the baud rate in MoCo, it is necessary to be able to tighten as much as possible the time window in which a symbol is contained. Before experimentally verifying the efficacy of self-assembled CQDs in increasing the symbol baud rate, numerical simulations were performed in order to observe the effects of the

## Self-assembled carbon nanoparticles as messengers for artificial chemical communication

diffusion coefficient on the width and overlap of two successive symbols. Communication velocity depends on the effects governing molecular propagation in the communication channel. The simplest model is usually the differential equation (eq. 11) of advection-diffusion.

---

$$\frac{\partial C}{\partial t} = \nabla \cdot (D \nabla C) - \nabla \cdot (vC) \quad \text{eq. 11}$$

---

$C$  is the concentration of the pulse of information particles released into the communication channel,  $t$  the time,  $D$  the self-diffusivity coefficient of the substance and  $v$  the flow velocity of the transport fluid. Dispersion effects during transport are therefore strongly correlated by the diffusion coefficient and velocity of the substance. Of course, the distance between transmitter and receiver also influences the broadening of a signal since diffusive and dispersive effects act for a longer time.

### 4.2.3 Molecular Communication Approach

By numerically solving eq. Y by means of a Python simulation using the FiPy library,<sup>145</sup> the effects that velocity and diffusion coefficient have on the ISI were obtained. Fig. 20 shows the signal pattern at the simulated detector, obtained from the release of two consecutive 1-symbol pulses, spaced 50s apart, as a function of time at various values of  $D$  coefficient and  $v_{\text{mean}}$  and setting a transmitter-receiver distance of 100cm and a capillary diameter of 2mm. Under these conditions, calculations show that the larger

## Self-assembled carbon nanoparticles as messengers for artificial chemical communication

the velocity drifts, the better the peak separation and, in turn, the higher the baud rate. In addition, a smaller diffusion coefficient allows more space to travel before looming overlap between consecutive pulses, causing the signal to be transmitted incorrectly.

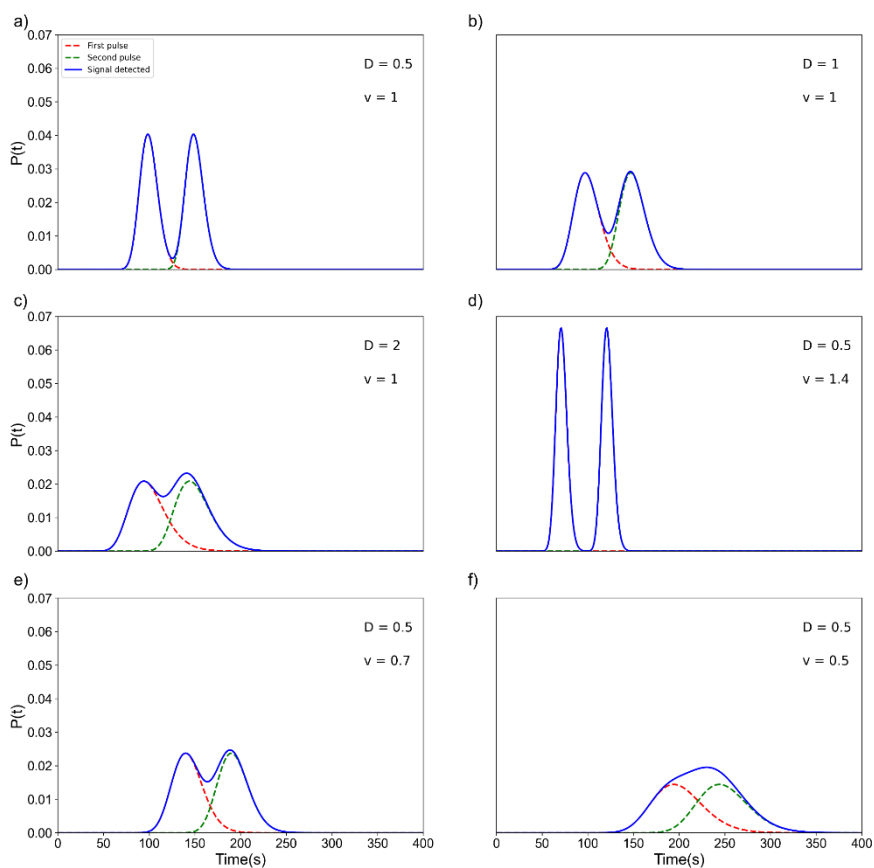


Figure 20 - Probability distribution function of the detection time for different sets of velocity and diffusion parameters related to the release of two consecutive 1-bit pulses.

## Self-assembled carbon nanoparticles as messengers for artificial chemical communication

Assuming that MoCo is applied by exploiting already existing communication channels, the flow rate is often not adjustable, so one can only work on the parameter  $D$  to optimize the baud rate. Therefore, the strategy adopted to reduce the diffusion coefficient of CQDs could be efficient to optimize the message transmission process in natural environments. Therefore, the molecular communication prototype described above was used to transfer a symbol through a capillary of the same size as the simulated one. Fig. 21b shows the experimental comparison between the transmission of the symbol signal by releasing a pulse of CQDs-triazine and CQDs-triazine@NDI. The results show that the signal width related to the release of a short pulse of information particles is narrower for self-assembled CQDs. The results therefore confirm the predictions of the theoretical calculations, namely that the use of supramolecular assemblies of CQDs with a low diffusion coefficient allows a sharper detector response. Fig. 21c shows the calculated probability distribution function of the detection time by fitting five values of  $D$  into the advection-diffusion equation (eq. 9). Both the shape and the amplitude turn out to be in accordance with what was obtained experimentally. This is a very promising result and paves the way for the development of a working artificial chemical communication system. Indeed, as pointed out in the previous section, the lower the  $D$ , the better the efficiency of artificial molecular communication for systems in which carrier flow is turbulent and the capillary is of non-micrometer size, since sharper peaks reduce intersymbol interference, allowing less temporal spacing between symbols. Furthermore, the relative values of  $D$  are congruent with the experiments, indicating that a lowering of the diffusion coefficient by about 4-5 times



## Self-assembled carbon nanoparticles as messengers for artificial chemical communication

(associated with crosslinking) corresponds to the decrease in the self-diffusivity coefficient detected using DOSY-NMR, although the width of the experimentally measured peaks cannot be determined by nanoparticle diffusion alone, but also depends on all the fluid-dynamic mixing phenomena that occur during transport.

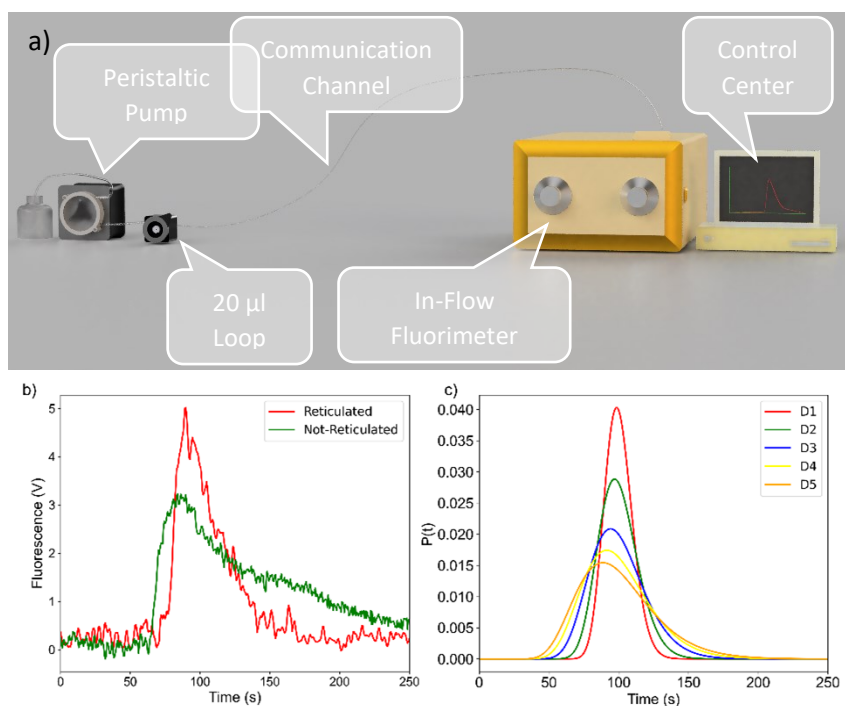


Figure 21 - (a) Schematic of artificial chemical communication prototype. (b) Received signal of a 1-bit pulse transmitted using non-reticulated NPs (green line) and reticulated NPs-Triazine@NDI (red line) as molecular messengers. Travel distance of 1.0 m, transport velocity of 1 cm s<sup>-1</sup>, NPs concentration of 0.85 g ml<sup>-1</sup>, loop volume of 20  $\mu\text{l}$ . (c) Probability distribution function of the detection time calculated by eqn (9) with several values of diffusion parameter  $D$  and using  $v = 1 \text{ cm s}^{-1}$ ,  $d = 1 \text{ m}$ .

## 4.4 Conclusions

Our results show that, under non-microfluidic experimental conditions, reducing the diffusion coefficient is a priority for reducing signal broadening. The formation of supramolecular assemblies is a successful strategy to achieve the reduction of the diffusion coefficient but still using fluorescent information particles with the peculiar optical properties described in the previous chapters. To achieve this reduction, carbon-based fluorescent nanoparticles were synthesized and their diffusion properties were modulated using cross-linking species where appropriate. The synthesis involved triazine functionalization of CQDs followed by cross-linking with NDI. Cross-linking was observed via NMR, DOSY and emission spectroscopy and was found to be achievable even with a very small amount of NDI and was confirmed by AFM. Supramolecular cross-linked CQDs retained the fluorescence properties but showed a decreased diffusivity coefficient by a factor of five. As a result, sharper and more intense molecular bits were transferred over 100cm long fluid paths with flow rates around 1cm per second. With this study, we want to demonstrate that the engineering of information particles produces excellent results in the development of an artificial molecular communication platform and opens the way to new methods of signal modulation. This would allow to claim that limits are dictated only by the imagination.

## Chapter 5

### Reactive nanomessengers for artificial chemical communication

The development of artificial molecular communication, however, needs to be taken a step further, with a view to applying it to the exchange of information for bio-implanted systems in living beings. The examples seen so far have focused on the development of information particles and little on the actual communication process. However, chemical communication is efficient in nature because highly specific messengers and receptors have been developed over millions of years of evolution in which each paired receptor/messenger is able to transfer information. Thus, the plethora of information required for the proper functioning of a living organism is stored and transferred by thousands of information particles. It is obviously unconceivable to use such many host-guest interactions for artificial molecular communication, as too many different sensors and information particles would be needed. The current aim of artificial molecular communication is to simplify and make the communication process robust and reliable, and to make it possible to use the digital transmission protocols already in use because they have been developed for some time. The digital logic currently used is based on a binary system, and as described in the introductory part of this dissertation, modulation methods for MoCo, based on binary logic such as CSK or OOK, have already been introduced.<sup>146</sup> In both cases, these are methods that exploit the number of particles to distinguish symbols from each other, rather than the identity of the molecule itself. OOK is also

simplified as it is based on a single concentration threshold. Any communication platform is subject to noise, which occurs during the transmission process or due to encoding and decoding noise by the transmitter and receiver.<sup>52</sup> Artificial molecular communication is also highly susceptible to noise, although of a different nature, so it is necessary to act either on the sources of noise when possible, or directly on the modulation method to make it error-resistant. To date, it has been seen that the bulk of the chemical noise that a communication channel introduces into the system derives mainly from the hydrodynamic dispersion effects of the messenger during transport from the transmitter to the receiver. Firstly, there is the reduction in signal strength that results from dilution induced by hydrodynamic mixing, for which *Tuccitto et al.* in ref. <sup>147</sup> proposed to exploit the concentration quenching effects of CQDs to optimize long range transmission without loss in signal strength. Secondly, the problem of synchronization between transmitter and receiver is critical. The use of fixed time slots for reading the signal requires perfect synchronization and any mismatch between the read clock and the write clock will cause errors that will propagate to the subsequent steps. From a transport point of view, the phase mismatch is caused by an unpredicted dispersion of the information particle. For example, if the transmission is subject to stochastic random walk phenomena (for Diffusion-only transport) or if the flow velocity within the communication channel is variable and not perfectly predictable (as in transport in biological flows) or when the distance between receiver and transmitter is not constant (as in mobile communication), phase mismatch is observed between transmitter and receiver. It has been shown in the previous chapters that molecular messenger engineering

opens multiple possibilities for the development and optimization of data transfer using information particles. For example, by adjusting the diffusion coefficient, depending on the fluid-dynamic properties, it is possible to minimize intersymbol interference and thus increase the baud rate of a communication channel. The proposed method for modulating the diffusion coefficient required the use of carbon nanoparticles, synthesized using a *green* technique,<sup>84</sup> and a surface engineering process.<sup>130</sup> Here we propose an artificial chemical communication system based on a new modulation technique, called Reaction Shift Keying modulation (RSK), which exploits the optical properties of CQDs synthesized by green techniques and without surface functionalization, to solve some of the previously mentioned problems. A prototypal artificial molecular communication system has been developed, from the design and simulation of the platform to the synthesis of the suitable information particles applied in an operational prototype system.

## 5.1 Materials and methods

Ammonium acetate, citric acid, copper chloride and sodium hydroxide were purchased from Aldrich and used as received. Solutions were prepared in water Milli-Q (18.2 Mohm). Carbon nanoparticles were synthesized by hydrothermal decomposition. 2.5 g citric acid and 2.5 g ammonium acetate were mixed and placed on a hot plate at 205°C for 15 minutes. When crystals turned from white to dark orange, the solution was cooled to room temperature, and 50 ml of 0.2 M sodium hydroxide solution was added, stirring strongly until completely dissolved. The

solution was purified using a dialysis tube (11 000 Da cut-off) in 1 litre of water for 24 hours, changing the water every hour for 5 times and then left until the last change. UV-vis analysis was performed using a Jasco V-650 and fluorescence analysis was performed using a Varian Cary Eclipse fluorescence spectrophotometer. Atomic force microscopy (AFM) images were obtained using a Nanoscope IIIa multimode apparatus from Digital Instruments (Santa Barbara, CA) used in air tapping mode on a mica substrate. Budget Sensors' Tap 300G silicon probes were used, with a nominal resonant frequency of 300 kHz and a nominal constant force of 40 N/m. The solution of CQDs has a concentration of 1 mg/ml, while the concentration of the quencher for RSK modulation is 2 mg/ml. The prototype molecular communication platform was assembled in-house (Fig.22). Flow was provided by a peristaltic pump (ISMATECH). A 6-port valve (Valco-Vici) with a 20 ml loop was used for the controlled injection of the information particles. A PEEK tee with a silicone septum was used to inject the copper chloride solution (2 mg/ml). A 1m Teflon capillary was used as a communication channel. An RF-535 flow fluorometer with a S1989 xenon lamp (Shimadzu) was used as a signal receiver. An Xtralien X-100 (Ossila, UK) was used as an analogue-to-digital converter and a PC was used for prototype management and data collection. A Python-based GUI was developed for data acquisition and processing. Numerical simulations for the solution of the diffusion-transport-reaction model of information particles were performed using a Python-based script developed ad Hoc. Python 2.7 and the FiPy library, an object-oriented partial differential equation solver based on a standard finite-volume approach, were used.<sup>145</sup>

**Reactive nanomessengers  
for artificial chemical communication**

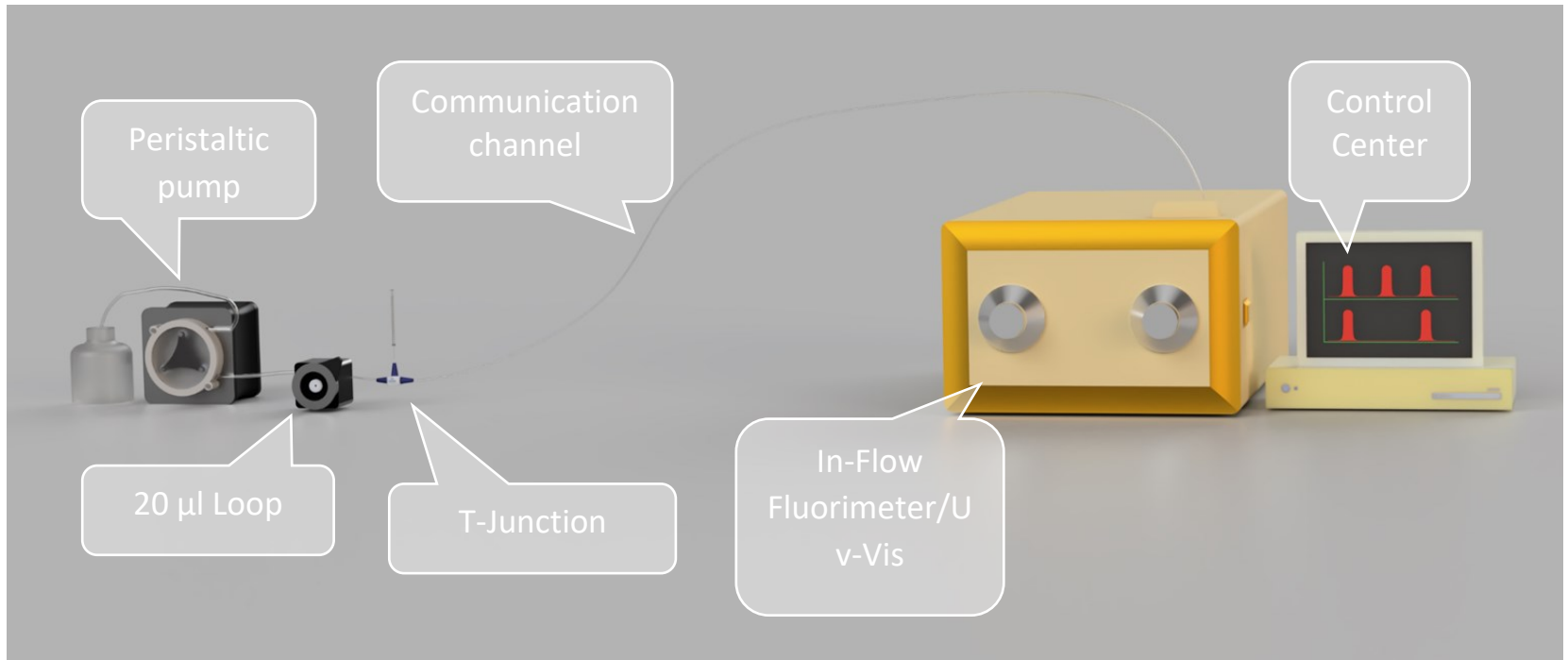


*Figure 22 - 3D project of RSK modulation prototype. Notice the presence of T-junction to inject the modulant.*

## 5.2 Result and Discussions

### 5.2.1 Theoretical and simulative approach

As already addressed in the previous chapters, the workflow to be followed requires first the development of the theoretical foundations on which to subsequently build the experimental approach. The first phase basically requires the prediction of the dispersion phenomena of the information particles during the transport from transmitter to receiver. As already widely discussed, the use of the advection-diffusion equation turns out to be reliable as a prediction model for these simple systems. The novelty here lies in the addition of the concept of chemical reaction within eq. 11.

---

$$\frac{\partial C}{\partial t} = \nabla \cdot (D\nabla C) - \nabla \cdot (vC) + R \quad \text{eq. 12}$$

---

Eq. 12 shows, in comparison to the advection-diffusion equation, the factor  $R$ , i.e. that which determines the reduction or increase of concentration due to a chemical reaction, dependent on the kinetic constant of the reaction and of course on time. The actual addition of this factor has already been seen in ref 120 in which the formation of the molecular messenger during transport makes it possible to keep the intensity (hence the signal strength) constant as the distance between transmitter and receiver varies. Here, it is proposed again for the application of a peculiar modulation method that has been called RSK. The computational analysis was carried out, in a first step, considering the absence of chemical reaction to study the dispersion effects during transport,



varying distance between transmitter and receiver and flow velocity.

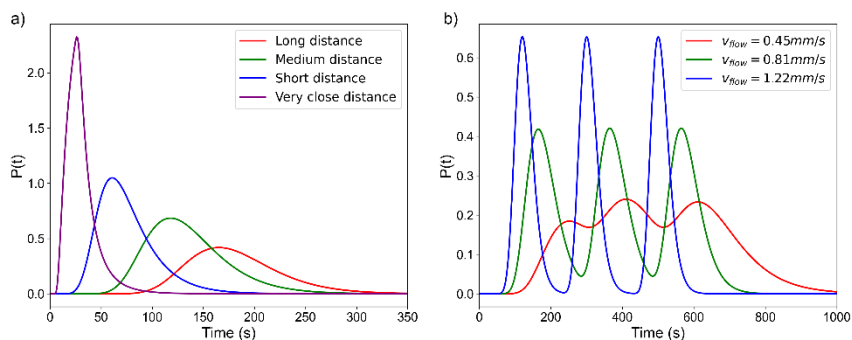


Figure 23 - (a) Detected simulated signal of bit-1 by a receiver placed at various distances; (b) detected simulated signal of sequence 1-0-1-0-1 transported by a flux of various velocities. Time unit is reported in simulation steps.

Fig. 23a shows the evolution of the information particles pulse, corresponding to a 1-bit pulse as a function of time, at various transmitter-receiver distances. As expected, hydrodynamic dispersion causes inexorable dilution, concentration pulse broadening and thus ISI phenomena, a consequence observed at the receiver since the signal intensity ( $I$ ) relative to the information particle is related to its  $C_{det}$  concentration. Using spectroscopic detectors, the intensity is usually linearly related to the concentration (for appropriately diluted solutions) according to Lambert Beer's law. In the case of a fluorescent information particle, the intensity signal at the receiver is proportional to two factors: (i) the fraction of incident light absorbed, which causes

excitation of the fluorophore, and (ii) the fluorescence efficiency, thus:

---

$$I(C_{det}) = kA(C_{det})E(C_{det}) \quad \text{eq. 13}$$

---

where  $k$  is a proportionality constant dependent on instrumental parameters. The absorbance  $A(C_{det})$  increases linearly with the concentration at the  $C_{det}$  detector, while the fluorescence efficiency  $E(C_{det})$  first rises and then falls with self-quenching.<sup>148</sup> In any case, the persistent dilution effect of pulse broadening makes it very difficult for the receiver to detect the messenger when the signal strength reaches the lower detection limit of the detector. If it is solved by increasing the signal strength appropriately (by increasing the starting concentration, by increasing the receiver sensitivity or by changing the detection method), the worst effect of OOK modulation is the variability of the time-slot width of bit-1 with respect to bit-0. Since bit-0 is modulated by the *silent* state of the transmitter, i.e. no messenger release, then only the bit-1 signal will be affected by hydrodynamic scattering and the resulting spread of signal width. As proof of this, Fig. 23b shows the result of simulating the transfer of the 1-0-1-0-1 sequence with OOK modulation by solving equation (XY) when three different flow rates are imposed. It can be seen immediately that the time slot of bit 1 increases in width with respect to the time slot of bit 0, until it becomes essentially undetectable. The simulations were carried out by modelling a tube with a diameter and length similar to those of a human blood vessel and three flow velocities simulating normal state, sleep and vigorous activity respectively. The simulations show that both the transmitter-

receiver distance and the transport speed, or, in other words, the time required by the messenger to reach the receiver, strongly influence the signal width of bit 1.

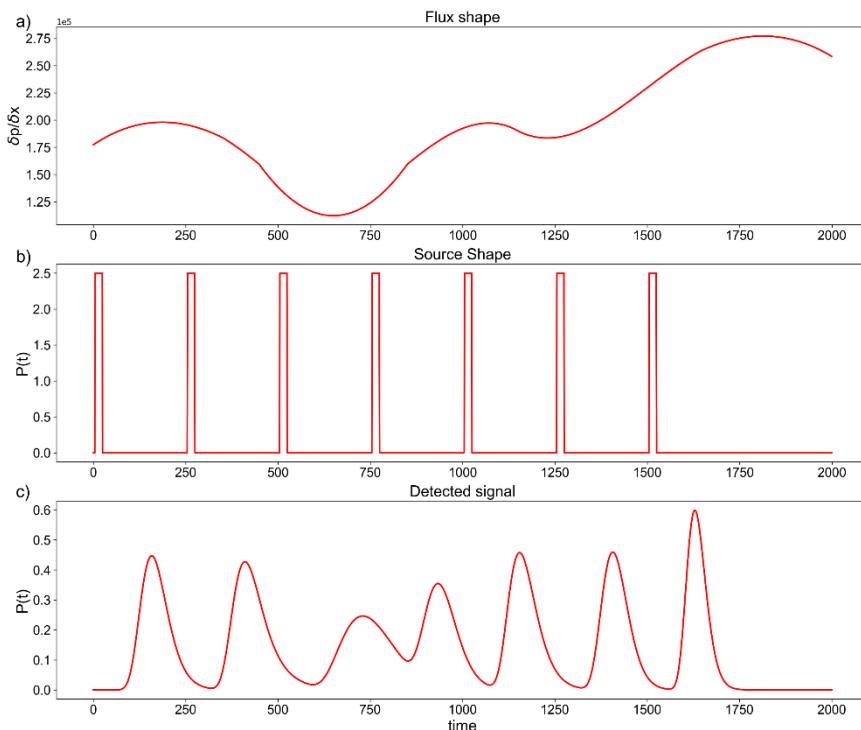


Figure 24 - (a) Trend of variable flow pressure during the simulation of communication procedure; (b) sequence of bit-1 released by the transmitter; (c) sequence of bit-1 detected by the receiver. Time unit is reported in simulation steps.

It is not sufficient to focus exclusively on fixed flow velocities as this is hardly applicable in a real case. A further simulation, shown in fig. 24, shows the dispersive effect that transport causes if the flow velocity varies over time during transmission. As done

previously, flow velocity variations corresponding, in terms of  $\delta P/\delta x$ , to a normal circulatory situation, one at rest and one under stress were simulated, the layout of which is shown in Fig. 24a. Given these conditions, the decoding process becomes very complex because even if the bit-1 pulse is released with a fixed and known time, the time-slot between two consecutive signals at the receiver changes according to the variation of the flow velocity, generating an asynchrony that does not allow to predict the time-slot of the next bit. In simpler words, the time-slot becomes a function of the flow velocity and therefore varies over time. Knowing the function that describes the variation of the velocity with time, then the width of the time-slot is also known and the receiver can be adjusted accordingly. However, in the real application, this is not likely to happen and the transmitter and receiver will remain out of synchronization. Furthermore, there is not only the time-slot to consider but also the signal distortion caused by the varying fluid-dynamic conditions. Here, we want to propose the possibility of overcoming this problem by exploiting the most important asset of chemical science, the knowledge of the reactivity of information particles, hence the idea of including  $R$  in equation (2). Building on the results obtained in last experiments, a new application is presented here: a modulation procedure that we call Reaction Shift Keying (RSK) following the concept proposed by Chou et al. where transmission symbols are generated by chemical reactions.<sup>149,150</sup> This new modulation scheme requires basic conditions to be set in order to obtain the logic schematically shown in Fig. 25. It is assumed that the information particle reacts at the transmitter with a substance, the modulant, according to a known kinetic law that we assume to be of the first order for simplicity of description. Therefore, the

chemically modified information particle will be transported to the receiver by the carrier flow. It is also assumed that the chemical modification (modulated reaction) affects some optical properties of the information particle. Given the known properties of CQDs, the modulant does not change the UV-vis absorption spectrum of the messenger, but quenches its fluorescence according to the Stern-Volmer law (i.e. quenching effect).

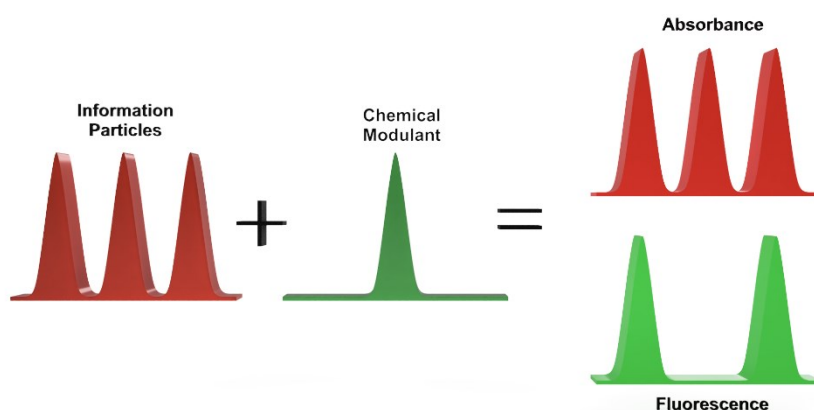


Figure 25 - Representation of reaction shift keying modulation.

RSK modulation presupposes the use of two symbols, produced at the receiver, encoded with the binary values "0" and "1" respectively. The formation of one symbol with respect to the other takes place using the same information particle (i.e. CQDs), but modulation by means of a chemical reaction occurs by using the modulant (i.e. quenching modulation), which allows a correct encoding of the information. The fundamental difference with the simpler OOK modulation is that the encoding of the binary character "0" is not achieved by the silent transmitter (no release)

but by the emission of an information particle which reaches the receiver after the chemical modification. The logic of the RSK modulation method is described below: the presence of a signal is only detected by means of UV-vis absorbance, which acts as a trigger for the start of the reading. Decoding, however, is charged to the fluorescence intensity reading. Therefore, if no absorbance signal is detected at the receiver, it is not yet time to decode any signal and the receiver remains in stand-by mode. As soon as absorbance is detected, the receiver decodes the value "1", but only if both absorbance and fluorescence signals exceed a set threshold. It decodes the value "0" if absorbance exceeds the threshold while fluorescence remains below. The absorbance intensity (ABS) is assumed to be described by the Lambert-Beer equation.

---

$$ABS(C_{det}) = \varepsilon C_{det} d \quad \text{eq. 14}$$

---

where  $\varepsilon$  is the molar extinction coefficient,  $d$  is the optical path and  $C_{det}$  is the concentration at the detector. As described in Eq. 11, the fluorescence emission signal intensity is proportional to two factors: (i) the fraction of incident light absorbed, which causes excitation of the fluorophore, and (ii) the fluorescence efficiency. In the case of irradiation with monochromatic light, the quenching of the fluorescence is assumed to be described by the Stern-Volmer relation, we obtain:

---

$$Fluo(C_{det}) \propto (1 - e^{-\varepsilon C_{det} d}) \cdot \frac{1}{1 - K_{SV} \cdot \tau \cdot C_{quencher}} \quad \text{eq. 15}$$

---

where  $K_{SV}$  is the Stern–Volmer constant,  $\tau$  is the lifetime of the emissive excited state of CQDs and  $C_{quencher}$  is the concentration of the quencher. Assuming also a single threshold for absorbance ( $\xi_{ABS}$ ) and one for fluorescence ( $\xi_{FLUO}$ ), the receiver decoding scheme must be:

---


$$s(t) = \begin{cases} \text{if } ABS(t) < \xi_{ABS} \text{ then } s(t) = 0 \text{ NO – SIGNAL} \\ \text{if } ABS(t) > \xi_{ABS} \text{ and } Fluo(t) < \xi_{FLUO} \text{ THEN bit} = 0 \\ \text{if } ABS(t) > \xi_{ABS} \text{ and } Fluo(t) > \xi_{FLUO} \text{ THEN bit} = 1 \end{cases} \quad \text{eq.16}$$


---

The symbol time-slot starts at  $t_1$  when the signal absorbance exceeds the threshold, i.e. when  $ABS(t_1) > \xi_{ABS}$  is satisfied, and ends at  $t_2$  when  $ABS(t_2) < \xi_{ABS}$  with  $t_2 > t_1$  as illustrated by the red lines in Fig. 26c,d. The decoding conditions of the symbol, depend on whether or not a threshold described by  $\xi_{FLUO}$  is exceeded. Using the new RSK modulation, simulation results show that it is easy to decode the message at the receiver even under drastic changes in the transfer rate and signal spread of the message, as shown in Fig. 26c,d.

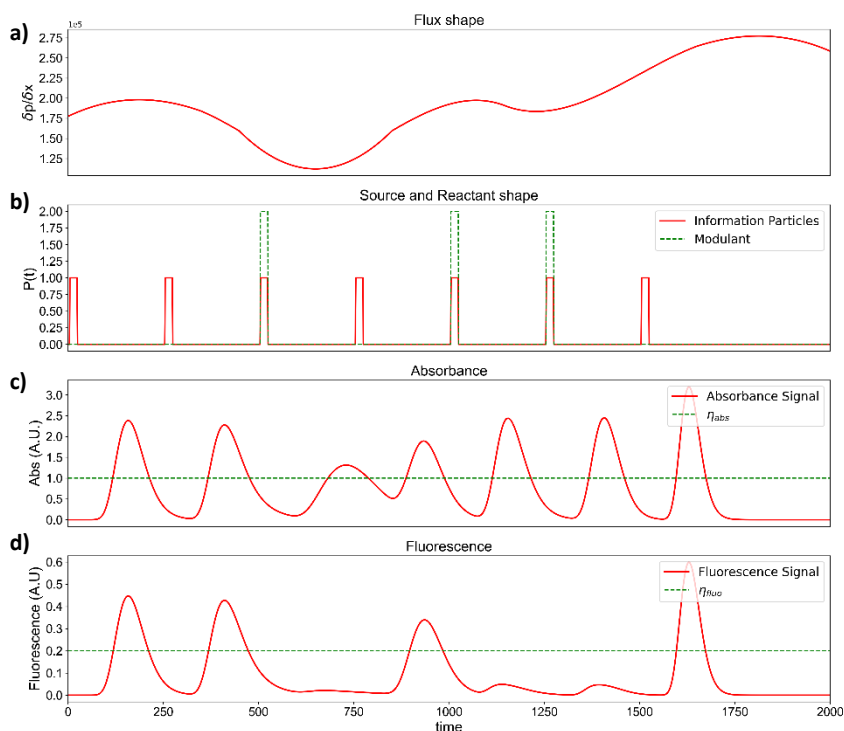


Figure 26 - (a) Trend of variable flow pressure during the simulation of communication procedure; (b) sequence of bit-1 released by the transmitter (blue line: messenger, red line: reactant); (c) sequence of bit-1 detected by the absorbance detector placed at the receiver; (d) sequence of bit-1 detected by the fluorescence detector placed at the receiver. The decoded binary sequence is reported at the bottom.

## 5.2.2 Nanomessengers characterization

In this context, the difficulty in applying the RSK modulation model stems from the search for an information particle that is both sensitive to a modulant and efficient, cheap and green. The literature proposes chemical messengers depending on the



propagation medium and the sensing system: molecules, proteins, aggregations and nanoparticles. However, there is not much experimental data and for the most part, it concerns the use of fluorescent carbon nanoparticles, showing that they can be excellent and versatile chemical messengers.<sup>130,147,151</sup> They can be encoded by means of OOK modulation and the resulting concentration pulses of fluorescent nanoparticles have been shown to be self-quenching. For the reasons described in Chapter 2, they represent a perfect candidate for testing the reliability of RSK modulation for MoCo in vivo. Several authors have shown that carbon nanoparticles exhibit strong quenching when exposed to very low amounts of Cu(II) ions up to a concentration of 5 nM.<sup>152</sup> In the blood, Cu(II) is present but not free because it is mainly transported by proteins, such as albumin, which is an important copper transporter in human blood.<sup>153,154</sup> Fig. 27a-b show the characterization by atomic force microscopy of the carbon nanoparticles synthesized using the method described in the previous paragraph. They show that the carbon nanoparticles have an average diameter of around 3 nm and appear approximately as discs. The UV-vis absorption spectra of nitrogen-doped carbon nanoparticles, CuCl<sub>2</sub> solution and a mixture of carbon nanoparticles and Cu(II) are shown in Fig. 27c. The nanoparticles show an intense absorption band in the UV region due to the electronic transitions of the sp<sup>2</sup>-rich aromatic carbon inner core and a weak band at about 335 nm related to the surface defects. As demonstrated in Fig. 27c, the presence of Cu(II) does not influence the UV-vis spectrum of the carbon nanoparticles except by slightly raising the baseline.

## Reactive nanomessengers for artificial chemical communication

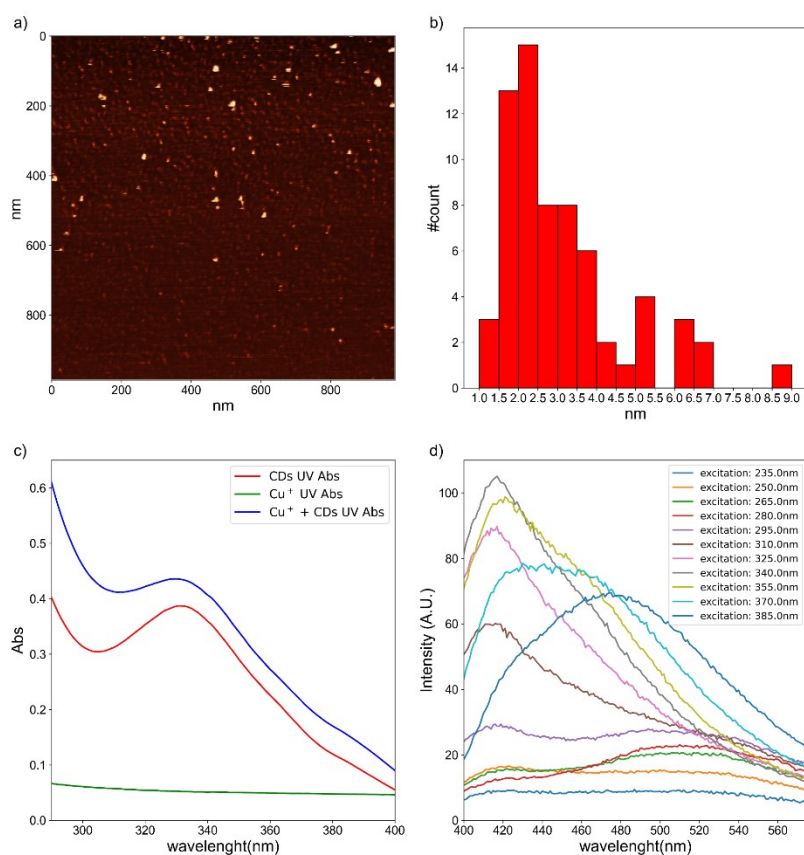


Figure 27 - (a) AFM phase image of nanoparticles deposited onto mica substrate (z scale: 0–201); (b) histogram analysis of nanoparticle height obtained by several sections of AFM height image (not-shown); (c) overlay of UV-vis spectra of aqueous solutions of carbon nanoparticles, CuCl<sub>2</sub> and 1 : 1 mixture of both, respectively; (d) overlay of fluorescence spectra of aqueous solutions of carbon nanoparticles acquired at several excitation wavelengths as reported in the labels.

Strong fluorescence emission is present around 450 nm, dependent on the excitation wavelength, and typical fluorescence spectra of CQDs are shown in Fig. 27d, emphasizing the effect that

the excitation wavelength influences the emission wavelength, which is more intense when irradiated with a wavelength of around 340 nm.

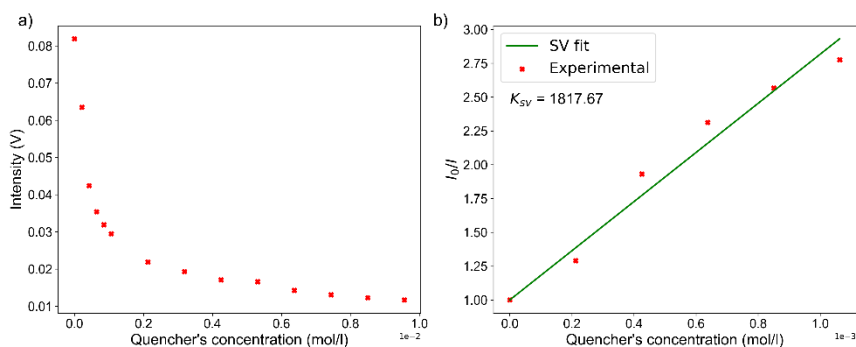


Figure 28 - (a) Fluorescence intensity of carbon nanoparticles as a function of the quencher concentration; (b) Stern–Volmer plot.

Fig. 28 shows the quenching effect caused by the presence of Cu(II) on N-doped CQDs. An increase in the concentration of copper ions leads to a sudden decrease in fluorescence yield (Fig. 28a). If we plot  $I_0/I$  according to the Stern-Volmer relation (fig. 28b), we obtain the linear trend of the function, whose angular coefficient consists of the constant  $K_{SV}$ . Summarizing the properties of carbon-based N-doped nanoparticles, they can be designated as ideal candidates for RSK modulation, as they are perfectly aligned with the model described above, i.e. detecting their presence by means of UV detection techniques and modulating the information contained by forcing quenching using bivalent copper ions. <sup>155–157</sup>

### 5.2.3 Artificial molecular communication platform

The information obtained above provided the basis for the design of an *ad hoc* experimental platform for the application of RSK modulation, so far only theorized, suitable for confined environments such as capillaries, to be used as a model for applications in biotechnology. The prototype chemical communication system is schematically described in Fig. 22: an injector loop is used as a transmitter to ensure that the information particles are always released in the same quantity, a cylindrical tube simulates the transport channel and UV-vis and fluorescence detectors are placed at the receiver. The peristaltic pump ensures a constant and controllable flow of the aqueous solution acting as liquid carrier. The modulant for RSK modulation (Cu(II) solution) is injected via a T-junction placed downstream of the molecular messenger injection valve, mimicking a continuous flow synthesis setup.<sup>158</sup> The results are shown in Fig. 29b,c: they show that the release of carbon nanoparticles allowed a binary sequence to be successfully decoded. In particular, starting from the initial idea of creating an environment in which certain conditions are uncontrollable, such as the speed of the flow, absorbance was used to detect the arrival of the messenger, i.e. to detect the presence of the information particles, while the actual decoding of bits 0 and 1 was performed using fluorescence measurements. The message transferred by this experiment is "100010", chosen because it is a challenging bit sequence due to the three consecutive 0 bits, which imply a high possibility of signal distortion due to overlapping pulses. Moreover, just to recreate the worst possible condition, this sequence has been transmitted in the slowest flow zone (Fig. 29a), recreating a challenging

environment with a high risk of intersymbol interference (ISI) and the proposed RSK approach still works well. The results reported here required the optimization of various parameters such as the concentration of messenger and quencher, the amplitude of messenger release, an appropriate time interval between the release of two consecutive information particle pulses, the right delay in quencher release, the optimal detector thresholds, etc. The development of artificial chemical communication systems for specific applications will require the fine-tuning of all the above experimental parameters and a systematic investigation.

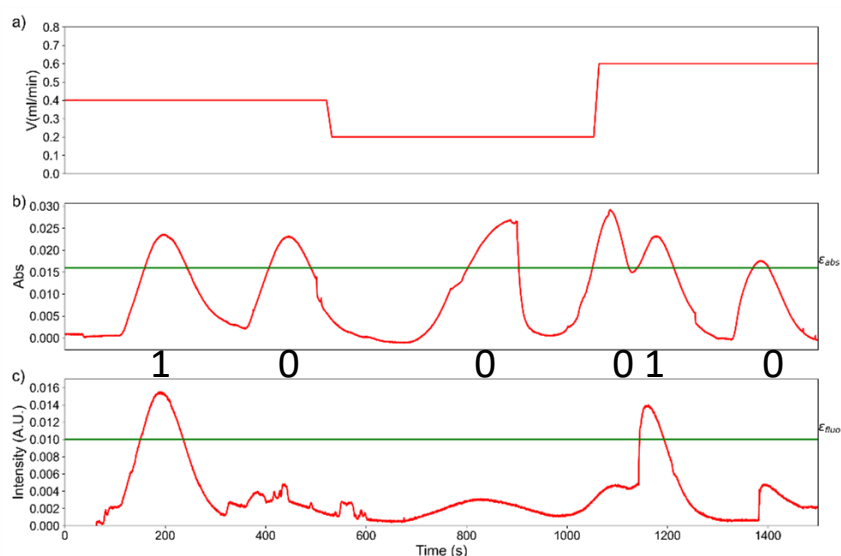


Figure 29 - (a) transport flow velocity trend during the communication time. (b) Absorbance and (c) fluorescence signals detected by the receiver when “1-0-0-0-1-0” sequence is released in a real-working chemical communication platform. First 1-bit was released at time  $t = 0$ . Subsequent pulses have been released with 200 s delay time among each other. Between (b) and (c), the decoded binary sequence according to RSK modulation is reported.

Of course, it is beyond the scope of the experiment to obtain a perfectly clean and defect-free signal: the proposed method has proved to be efficient despite the difficult scenario, but the improvement margin is considerable and requires the contribution of experts in fields other than chemistry, but which are close to the concepts of MoCo and development of communication platforms. However, the results reported here unequivocally show how RSK modulation is effective and flexible for artificial molecular communication when flow conditions are variable and above all uncontrollable.

### 5.3 Conclusions

To sum up the purpose and results of the entire experiment, it is possible to say that the development method is successful. The aims of this experiment have been to theorize a model to be applied to the problem, to engineer the appropriate information particle and finally, to observe experimentally the results of the model. In this specific case the problem due to the non-time synchrony between transmitter and receiver has been addressed: if the clock that marks the separation between a time-slot and the other is not constant, it is unthinkable to apply a classical OOK modulation method. Therefore, a new modulation procedure, called reaction shift keying (RSK), has been theorized and developed for the transmission of information through information nanoparticles even in the absence of synchrony. The approach requires a chemical messenger with two measurable and independent properties used, respectively, to detect the presence of the information particles and to decode it. This has

been achieved by means of an artificial molecular communication system that exploits fluorescent carbon nanoparticles as chemical messengers and their chemistry with Cu(II) ions for modulation of fluorescence properties, allowing to encode the required information by RSK modulation. In principle, any other fluorophore with similar properties can be used but the motivations described in Chapter 2 lead to continue development using CQDs. We believe that RSK modulation will represent a fundamental improvement for the development of truly functional chemical communication systems, since it overcomes all limitations related to flow rate and receiver distance variations, which appear in many applications where MoCo can be applied.

## Chapter 6

### Fluorescent nanoparticle-based Internet of things

Face-to-face communication systems in which the transfer of information takes place exclusively between two interconnected devices are a perfect basis for understanding the mechanisms involved in MoCo and acting to optimize the method. From an application point of view, however, it is reductive: although MoCo is a modern and innovative concept, the absence of advanced functionalities that have become a prerequisite makes the development of this technology an end in itself. In this regard, when introducing MoCo, it was stated that the natural application is towards interconnectivity, IoT and communication networking between nanodevices. Although the conception of an IoT system on paper (Fig. 30) seems simple if we take it for granted that each device is properly programmed, interconnecting the latter by means of MoCo requires a great deal of engineering work on the experimental system, a great deal of optimization and an error reduction procedure. The effort made in the work described below has resulted in the first working IoT system based on MoCo. For the development of a reliable chemical-IoT, information particles must travel from a central source (server) to several receivers (clients), who will receive the information to perform the task for which they are programmed. In this specific case, wanting to emulate a biological scenario, the server is equipped with sensors of specific physiological properties, which sends commands to the clients, i.e. actuators that allow them to act and fix these properties.



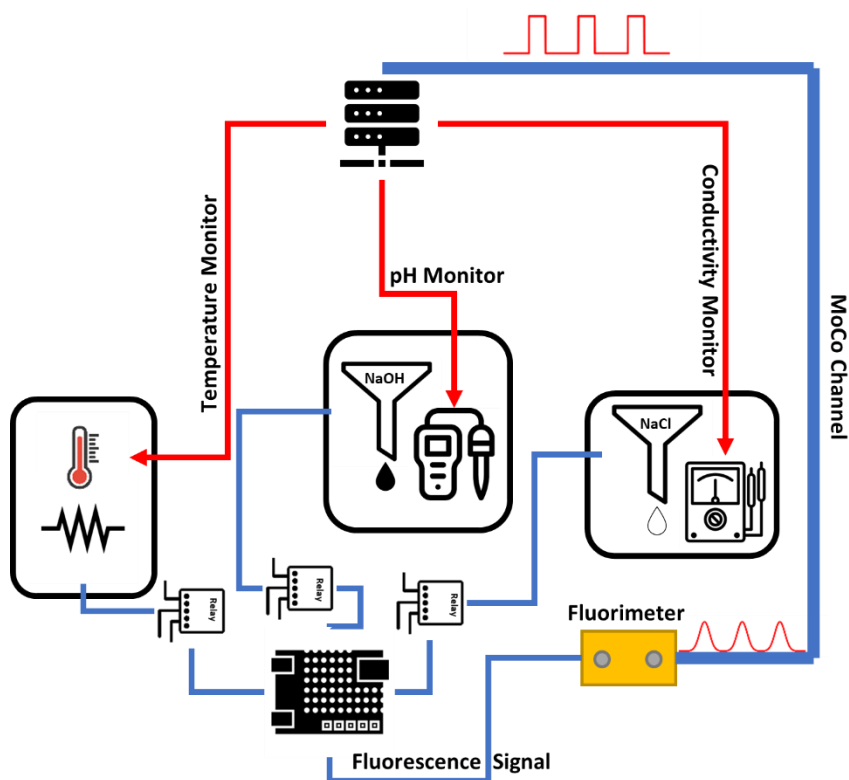


Figure 30 - Schematic representation of a conceivable molecular-IoT architecture.

For simplicity, a single-bit approach (ON / OFF) can be used to change the actuator state, thus ensuring the shortest communication time. Obviously, the more clients there are in the network, the more distinct commands are required i.e. more information particles are needed to avoid unwanted activations. The choice of information particles falls again into the CQDs. Here, we show that a mixture of carbon nanoparticles, characterized by discrete fluorescence wavelengths, can selectively activate three distinct actuators upon change of three distinct physiological

parameters.<sup>159</sup> The preliminary results achieved by this pioneering work serve to lay the groundwork for progressively increasing the complexity of communication platforms based on artificial molecular communication, urging efficient and reliable information exchange between liquid-communicating devices.

## 6.1 Materials and methods

Since the aim of the work does not focus on the synthesis of the molecular messenger, which has already been discussed at length, in order to devote most of the time to the development of the model in question, carbon nanoparticles (CQDs) were purchased (from Aldrich) and used as received, since they were already distinguished by their fluorescent properties. In particular, three types of CQDs were purchased according to their emission wavelength: blue (B-CQDs), cyan (C-CQDs) and green (G-CQDs). CQDs were adequately diluted in ultrapure water obtained by filtration (from Millipore). The fluorescent properties were also confirmed by analysis with a Cary fluorimeter (from Agilent) using a 5 nm slide. The entire IoT prototype was built in-house and uses a hybrid communication system, part electrical and part molecular communication. The control center consists of a standard PC running Linux. As this is a non-standard system, the scripts for sensors data collection and for the commands to open/close the valve to release the nanomessengers were developed *ad hoc*, using Python as programming language. The temperature sensors (thermocouple, from RS Components), the pH sensor (pH sensor from RS Components), the salt conductivity sensor (from Hanna) and the valves for releasing the nanomessengers (from Valco)

interfaced with the control center by means of a single-board microcontroller (STM32 Nucleo-64 from RS Components). MoCo is via a microfluidic system, the flow of which is ensured by a piston pump controlled by a stepper motor (nema17, 4.8kg/cm, 200steps) to ensure constant speed, while a Teflon tube connects the control center and sensors with the actuators. The piston pump was designed in house and built by purchasing components from RS Components and then engineering and printing some PETG parts with a 3D printer (Alfawise u30 pro). The reading of the fluorescence emitted by the information particles was carried out in flow by means of an HPLC detector (Shimadzu). Actuator A (acting on temperature) consists on a relay that turns on/off the heater triggered by the detection of B-CQDs. Actuator B (pH-related) opens/closes the valve that adds a basic solution ( $\sim 1$  ml NaOH, 0.1 M) to the solution monitored by the pH meter when C-CQDs are detected. Actuator C adds a saline solution ( $\sim 1$  ml NaCl, 0.01 M) when G-CQDs are detected. The simulations were performed by solving the advection-diffusion equation (eq. 3) numerically by means of a Python script, modelling an appropriate mesh thanks to the tools provided by the NumPy and FiPy libraries.

## 6.2 Results and Discussions

### 6.2.1 The model

Referring to a possible application in biology, a schematic representation of a molecular-IoT architecture has been designed and presented in Fig. 30. The devices that make up this model are four and defined as follows: a HOST device that receives and

processes the physiological parameters obtained from the sensors (the so-called control center), and its three sensors which are instead actuators that can be activated by stimulus received from the control center through molecular communication. When the control center detects that the monitored parameters are out of control (out of established set-point), the HOST system releases the related information particle to the actuator transmitting the information, i.e. through activation. In a simple inversion logic scheme, the control center modulates the release of the short concentration pulse of the information particle. When it reaches the target client device, it triggers the state of the actuator, activating it (OFF → ON) if in stasis and stopping it (ON → OFF) if in operation. In this way, it will be possible to interconnect the sensory and functional parts of the molecular-IoT architecture in line with a typical biomimetic regulation scheme. In other words, the transmitter sends information particles to reverse the state of the actuator, while remaining silent (not transmitting) when no action is required. Since the activation/deactivation of each device must be selective and independent, an information particle which is different for each device is required. Thus, the reaction of the  $i$ -th receiver device  $\Gamma_i$  depends on the amount of detected messengers  $C_i(t)$  and on the property of the  $j$ -th information particle to which the  $i$ -th receiver is selectively susceptible according to a specific response  $\phi_{i,j}$ , so that, for a three-device system:

---


$$\begin{cases} \Gamma_A(t) = \phi_{A;k} \cdot C_k(t) + \phi_{A;l} \cdot C_l(t) + \phi_{A;m} \cdot C_m(t) \\ \Gamma_B(t) = \phi_{B;k} \cdot C_k(t) + \phi_{B;l} \cdot C_l(t) + \phi_{B;m} \cdot C_m(t) \\ \Gamma_C(t) = \phi_{C;k} \cdot C_k(t) + \phi_{C;l} \cdot C_l(t) + \phi_{C;m} \cdot C_m(t) \end{cases} \quad \text{eq. 17}$$


---

Ideally, the matrix of response coefficients  $\phi_{i,j}$  is the identity, which enables each communication to be considered as end-to-end. Once again, the function  $C(t)$  comes into play, which is critical in order to correctly determine the thresholds that trigger the state switch of the actuators. Obviously, the fluid-dynamic properties of the designed system must be considered again, since during the transmission towards the receivers, an exponential decrease of the concentration of the various information particles is expected, according to the solution of the differential equation:

---

$$\frac{\partial C_j}{\partial t} + v\nabla C_j = D_j\nabla^2 C_j \quad \text{eq. 18}$$

---

where  $C_j$  is the concentration value of the  $j$ -th messenger in space at time  $t$ ,  $D_j$  is its diffusion coefficient and  $v$  is the velocity of the transport flow. Here again, the same argument developed in the previous chapters applies: each system is endowed with different fluid-dynamic properties, in fact, if  $D$  can be considered as a property dependent on the geometry of the information particles and the viscosity of the medium in which it is located (see Stokes-Einstein equation<sup>143</sup>), the  $v$  depends on a large number of factors, such as the pressure gradient of the capillary, the geometry of the capillary if different boundary conditions are imposed. This means that the dispersion process of the information particles during transport must be analyzed from time to time. All parameters, such as the time distance between one information particle pulse to the other or the adjustment of the detector thresholds, must be reconsidered and set for the specific system. In order to optimize times and avoid excessive consumption of reagents, this

is done by acting as in the flow, i.e. by promoting a first phase based on fluid-dynamic simulations of the model. Moreover, this approach allows not only to acquire predictive knowledge, but also to investigate the phenomena involved as well as to proceed to a preventive optimization of the system. Indeed, one might think that the baud rate (i.e. the information transfer speed) could simply be adjusted by the flow speed. However, the information transfer rate depends on two parameters: the time required by the information particles' pulse to reach the detector, which is closely related to the flow velocity, but also the time required by the pulse to cross the detector and thus to exit the information loop. The latter consists of the pulse width and represents the minimum time between two actuator triggers, is related to the ISI concept and depends on several parameters. As can be easily guessed, the effect of the source-detector distance is proportional (as expected) to the width of the information particles' pulse, since the longer the flow path, the greater the dispersion phenomena. The simplest solution to this problem seems to be to increase the flow velocity, as this would reduce the time during which the pulses are subject to dispersion-induced broadening. As already briefly described in Chapter 3, it is well known that in a capillary tube the flow gradient between the center and the wall is proportional, but not linear, to the flow velocity.<sup>160,161</sup> The higher the average cruising velocity, the greater the difference between the internal (center of the tube) and external (proximity to the wall) drift. This induces a distortion of the molecular messenger pulse profile, reduces the optical path of the detector and consequently there is a damaging reduction in signal intensity which undermines its detection by the detector. Increasing the flow rate does not correspond to the effective baud rate solution

and the model must be studied to optimize both the information transfer rate and the pulse intensity. The study of the effect of the transport speed on the quality of the transmitted signal was carried out by means of computational simulations, by developing the mesh (a cylindrical capillary channel with a diameter of 0.25 mm and a length of 1000 mm in which there is a laminar flow regime) and by means of the numerical solution of eq. 15. The results were compared by varying the parameter  $v$  (which we remind to be a tensor and not a scalar value) in the advection-diffusion equation. Fig. 31a shows some interesting snapshots obtained for different flow velocities. To make it easier to interpret graphically, the X-axis scale (transmitter-receiver distance) is larger than the Y-axis (capillary diameter). The false-colour images clearly show that the higher the flow velocity, the greater the dispersion induced at the pulse of information particles, causing the signal intensity to decrease and the physical width within the channel to increase. A similar effect, but from the detector's point of view, is shown in Fig. 31b, which represents the trend in signal intensity (i.e. messenger concentration) detected by receiving devices placed at different distances as the travel drift changes. Caution should be exercised when interpreting this data: the further is the receiving device, the wider the time window in which the signal is present, as well as having a lower maximum intensity. However, fixing the distance of the receiver and observing the signals closely, an anomaly can be observed: it almost seems that at slower speeds the total concentration of the information particles increases, as there is an increase as well as a widening in the intensity of the signal.

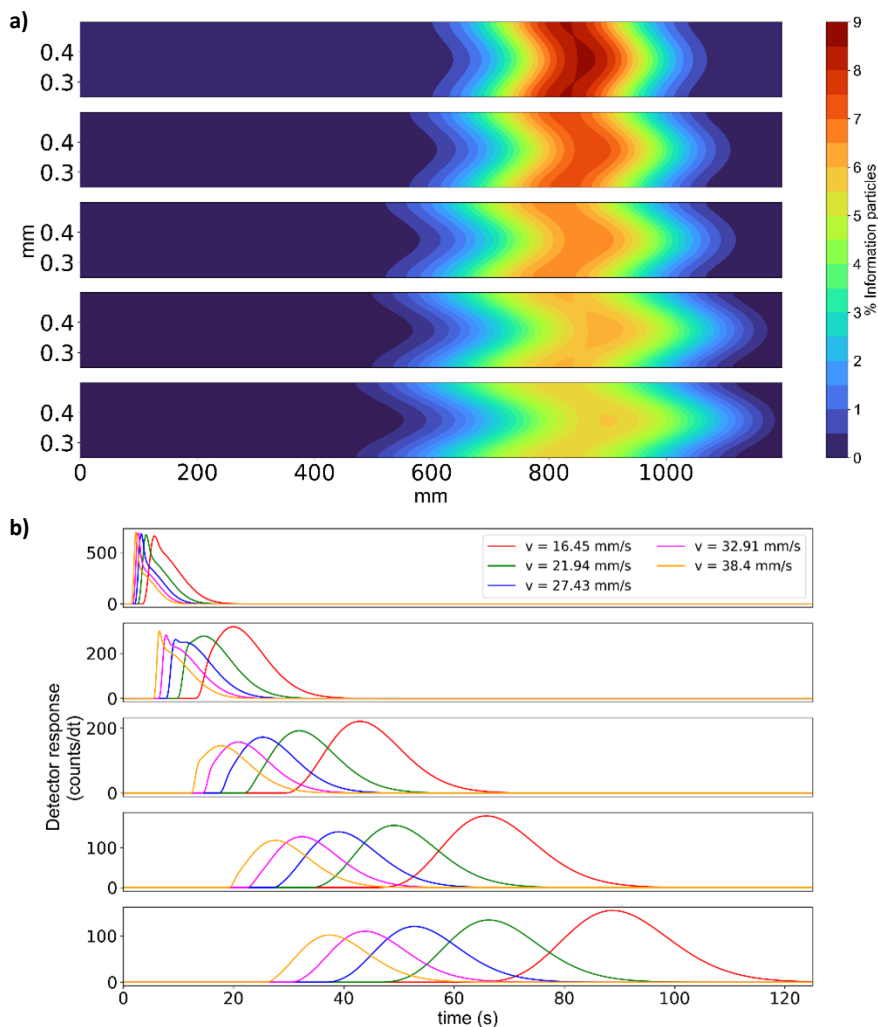
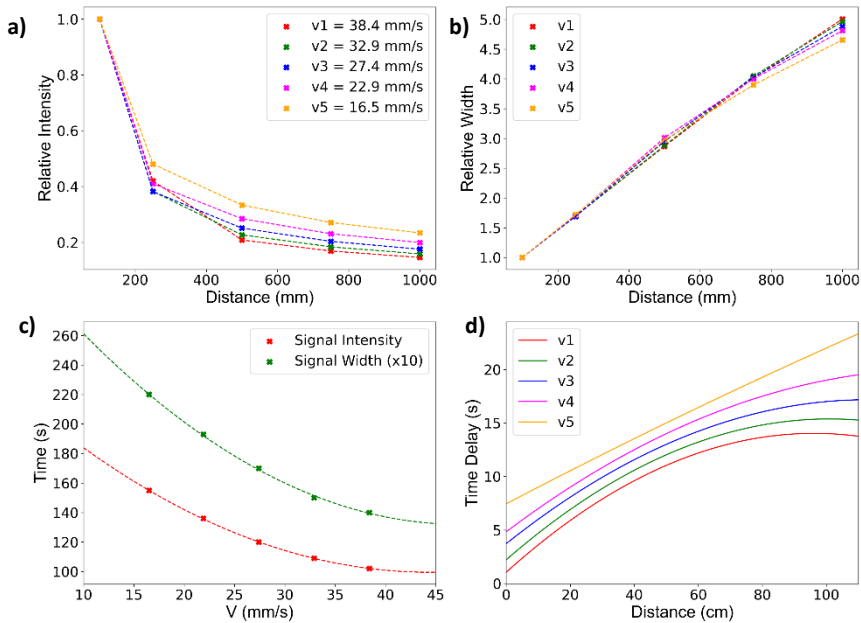


Figure 31 - (a) False color maps of simulated molecular messenger concentration distribution inside the capillary pipe acquired at different flow velocities (from top to bottom:  $v_1 = 16.45 \text{ mm s}^{-1}$ ,  $v_2 = 21.94 \text{ mm s}^{-1}$ ,  $v_3 = 27.43 \text{ mm s}^{-1}$ ,  $v_4 = 32.91 \text{ mm s}^{-1}$ ;  $v_5 = 38.4 \text{ mm s}^{-1}$ ). (b) Actuators' response placed at various distances as a function of time.





*Figure 32 - (a) Relative signal width as a function of transmitter receiver distance at various velocities. (b) Normalized peak intensity as a function of transmitter receiver distance at various velocities. (c) Signal intensity and width ( $\times 10$ ) detected as a function of time. (d) Time delay between successive pulses required to avoid their overlap as a function of the travel path calculated for 5 different flow velocities.*

This is a false supposition and can be interpreted as follows: since at lower flow velocities, the pulse takes longer to pass through the detector, the measured absolute amplitude is the highest at lower velocities and this explains the signal broadening in the time domain. Similarly, in our simulation, the peak height turns out to be higher at lower velocities, irrespective of the detector distance, as evidence of what we saw in the space domain simulations (fig.31a). In Fig. 32 these results are summarized and graphed. Fig. 32a shows the actual hyperbolic relationship present between

signal strength and receiver distance, a hyperbola which is translated upwards by reducing the flux velocity. Inversely, signal broadening increases linearly with distance traveled and, when normalized for higher velocity, little affected by the flow velocity itself (Fig. 32b). The effect of flow velocity on pulse width and intensity is therefore summarized and appropriately scaled in Fig. 32c. For both parameters there is a quadratic relationship, suggesting the establishment of a fluid dynamic regime with Taylor dispersion.<sup>162</sup> This is because, while the dispersion coefficient of the messenger along the direction parallel to the flow is independent from the flow velocity (since it follows Fick's law of diffusion), transversal to the flow direction it is proportional to the mean square of the flow velocity. This implies the quadratic relationship between peak intensity reduction and flow velocity. However, even though from a purely dynamic fluid dispersion point of view slow flows allow better results, it cannot be ignored that the absolute width of the signal read by the receiver increases with decreasing flow velocity. The increased signal width will require a shorter path to induce overlap between consecutive signals. This concept was developed in Fig. 32d, where the delay between two successive peaks required to avoid overlap is reported as a function of flow velocity and path length. Simulations have shown that before the molecular-IoT platform can be trained, it is essential to find a balance between the throughput and the distance between two successive pulses to avoid overlap. In order to implement the technological transfer of this theoretical investigation to its practical implementation, a chemo-cyber interface is defined here as the set of processes required to translate information from the chemical domain of

molecular messengers to the electronic devices that constitute molecular-IoT networks, and *vice versa*.

### 6.2.2 The experiment

The design of a molecular-IoT interface is a critical part of this kind of work, since it is not enough to obtain good quality simulations, which are necessary to know and predict the fluid-dynamic properties of the system, but another challenge for the realization of these interfaces lies in the part of detection, through physico-chemical processes, of the information particles. The ability to accurately detect the encoded information and to transduce it into the correct modulation of the electro-magnetic parameters of the devices (biosensors, actuators, etc.) is indispensable in this project. The literature teaches that the most obvious solution is the use of specific sensors based on the highly selective host-guest interaction resulting in the production of an electrical signal.<sup>163</sup> The problems that arise from the use of a sensing technology based on highly selective systems on applications in the biological domain lie in their high latency, sensitivity to noise, lack of standardized response,<sup>164</sup> and, unverified biocompatibility.<sup>165</sup> The problem arises from the fact that active part of the sensor must be in contact with the messenger to which it is selectively sensitive, i.e. it must be immersed in the fluid carrying the information particles. Since the beginning of this project, the application target has been the biomedical field, therefore serious biocompatibility problems cannot be accepted. Among the possible solutions, which have already been extensively described in chapter 2, there can be methods of remote detection of the

information particles by means of magnetic transduction<sup>166,167</sup> or optoelectronics.<sup>168</sup> This last case is the one chosen for the development of this project, in fact the information particle is detected by fluorescence by exciting it with an appropriate wavelength. The detection of its photoemission is done by means of an appropriate optoelectronic transducer set to the specific wavelength without any direct contact.<sup>169</sup> Carbon-based fluorescent nanoparticles (CQDs) have been shown several times to be good candidates for this purpose. CQDs have high quantum yield, high stability, good biocompatibility, low toxicity and high water-solubility, e.g.<sup>78</sup> all excellent properties for bioimaging and biosensing applications. The synthesis can take place following many procedures, countless examples are found in the literature, such as the simple oxidation of carbon in the presence of acids at various temperatures.<sup>170</sup> Notable morphological features include a size range of 1-10 nm, 2D morphologies and a zigzag edge structure consisting of 1-3 atomic layers. Although not described in a highly specific manner for the sake of brevity (and in order not to distract the discussion from the information to be conveyed), the simulation modelling efforts allowed us to narrow down the field to the best performing fluid dynamic conditions to create a truly functional molecular-IoT platform, starting from a simple end-to-end communication. The first phase concerning the development of the molecular-IoT platform required a not inconsiderable process of experimental optimization, always based on the results achieved through simulations. First, the transport and dispersion process of CQDs was analyzed: fig. 33a reveals the response of the fluorescence detector when a single information particle pulse is released into a transport medium travelling at various flow velocities. As expected for the fluid

dynamic conditions set in the model, the experimental results imply the presence of Taylor dispersion and a predominant laminar flow. In fact, according to our simulations, an increase in the drift velocity leads to a reduction of the maximum signal intensity and thus of the signal energy because the information particle pulse is much more dispersed for higher velocities (compared to a lower one).

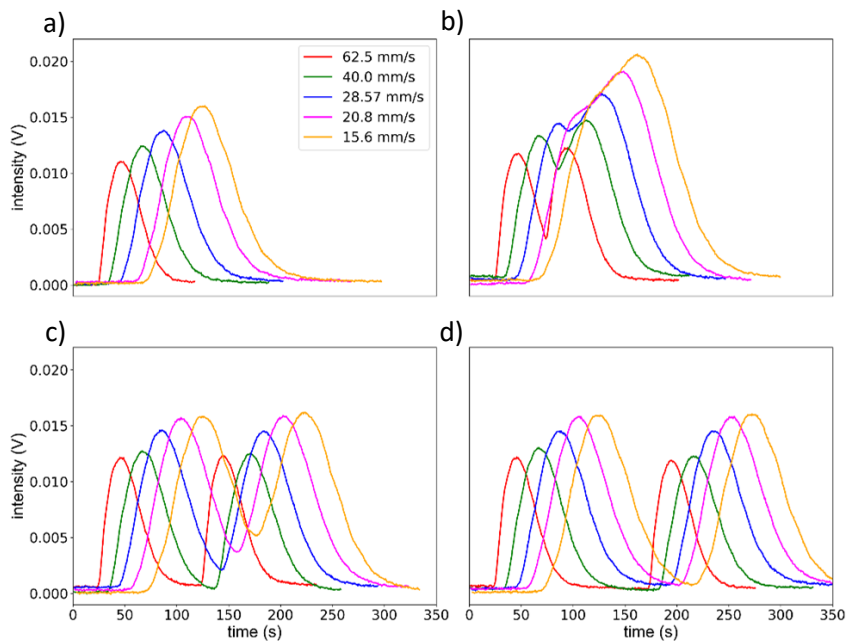


Figure 33 - Fluorescence detector response when (a) a single pulse of fluorescent nanomessengers is released or two subsequent pulses are released with (b) 50 s, (c) 100 s, and (d) 200 s of delay time (velocities values in the legend).

The amplitude of the signal detected by the receiver, on the other hand, remains narrow because the high speed allows the pulse of

information particles to pass quickly through the detection zone. The choice of speed is therefore critical to enable correct signal detection (ideally at high intensity), especially if successive pulses must be sent very close together (without incurring ISI). The latter concept was developed by detecting two successive pulses at various flow rates and various distances between releases and shown in Fig. 33b-d. To investigate this detail statistically, an extensive optimization campaign of the two parameters was undertaken, revealing that the absolute peak intensity and the relative peak-to-valley intensity are affected by the transport velocity and the delay time in opposite ways. It is now clear that to maximize intensity, a low flow velocity should be used, but to avoid peak overlap it is better to use higher velocities. So, the question arises, which is the best compromise? To be more comprehensible, fig. 34a shows a 3D representation of both parameters extrapolated in matrix form from the experimental measurements. Because they are numerically not directly comparable, the matrices were centered by subtracting the mean and scaled by dividing them by the standard deviation. The data points of absolute intensity (green) and relative valley peak (red) were subsequently interpolated with biquadratic planes. Briefly, the versatility of the 3D plot comes from the ability to note where the two planes intersect, resulting in a curve (blue line) that represents the optimization function of the transport process: the relationship between flow velocity and delay time between symbols to produce the most intense signal without inducing high ISI. This optimization curve is geometrically a branch of an ellipse (Fig. 34b) whose coefficients must be determined experimentally. Given that in most practical cases, especially in the biological domain, it is expected that the flow velocity is not controllable but

is dictated by the physiological conditions themselves, e.g., the velocity of blood flow, plant sap, pipeline flow, etc., it is not possible to control the flow rate. The optimization curve extrapolated using this statistical method will provide the appropriate delay time value between two consecutive pulses in order to maximize the baud rate without incurring into errors. The results obtained through the simulations lay the foundation for the optimization of any MoCo system in a microfluidic environment with purely laminar flows. After evaluating the optimal experimental conditions for the operation of prototype molecular-IoT systems, we have identified the most suitable information particles for selective and simultaneous communication between three actuators. One of the main features of CQDs, which make them extremely versatile for these applications, is the possibility to modulate their fluorescence by varying the composition of the carbon core, carrying out the synthesis by different techniques, isolating only a small size range etc.<sup>144</sup> About the CQDs used for this work a unique excitation wavelength, 280nm, has been identified at which the three different CNs emit at three different wavelengths from which they take their name: B-CNs, C-CNs and G-CNs. In the proposed molecular-IoT architecture, the device, acting as a sensor station and acting as a control center for the actuators, will release the appropriate CQDs to reverse the actuator's operational state. B-CNs have been selected for actuator A, C-CNs for actuator B and G-CNs for actuator C.

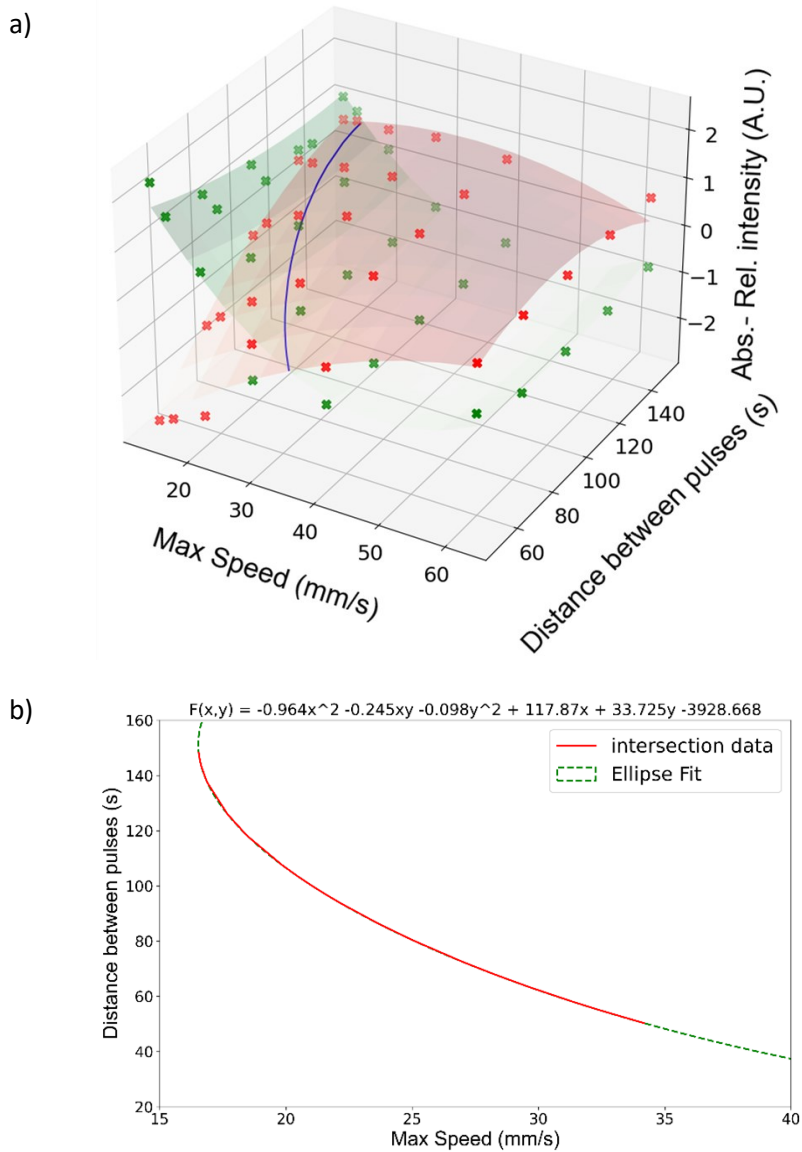
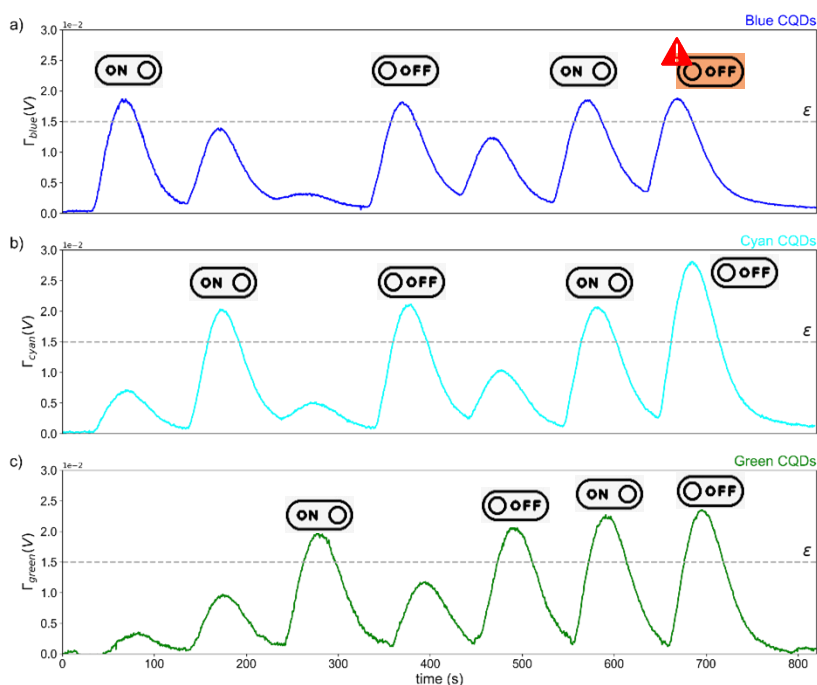


Figure 34 - Optimization results. (a) 3D representation of absolute (green dots) and relative peak–valley (red dots) intensity as a function of fluid velocity and pulse delay. (b) 2D plot of the two-plane intersection curve, the blue line in (a), and the fit (green dotted curve).



Finally, the actual working prototype platform was assembled to verify what has been theorized. Fig. 35 shows the complete response and effect of interference between different CQDs for selective activation/deactivation of the actuators (individually or simultaneously) by detecting the different wavelengths of fluorescence emitted by each information particle. The icons ON and OFF shown in Fig. 35 reveal the times when the control center intended to activate/deactivate specific actuators.



*Figure 35 - Actuators' response to the release of specific messengers' sequence: 1. blue-CQDs, 2. cyan-CQDs, 3. green-CQDs, 4. blue-CQDs and cyan-CQDs, 5. green-CQDs, 6. all CQDs, 7. cyan-CQDs and green-CQDs.*

From the reported results, the CQDs proved to be excellent candidates in terms of selectivity of specific actuator activation, as

only one error was found at about 700 seconds. The error consists of an unintentional deactivation: the C-CQDs and G-CQDs were delivered to deactivate actuators B and C but actuator A was also deactivated. This unwanted event can be attributed to the very large high fluorescence intensity of C-CQDs, which affected the detection of a false positive at actuator A. Considering the very high intensity of the C-CQDs, this was a release problem and therefore solvable with improved valve calibration. After the preliminary study and optimization of the molecular-IoT prototype, we finally got back to the scope of the work: the control of three physiological parameters through the feedback action between the HOST (control center) and the CLIENTS (three actuators). Fig. 36 shows the results of the first working molecular-IoT architecture. First, three parameters (temperature, pH and ionic conductivity) typical of a physiological solution were selected. Whenever a sensor measures a value outside a preset threshold, the control center releases the specific CQDs for the selected actuator to reverse its operation. The HOST then sends the reversal information to keep any parameter close to the threshold. Going into more detail about the device: the temperature actuator turns on/off the resistor to maintain the temperature at 50 °C. The pH actuator controls the release of a sodium hydroxide solution into the acetic acid solution to obtain buffer at pH = 5 . The salinity actuator releases a fixed dose of sodium chloride solution to increase conductivity to the set threshold (effectively acting as a button instead of a switch). For simplicity, the saline solution being monitored is not the same as the one through which the information particles travel. Ideally, the possibility of combining the two is not precluded as the fluorescence properties are not strongly influenced by the

variation of temperature, pH and salinity in the range explored. The results obtained are encouraging and demonstrate the feasibility of the project: the molecular-IoT platform allows the parameters to be controlled at the selected threshold, despite the obvious delay between the signal emitted by the control center and the response of the actuator, due to the transport time through the capillary (about 80 seconds in the conditions under analysis).

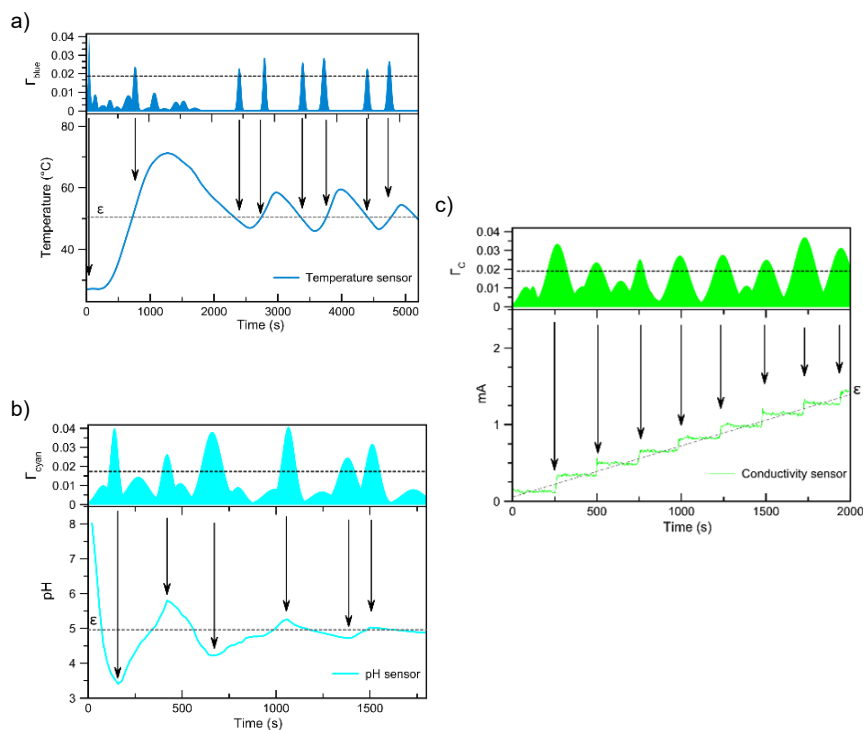


*Figure 36 - (a) Temperature controlling of actuator A. (b) pH controlling of actuator B. (c) Conductivity controlling of actuator C. Fluorescence responses of each actuator are also plotted.*

In addition, the temperature value is affected by a further delay due to the thermal inertia of the solution. It is clear that the experimental prototype should be considered for what it is: handcrafted in the laboratory in the absence of specific electronic and computer skills. Any additional optimizations are beyond the scope of this work, which only want to demonstrate how MoCo can allow to obtain communication networks much more complex than a simple interaction between only two interlocutors.

### 6.3 Conclusions

The difficulty in applying an idea usually clashes with the impossibility of its realization. For MoCo, this was not the case: although it had been theorized many times and although it is contemplated in the literature as the solution to some problems concerning the media, nothing overly complex had been realized so far. Finally, a well-functioning prototype of a molecular-IoT platform, which required effort in design, simulation, theoretical analysis and implementation has been proposed. The use of fluorescent CQDs proved again to be efficient due to the different emission wavelengths, allowing the selective remote recognition of actuator-specific information. Theoretical and experimental studies of the fluid-dynamic conditions and the analysis of the physical-chemical properties of the CQDs have made it possible to create a truly operational system, capable of autonomously regulating certain physiological parameters. Although the system is only a prototype implementation in vitro, the feasibility has been demonstrated and it is hoped that with the collaboration of other fields of communication science, it will be possible to

## Fluorescent nanoparticle-based Internet of things

implement molecular-IoT in truly practical contexts. We like to imagine it as the next generation of MoCo systems, which can be a powerful method to ensure the achievement of precise medical diagnoses and/or treatments.

## Chapter 7

### Graphene Quantum Dots enable digital communication through biological fluid

This chapter seeks to find an approach to MoCo that is less ideal and more attentive to a real problem, in which this new bio-inspired communication method can make a real contribution. Most of the work in the literature has focused on just three key aspects of MoCo: the information particle, modelling the phenomenon of transmission-transport-reception of information particles, and modulation methods. There are few practical examples in which a truly functioning prototype is shown, and these include all the variants of ours. We are pushing towards these new methods of communication because the new frontier of science is directed towards man-machine interaction, what in science fiction films was called cybernetics. The very first objective of science in this context is obviously the medical field, as it must have priority in order to improve the quality of life of human beings. The simplest objectives that can be implemented in a system equipped with MoCo concern the real-time monitoring of key biological parameters: we have seen in the previous chapter a molecular-IoT system where, however, the sensors of the physiological parameters sent the information electrically, only the command of actuation took place via MoCo. Parameters such as blood pressure and body temperature are also easily obtained from very small sensors and can easily be incorporated into nanodevices. In addition, nanodevices do not require high energy to operate, so body heat alone, or movement or blood flow, would

## Graphene Quantum Dots enable digital communication through biological fluid

allow them to function without relying on energy storage. A complete liberation of these devices from cables or harmful electromagnetic radiation<sup>171</sup> would allow the development of new medical treatments for those suffering from diseases that require continuous treatment or monitoring. The closest thing to this, but already in common use, are wearable devices that can provide information on parameters such as physical activity, heart rate and sleep monitor.<sup>172-174</sup> However, these devices have serious limitations due to their limited number of sensors that cannot locally monitor a specific organ or body part. For example, patients undergoing hip implant surgery are prone to inflammation in the vicinity of the operation, which, if not treated promptly, can lead to severe and acute inflammation, requiring further surgery.<sup>175,176</sup> Continuous localized monitoring of tissue temperature around the prosthesis would allow the effects of hyperthermia to be anticipated and treated pharmacologically, eliminating the need for further surgery. A secondary area in which MoCo can make a positive contribution is away from the medical field and concerns underwater communication. In these conditions, the limitation comes from the difficulty of electromagnetic waves in travelling the distances reached on land, since the attenuation of the signal is considerably accentuated.<sup>177</sup> Although this drawback can be partially overcome by the construction of fixed repeaters, the signal can always suffer from additional noise or loss of information. If immediate communication of a position is crucial for rescue operations, such as for submarines, ships or aircraft, it therefore remains an inadequate form of communication. Although it is not the subject of this specific project, this may be a potential point of development for the application of MoCo to replace

electromagnetic waves. The state of the art in working prototypes that exploit MoCo is currently mostly oriented on non-specific communication using basic signal modulation methods for encoding and decoding information. Resuming what has already been extensively described in the introductory chapter, typical modulation methods are essentially based on the type of information particles (MoSK, molecular shift keying) and/or concentration (CSK, concentration shift keying).<sup>52</sup> The most common is called OOK (On-Off keying).<sup>177</sup> Based on CSK modulation, it is a method in which information is transferred using only two states: on-off, typical of binary language. The time window must be fixed between successive symbols, while the logic can be easily described:

---

$$S(t) = \begin{cases} 0 & \text{if } C(t) < C_{threshold} \\ 1 & \text{if } C(t) > C_{threshold} \end{cases} \quad \text{eq. 19}$$

---

Where  $S(t)$  is a function of  $t$ , which can potentially be defined as a number of particles or concentration, and  $C_{threshold}$  an arbitrary threshold dependent on the specific operating conditions. This modulation strategy matches well with binary coding as it naturally adopts a 1-0 logic. The problem is that it requires the release of many bits for the complete transfer of very simple information. This contrasts with what afflicts artificial MoCo within natural communication channels: transfer is too slow because it is limited by the drift speed of the transport medium (e.g. blood for animals or sap for plants). Instead, the aim is to recreate a system for rapid communication of changes in physiological parameters (e.g. temperature), whereby the speed



of information transfer must not be limited by the speed of the transport stream. When using a binary coding system, a single letter requires 8 bits (corresponding in MoCo to eight time slots by modulating OOK) with extended ASCII coding. To avoid intersymbol interference (ISI), the time-slot must be larger than the dispersion of the information particle pulse,<sup>159</sup> which in turn also depends on the geometrical and physical parameters of the transport channel.<sup>151</sup> Thus, although it has been demonstrated that the transfer of complex messages, such as temperature values or other physiological information,<sup>50</sup> becomes an end in itself due to the time required to complete the message. Increasing the speed of the molecular messenger vector in some cases helps the baud-rate, within certain limits, and therefore may seem a practical and simple solution. However, having set implanted biodevices as the scope of MoCo, the speed of the carrier flow (e.g. blood) cannot be controlled from the outside. A diametrically opposed solution could be to increase the amount of information encoded/stored within a single messenger release, i.e. to increase the amount of information per symbol, thus reducing the number of information particles per information. Also in this context, modulation methods have been proposed, such as the method called n-CSK (n-ary Concentration Shift Keying) where the information is written with different  $C_{threshold}$  values. However, in n-CSK the error associated to the ISI strongly depends on the number of thresholds chosen, and therefore on the number of bits per symbol.<sup>50</sup> The alternative is called n-MoSK (n-ary Molecule Shift Keying) if the information written in each time slot depends on the type of molecule.<sup>52</sup> Using these more complex modulation methods we enter the concept of high information density MoCo.

## Graphene Quantum Dots enable digital communication through biological fluid

---

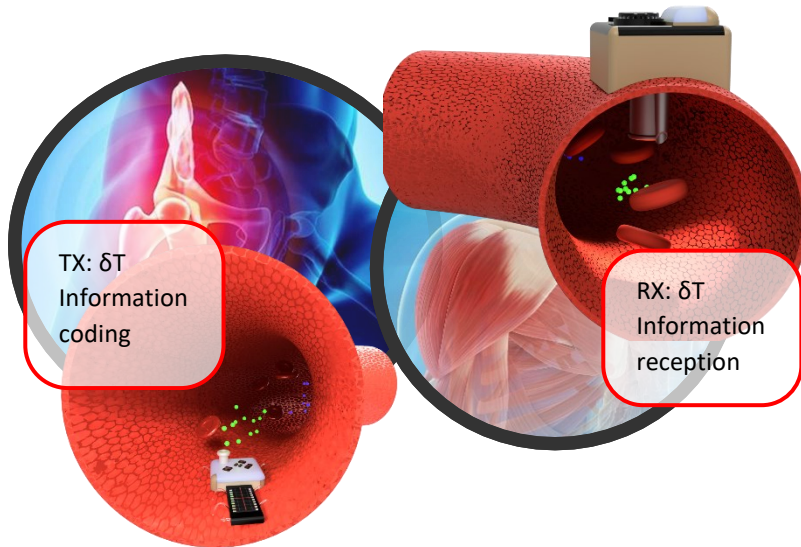


*Figure 37 - A schematic concept for in-vivo Molecular Communication. A micro-robot monitors the temperature of a tissue using a specific sensor. It communicates temperature level encoding information inside fluorescent information nanoparticles and releasing them in the blood flow. Another micro-robot detects the information nanoparticles using a fluorescent detector and decodes the information. It could then release medication if necessary.*

---

While the same technologies described in the previous chapters can be used for n-CSK, for n-MoSK it becomes more complicated to distinguish between different species using a detection method that is easy to implement. This has meant that the actual implementation of this modulation method has not yet been reported. It seems clear that, again, the choice of molecular messenger is of crucial importance to overcome these technological limitations. Ideally, an effective application of the n-MoSK modulation scheme requires a receiver capable of detecting

## Graphene Quantum Dots enable digital communication through biological fluid

the correct structure of the molecules, such as a mass spectrometer,<sup>178</sup> which is invasive and time-consuming in terms of computational analysis. For in vivo or emergency MoCo applications, two things are essential: a non-invasive receiver and rapid detection of the information particle. Technology currently provides very efficient and compact optical detection tools, such as micro-fiber optics,<sup>179</sup> so one can think of still exploiting absorbance/fluorescence properties for the detection of molecular messengers in biological fluids. Building on the assumptions made in Chapter 2, where carbon-based nanoparticles were described as jokers for MoCo, CQDs were also proposed for this work as information particles to realize a high information density MoCo prototype that exploits n-MoSK modulation and the peculiar fluorescence properties of CQDs. This was the first ever working prototype of high information density MoCo, and we want to use the transmission of temperature variations as an example (the logic scheme is described in Fig. 37). The transmitter encodes temperature values by having at its disposal three discrete Graphene Quantum Dots, denoted as B-GQDs (Blue), C-GQDs (Cyan) and G-GQDs (Green) and mixtures of them. Of course, even in this case, pulses of information particles travel through the communication channel and therefore the fluid-dynamic properties of the environment must be clarified immediately.

**Graphene Quantum Dots enable digital communication  
through biological fluid**

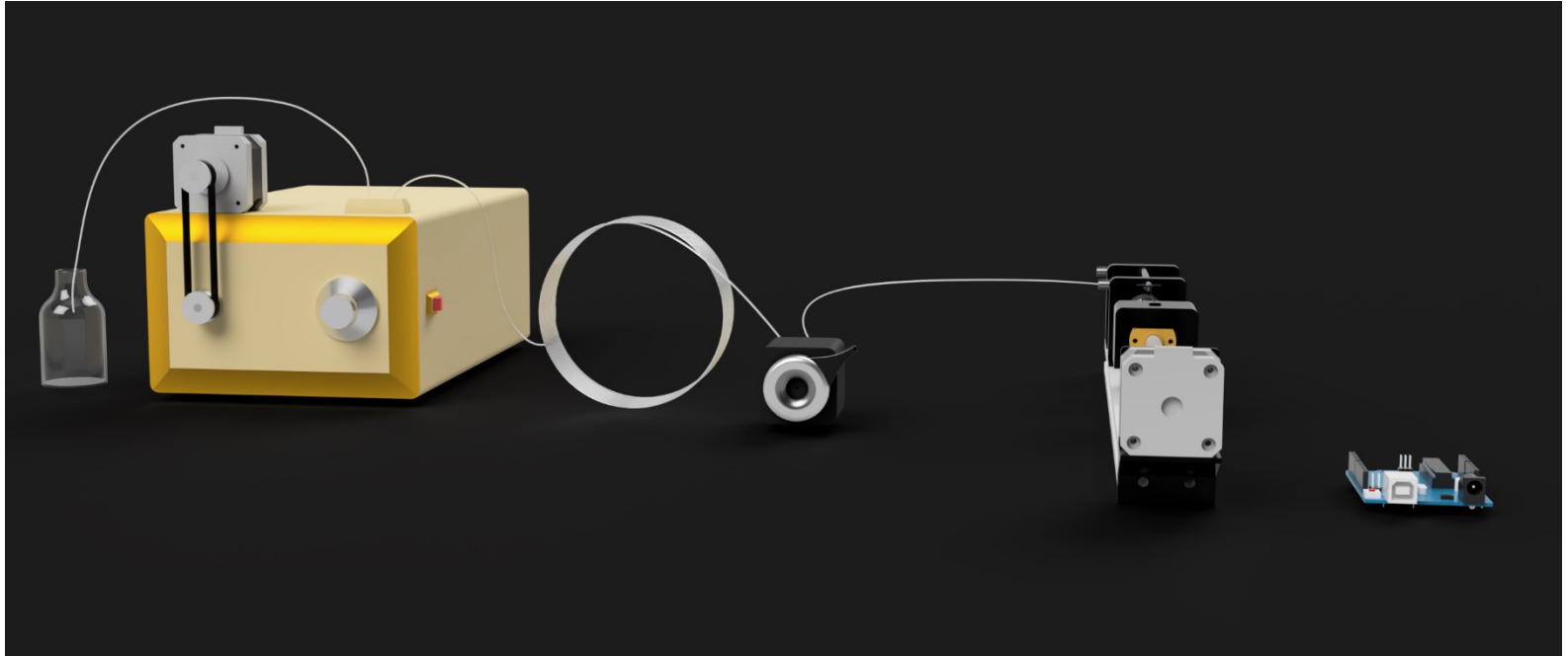


*Figure 38 - A schematic representation of the prototypal molecular communication system. To be noticed the motor that scan the emission wavelength.*

## 7.1 Materials and methods

Blue, cyan and green QDs were purchased (Aldrich) and used by diluting appropriate proportions in ultra-filtrated water (Millipore). Fluorescence characterization was carried out using a Cary fluorometer (Agilent) with an open slide at 5 nm. The high information density MoCo prototype was built in house and follows the scheme shown in Fig. 38. The control center consists of a standard PC interfaced to a microcontroller based on the stm32 chip (STMicroelectronics) for voltage readout, analogue-to-digital conversion and control of the stepper motor that moves the fluorometer reticle. The detection of the fluorescence emitted by the information particles was performed in flow by means of an HPLC detector (Shimadzu) modified to allow a time scan of the emission wavelength. The programming of the microcontroller was done *ad hoc* using the IDE provided by Arduino and the build libraries for STM32-based chips. A custom Python script was developed to interface the PC to the microcontroller and for data acquisition. The microfluidic communication channel consists of a piston pump controlled by a programmable stepper motor to ensure a constant flow rate and a Teflon tube connecting the transmitter and receiver. The piston pump is also designed in-house and built using a combination of purchased electrical and mechanical components (from RS Components) and components designed and 3D printed in PETG (Alfawise u30 pro). The simulations were performed by numerically solving differential equations using a Python script and the NumPy and FiPy libraries.<sup>145</sup>

## 7.2 Results and discussion

### 7.2.1 The Model

For the development of the entire research project, we focused on MoCo systems in the advection-diffusion regime, in which a transmitter releases pulses of information particles within the communication channel and through advective flow is transported and dispersed according to the laws of fluid dynamics. The variation of concentration in each area of the transport channel is a function of time and is described by the well-known advection-diffusion Eq. 20 (ADE).

---

$$\frac{\delta C}{\delta t} = \nabla \cdot (D \nabla C) - \nabla \cdot (vC) + S \quad \text{eq.20}$$

---

Where  $C$  ( $mol/L$ ) is the concentration of the chemical messenger, the time  $t$  ( $s$ ),  $D$  the coefficient for the dispersion contribution ( $mm^2/s$ ) from stochastic diffusion and turbulence caused by flow in the channel,  $v$  the flow velocity ( $m/s$ ) field extrapolated from the *Navier-Stokes* equations, and  $S$  is the source ( $mol/L$ ). Although no additional geometric and environmental parameters are considered, with the results described in the past few chapters it has been established that this simple model often provides reliable predictive results. The mesh in which the simulation is performed consists of a domain (relative to a pipe) with walls at zero slip velocity. The input of the velocity vector is allowed through one of the two openings and is parallel to the rotational symmetry axis of the domain and maintains a constant value there. The opposite opening is set as an outlet with a pressure of

1atm (ambient). The source of the molecular messengers is defined as the initial condition, i.e. when  $t=0$ . Obviously, the passage of matter through the closed walls of the domain is not allowed by the boundary conditions. Given the initial state  $S$  as probability 1, eq 21 is revised as follows:

---

$$\frac{\delta P}{\delta t} = \nabla \cdot (D\nabla P) - \nabla \cdot (vP) + P_{source} \quad \text{eq. 21}$$

---

$P(t)$  is the probability distribution of the messenger calculated by numerically solving eq. 17<sup>145,180</sup> and  $P_{source}$  is the initial condition. The geometry of the domain is as follows: 200 mm in length and 0.35 mm in radius, average velocity of 0.4 mm/s, diffusion coefficient of 1.2 mm<sup>2</sup>/s, and the initial width of the information particles pulse of 5 mm. The probability distribution of observing the molecular messenger at the receiver over time, starting from these initial conditions, is shown in Fig. 39a. As can be guessed, a pulse of information particles whose initial  $P(t)$  is worth 1, at the receiver becomes a broad, distorted signal of Gaussian-like shape. In a real MoCo apparatus, the concept of probability becomes proportional to the concentration of the messenger and depends on the time-dependent detection of one or more physicochemical properties of the messenger. In literature, the time-dependent measurement of fluorescence has been reported as a congenial physical property for CQDs.<sup>120,130,147,159,181</sup> Recall that fluorescence intensity is a function of concentration according to Eq. 13 and within certain limits (low concentration) the fluorescence intensity can be linearly correlated with it.<sup>102,182</sup> Under these conditions, then, the fluorescence intensity at the receiver as a

function of time for a single signal will have the same shape as Fig. 39a. However, a high-density MoCo system requires the release of different information particles to encode with n-MoSK modulation. Maintaining a fixed detection wavelength does not guarantee discrimination of the different symbols. Having a system capable of acquiring the entire fluorescence spectrum, instant by instant (CCD detectors coupled to prisms) one could record the entire information content of the symbol, correctly discriminating it from the others. To further clarify this concept, a 3D graph was developed (shown in Fig. 39c) representing what the receiver would "see" if it could acquire the entire fluorescence spectrum for each  $dt$  interval. This graph is obtained by merging a generic fluorescence spectrum (a Gaussian curve is simulated) shown in Fig. 39b and the same  $P(t)$  in Fig. 39a. Although the technology allows instantaneous multi-wavelength fluorescence detection with complex optical instrumentation, to miniaturize and simplify as much as possible, the model proposed here is based on cyclic scanning of the wavelength range as it is considered more easily achievable in an implanted miniaturized device. By better analyzing Fig. 39c, the red line drawn on the surface represents the cyclic scans along the wavelength axis following a  $\cos(\mu t)$  function. Finally, on the plane  $P(t)$  vs Time, the projection of the red line is shown, i.e., the signal detected by the receiver during the scan. It is clear that the shape of the detected signal has a complex dynamics and will depend on several parameters: i) the initial profile of  $P(t)$  obtained by solving the advection-diffusion equation, ii) the fluorescence spectrum of the information particles considered iii) the frequency at which the scanner oscillates iv) the phase between the position on the scanner wavelength axis and the time instant at which the



information particle is released from the transmitter and v) the flow velocity of the channel transport vector.

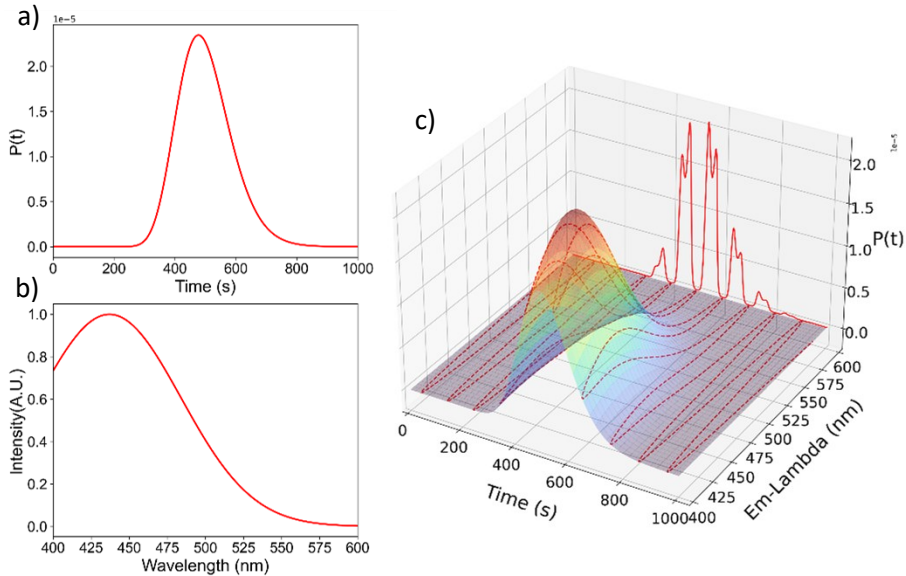


Figure 39 - (a) The probability distribution obtained solving the Advection Diffusion Equation using 200 mm path length, 0.35 mm radius, 0.4 mm/s flow velocity, 1.2 mm<sup>2</sup>/s diffusion coefficient and 5 mm initial pulse width. (b) Simulated fluorescent spectra approximated to a Gaussian with  $\mu = 437$  and  $\sigma = 47$ . (c) 3D plot of the signal reached by the receiver if it is able to acquire the entire spectra for each  $\delta t$  interval. The red line traced on the surface represents the back and forth explored by the receiver if it can scan the wavelengths according to a  $\cos(\mu t)$  function. On the plane  $P(t)$  vs Time is shown the projection of the red line obtained by several scans representing the signal that the receiver detects by scanning.

All these parameters were analyzed for model design optimization and the most interesting ones will be reported later. Fig. 40a shows the signals obtained from the simultaneous release of two

information particles with distinct fluorescence spectra (different Gaussian shapes). Both signals are markedly different including their respective Fourier transforms (see Fig. 40c). Fig. 40b shows the signals detected by the receiver when a single fluorescent information particle is released at different times. Again, the signals are not overlapping even though they are for the same substance. This is due to the phase-related parameter between scanner and release time. This makes it difficult to recognize the information particle if the transmitter and scanner are not perfectly programmed and synchronized. A similar effect occurs when the velocity of the transport medium varies, which is very common in the case of biological fluids, but this aspect will not be discussed in this chapter. However, the signals are superimposable in Fourier transform space (Fig. 40d), suggesting that it is therefore better to analyze the Fourier transform signal rather than the raw receiver signal. Furthermore, approximating the fluorescence spectra of information particles by a simple Gaussian curve is not representative of reality since real fluorescence spectra are not free of noise, not symmetric, and often have "shoulders" and "tails". Therefore, hybrid simulations were performed to build the model where, rather than the simulated fluorescence spectra, the experimental spectra of the three CQDs (shown in Fig. 41) were used, also considering the respective binary and ternary mixtures while keeping the excitation wavelength at 290 nm.

## Graphene Quantum Dots enable digital communication through biological fluid

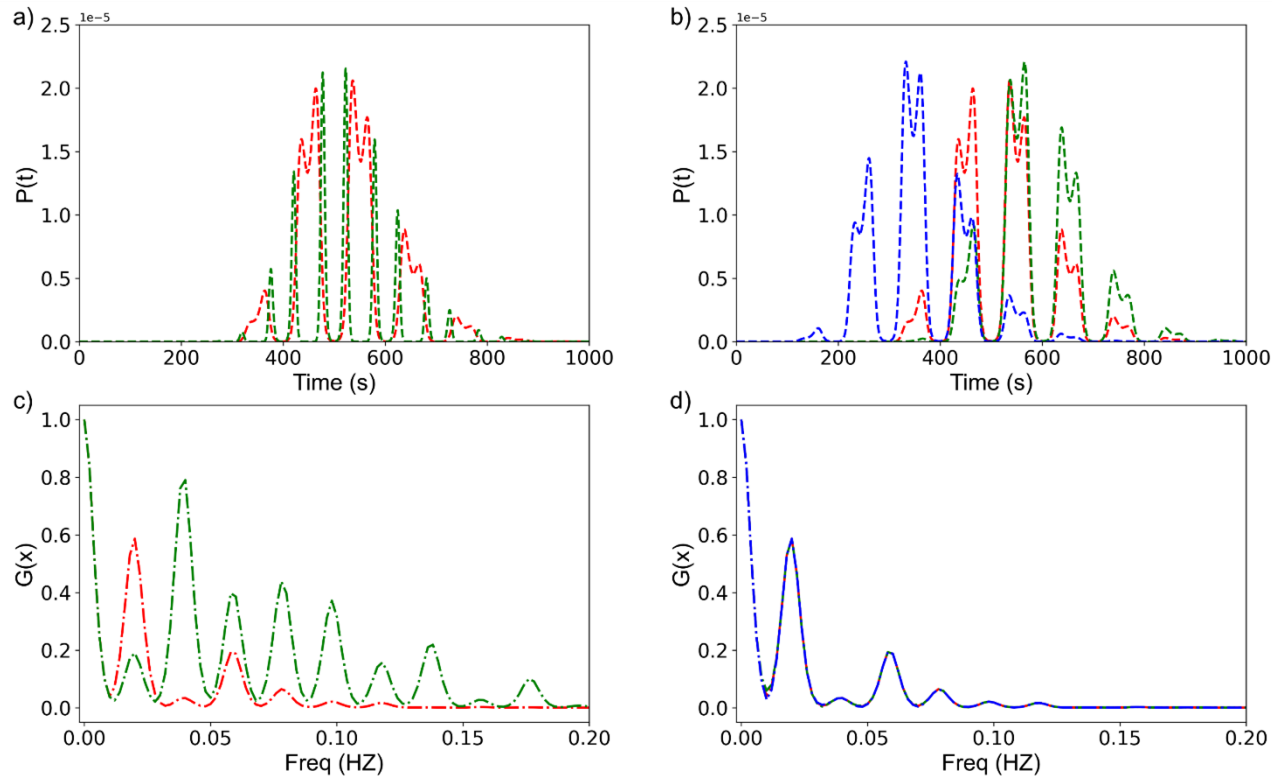
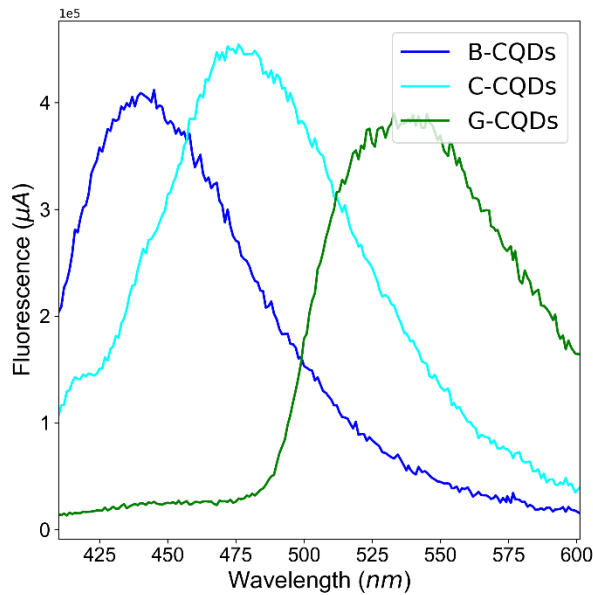


Figure 40 - (a) Signals obtained from simultaneously releasing of two information nanoparticles having distinct fluorescence spectra. (b) Fourier transformations of signals in (a). (c) Signals detected by the receiver when the same fluorescent information particle is released at different times. (d) Fourier transformations of signals in (c).



*Figure 41 - Experimental Fluorescent spectra of the three commercial GQDs at 290 nm excitation wavelength.*

Having available 3 different information particles (including mixtures), "the alphabet" will contain as many as 23 discrete symbols (including the no-signal symbol) that can be transferred per single time slot according to Eq. 22.

$$\text{Symbol content} = \begin{cases} \text{if } C_{(B-CQDs)} > k \text{ first bit is 1, than 0} \\ \text{if } C_{(C-CQDs)} > k \text{ second bit is 1, than 0} \\ \text{if } C_{(G-CQDs)} > k \text{ third bit is 1, than 0} \end{cases} \text{ eq.22}$$

Where  $C_x$  is the concentration of a specific information particle and  $k$  is an arbitrary threshold chosen as a function of receiver sensitivity. Fig. 42 gives some examples of how the signal looks if

## Graphene Quantum Dots enable digital communication through biological fluid

the scanning receiver receives four discrete symbols. The more complex the message is, the more difficult identification and recognition are, and this is compounded by the difficulties associated with imperfect synchronization between transmitter and detector. This leads to very different signal forms at the receiver, even when transmitting the same symbol. Applying MoCo in cyber-medicine implies fast and unambiguous recognition of the released symbol, so when the symbol travelling through biological fluids reaches the receiver, it must be recognized and decoded instantly. In order to discriminate the different symbols correctly, it is proposed to use machine learning to create a learning set instructing the control center and to improve the way the model works. To cover the full range of possible situations, a set of 35 simulations was built for 7 symbols and 5 different arrival times delayed by 33 seconds from each other. Each signal obtained was subsequently converted into Fourier space. From the tests carried out, we have found that, for the construction of an efficient data set for these types of signals, it is sufficient to consider the first four relative maxima of the Fourier transform, relative to the three GQDs and their respective frequencies, but excluding the frequency 0Hz. The starting matrix thus obtained will therefore be a 4x35 and is the basis of this learning system. In order to study the correlation between all the 35 signals (which we define as objects), described in the matrix of 4 relative maxima (defined instead as variables), multivariate principal component analysis (PCA)<sup>183</sup> was applied to reduce the number of variables and better visualize the families of signals. The strength of this type of analysis is the ability to create space consisting of perpendicular axes (called principal components) in the directions of maximum dispersion of the matrix points.

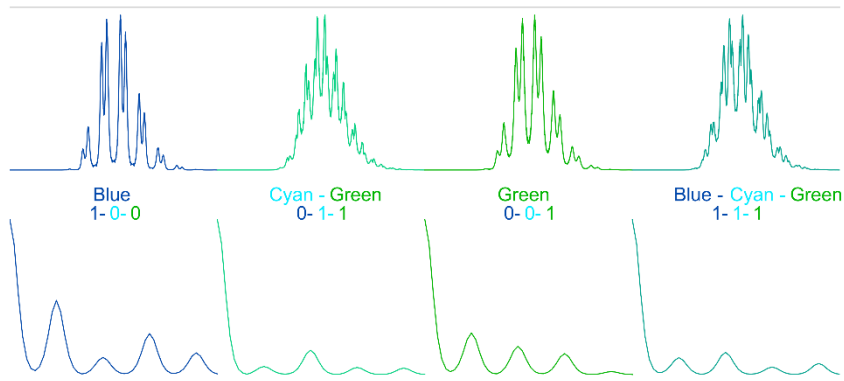


Figure 42 - Detected signals of GQDs by scanning receiver. From sx: B-GQDs, C\_G-GQDs mixture, G-GQDs and B\_C\_G-GQDs. In bottom of image, fourier transformation of the signals and respective binary encoding meaning according to Equation 18.

Potentially, an infinite number of principal components can be used but, given that the first principal component (PC1) follows the direction of maximum dispersion of the points, the second principal component (PC2) follows the direction of maximum dispersion of the points perpendicular to the direction of the first component, and so on, an increase in the number of axes allows the addition of further, but often useless, information. In relation to our problem, we focused on the analysis of the Scores-Plots obtained from this transformation of the variables. The objects clustered in the Scores-Plot are seen by the model as "correlated". The Scores-Plot in Fig. 43 shows in fact that with this approach we obtain 7 dense clusters, which are not immediately identifiable due to their proximity. The inset shows a zoom-in of the B\_C-GQDs cluster that confirms that the red spots in Fig. 43 are in fact clusters of points that are very close to each other.

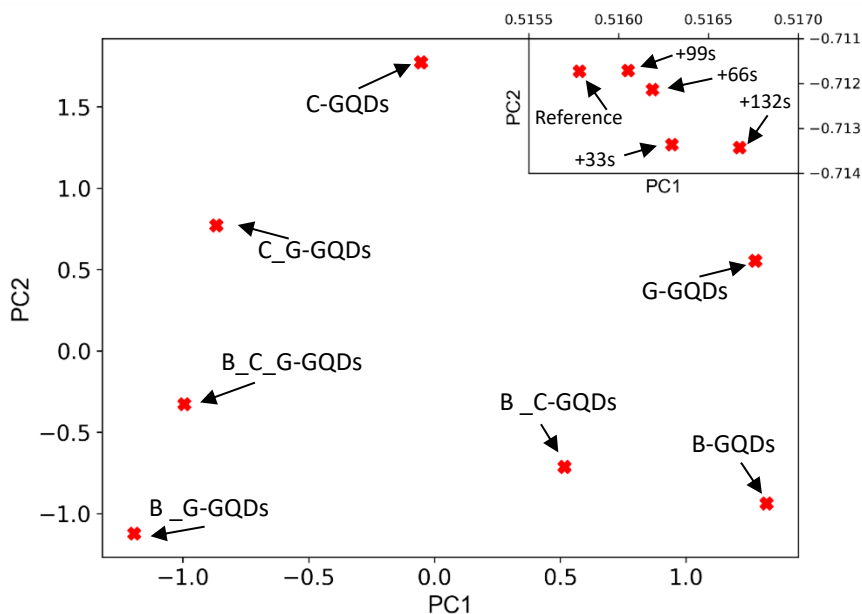


Figure 43 - Learning-plot obtained by PCA from the 35 simulated signals. We observe 7 dense clusters consisting of 5 points each. The inset represents a zoom near the cluster of B\_C- GQDs. "Reference" is the reference signal point compared to the other four that are out of phase of a  $\Delta T$  written in the figure itself.

Although the signal profile is relatively convolved, the use of the Fourier transform of the signal makes symbol identification easy and by means of only 2 PCs and the problem of non-synchronization is assumed to be negligible.

### 7.2.2 The experiment

Following the guidelines already seen in all the problems addressed during the writing of this dissertation, a test set, based

on the prototype platform for MoCo described above, was set up for the experimental testing of this decoding method. This was to reproduce in vitro what was in principle modelled to solve decoding in n-MoSK MoCo. As a first experimental step, the signals of all the CQDs used for this experiment (blue, cyan and green) were acquired by setting the scan at the same phase angle as in the simulations and reporting the signal obtained in Fig. 44a. The logic described in eq. 18 was therefore associated representing several specific sequences of bits 1 and 0. Each signal has a shape dependent on the fluorescence spectrum of the starting solution, a complex shape but of the same type seen with the previous simulations. The treatment of the data subsequently underwent the same study done with the simulated data: the first four relative maxima of the normalized Fourier transform were extrapolated, excluding the frequency 0, and finally the experimental dataset was fitted with the model relative to the learning dataset (already shown in Fig. 43). Fig. 44b shows the PCA Score-Plot hosting these experimental data as test dataset. In the first analysis we see that the model is more predictive for mixtures of two or more GQDs as the fluorescence spectra cover a larger portion of the analyzed spectrum region. Small experimental errors, resulting from the DIY nature of the prototype, are emphasized with narrower fluorescence spectra and with B-GQDs there is a particularly significant difference along PC2 of the learning plot. By implementing a predictive method with autolearning, perhaps based on artificial intelligence, one would expect more accurate and reliable symbol recognition. However, this will be the subject of future projects, perhaps more specific, to be developed in collaboration with scientists with expertise in electronics and computer science. Nevertheless, these results are



## Graphene Quantum Dots enable digital communication through biological fluid

to be considered encouraging, driving the applications of this innovative method of high-density information MoCo. In line with the usual application assumptions for MoCo, this modulation method finds its ideal application in the field of information transfer via implanted physiological sensors and actuators,<sup>159</sup> which has already been discussed in the previous chapter. Having a more refined alphabet at our disposal, one can think of exploiting high information density MoCo in sensory monitoring, control and possible intervention through drug administration. For example, in monitoring tissue temperature and the possible onset of bacterial inflammation. We report a case history known in the literature to be used as a starting point for application of this modulation method: HMEC-1 cells (Human Dermal Microvascular Endothelial Cell Line) show temperature variations in the presence of LPS (lipopolysaccharides) of the bacterial shell. The measured changes in  $\Delta T$ <sup>184</sup> are of the order of magnitude of approximately  $\pm 0.2^\circ\text{C}$ ,  $\pm 0.4^\circ\text{C}$ ,  $\pm 0.8^\circ\text{C}$  and  $\pm 1.2^\circ\text{C}$  with increasing concentrations of LPS. Imagine having an implanted temperature sensor that could constantly communicate significant temperature changes, corresponding to the presence of LPS interacting with the cell. Imagine also that this communication occurs through the release of information particles within the human circulatory system (the communication channel). A receiver located elsewhere in the body (maybe peripheral and more easily accessible) would decode the information sent by the temperature sensor and trigger the antibiotic release if necessary.

## Graphene Quantum Dots enable digital communication through biological fluid

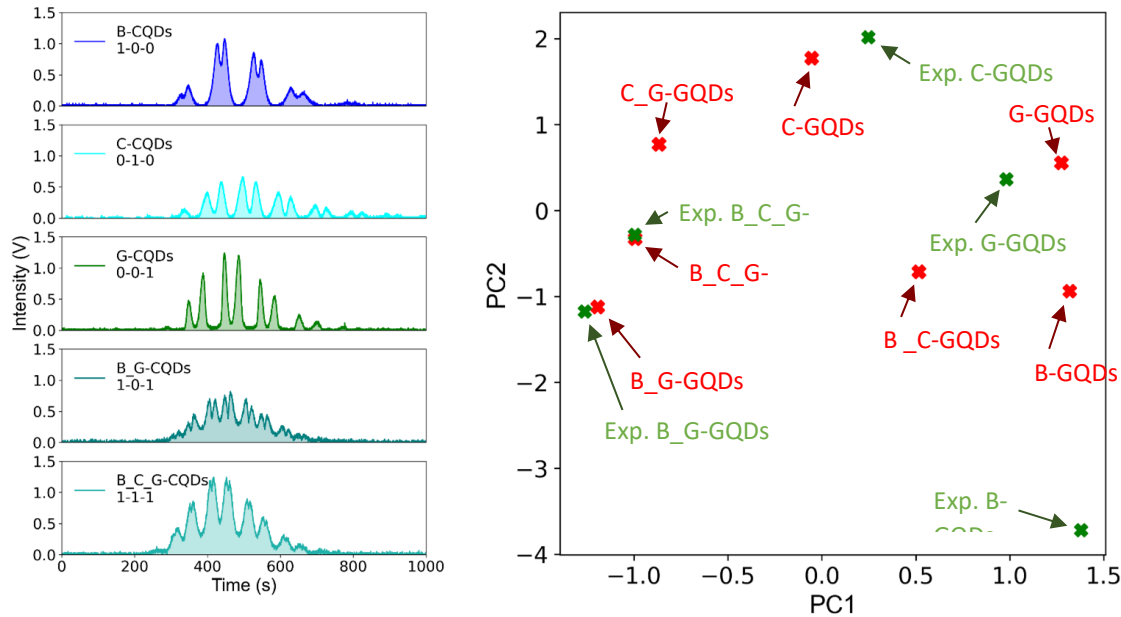


Figure 44 - (a) Experimental signals detected by scanning receiver. From Top to bottom: B-GQDs, C-GQDs, G-GQDs, B\_G-GQDs mix, B\_C\_G-GQDs mix and respective binary encoding meaning according to equation 18. (b) Fit plot of experimental signals. In blue the points relative to the learning-plot previously obtained by the simulated signals. In orange the points relative to the experimental signals fitted on the learning dataset in Fig. 43.

## Graphene Quantum Dots enable digital communication through biological fluid

In this context, an OOK modulation method based on binary coding is not applicable because, in addition to the physical limitation resulting from the speed of flow determined by the physiological state of the individual, it would require a high number of symbols to transfer complex information. Again, for the sake of example, Fig. 45a shows the number of signals required to send information with the OOK modulation method and how long it takes to transfer a single  $\Delta T$  value if encoded in ASCII code (the one typically used in common language). Our proposed high information density MoCo method involves the use of three CQDs, including mixtures, having 8 discrete symbols available per single release, pushing octal coding. The benefit of an octal encoding is considerable due to the reduction in the number of symbols to be sent to transfer the message. Considering that we are dealing with a highly specific situation, it is reasonable to think of implementing an encoding made specifically for the system. This allows, not only to further reduce the number of symbols to be transferred per  $\Delta T$  which must be encoded, but also to sacrifice some of the symbols available for status control functions, e.g. a system status check. Table 1 shows the proposed logic: the PCA results obtained earlier are the basis. The B\_C\_G-QQDs show a lower reading error, so they have been chosen for the most frequent type of information, i.e. the check-status.

## Graphene Quantum Dots enable digital communication through biological fluid

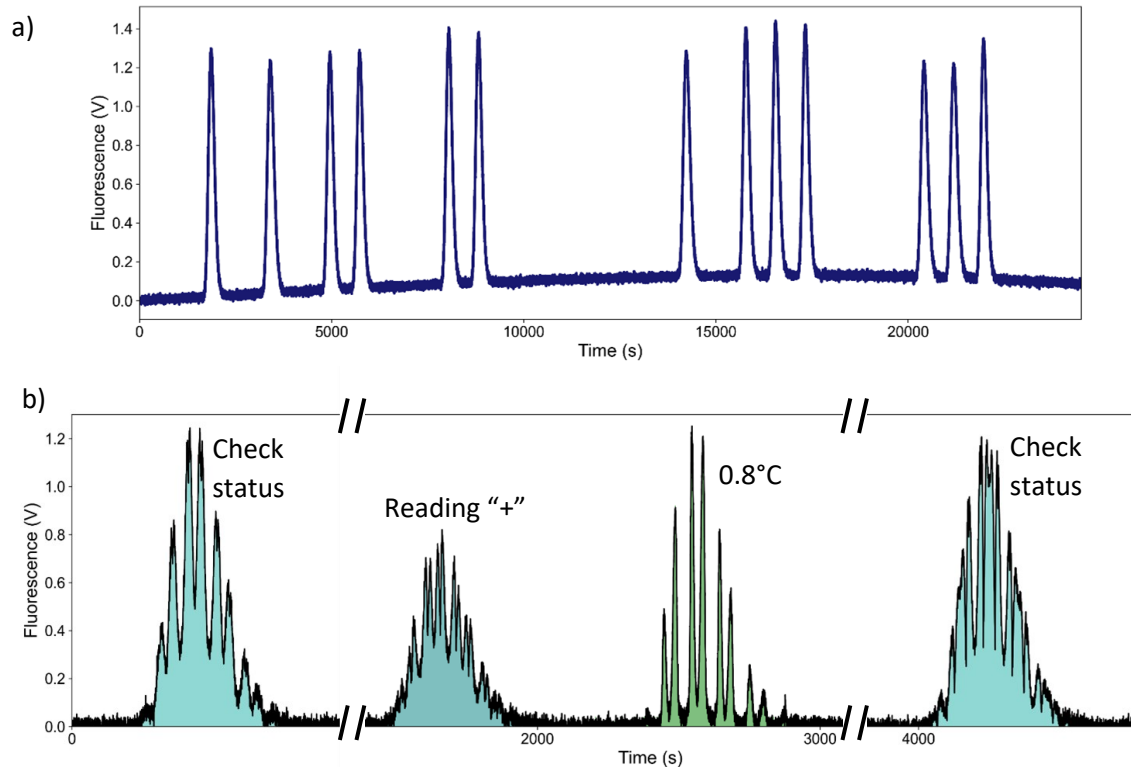


Figure 45 - (a) Transfer of the value  $p$  0.8, in reference to a temperature variation, using ASCII language in binary coding. (b) Transfer of the value  $p$  0.8, using a specific encoding method described in Table 1. It should be noted that the signals labeled with "check status" are not useful for the transfer of information but are used for a check of the state of operation of the communication.

<b>Symbols</b>	<b>Coded Information</b>
Null	No signal
B-GQDs	0.2°C
C-GQDs	0.4°C
G-GQDs	0.8°C
B_C-GQDs	1.2°C
B_G-GQDs	Reading positive variation
C_G-GQDs	Reading negative variation
B_C_G-GQDs	Checking Status

*Table 1 - Symbols encoding table for HMEC-1 cell monitoring*

The C\_G-GQDs and B\_G-GQDs contain the information of the start of the reading and the positive and negative temperature change, respectively. In the light of the temperature variations being considered discrete, the other combinations contain the information of the absolute value of the temperature variation. The example can be found in Fig. 45b, where the complete transmission of the temperature variation information is shown following the specific encoding described in Table 1. Specifically, the transmission of  $DT=+0.8$ . As accepted, through the release of B\_C\_G-GQDs, the periodic "control" signals necessary to verify the correct working status of the communication channel are transferred and are indicated with the blue color. In the time window between 1500 and 3000 s all the information to be sent is present. The first signal in this interval represents the start of the reading, indicating a positive variation and obtained by releasing the B\_G-GQDs. The absolute value of the variation, 0.8°C, is finally encoded in the signal obtained by releasing the G-

GQDs. Thus, comparing the OOK modulation with the optimized n-MoSK, keeping all other experimental parameters constant, approximately 25,000 s (7 h) binary-encoded OOK modulation is required (see Fig. 45a). The need for more complex modulation methods is obvious, and the one presented here is just one example of how to exploit the chemical properties of carbon-based fluorescent nanoparticles for the development of *ad hoc* codecs tailored to the system, significantly reducing the message transmission time. Following the coding described in Table 1, a transmission time of only 1500s was obtained (from the 1500s and 3000s seen in Fig. 45b). The time saved allows other symbols to be used for error checking or other operational functions. Fig. 45b (signal at 500s and signal at 4250s) gives an example of the transmission of control information. Further improvements and refinements are certainly possible, and the model is far from perfect. It is not the purpose of this experiment to obtain a perfect prototype, but we try to convey the idea of how to apply information-dense MoCo in bio-medical contexts.

### 7.3 Conclusions

The development of the high information density MoCo model, based on n-MoSK modulation, emerged from the need to increase the baud rate, which is slow due to the nature of the communication channels in MoCo. Rather than optimizing the actual transport process, which is not always externally controllable, it was decided to increase the density of information carried by molecular messengers by simultaneously employing and detecting messengers with known physico-chemical

## Graphene Quantum Dots enable digital communication through biological fluid

properties. Three fluorescent CQDs, characterized by three different fluorescence spectra, were used individually or mixed to obtain  $2^3$  symbols to be used when needed. Signal processing methods (Fourier transform) and statistical methods (Principal Components Analysis) allow us to discriminate the signals generated by these fluorescent substances, even by making the detection method unconventional. We denote that by employing a simple machine learning approach, it is possible to overcome any interference/artifice caused by imperfect synchronization between source and detector and train a model for increasingly reliable and rapid recognition. In addition, increasing the number of symbols available allows the application of the most suitable coding: from an n-ary system to communicate universally at the expense of baud rate, to an *ad hoc* coding to be tailored to the system in which the concept of MoCo is to be applied.

## Chapter 8

### Fluorescent nanoparticles for secure communication among implantable medical devices

Throughout the research project, the focus was mainly on the concept of molecular messengers and signal modulation to optimize the baud rate of the communication channel. However, what is still missing is a secure interconnection between implanted biodevices.<sup>185</sup> There is no secure platform for information exchange<sup>186</sup> required to turn isolated bionic devices into a part of a connected system that communicates, working in unison, under the control of a rational central system. The problem is global and of great impact, suffice it to say that a total of 34.2 million people of all ages - or 10.5% of the US population - had diabetes.<sup>187</sup> To help them, a growing number (more than 300,000 units) of continuous glucose monitoring and insulin delivery devices are being used by diabetic patients to deliver insulin into their circulatory system. This assembly is called a bionic pancreas and is also called an *automatic closed-loop insulin delivery system*.<sup>188</sup> To function, it requires the interaction of three primary components that are wirelessly interconnected. A real-time continuous glucose monitoring sensor inserted into the subcutaneous space,<sup>189</sup> which measures glucose concentrations in the interstitial fluid and wirelessly sends information about the detected glucose concentrations to a device via a transmitter that houses the dosing algorithm that calculates the correct amount of insulin to be delivered based on the prediction of glucose levels, with the goal of maintaining blood glucose levels within a specific target range. Finally, it wirelessly communicates instructions to an insulin<sup>190</sup> or glucagon pump<sup>191</sup> directed by the dosing algorithm,



## Fluorescent nanoparticles for secure communication among implantable medical devices

which delivers insulin through a subcutaneous cannula. These implantable devices must be reliable, safe and secure.<sup>192</sup> Intracorporeal communication between implantable devices must take place in "hostile" environments because they are subject to fraudulent attacks or eavesdropping, with significant safety concerns for patients. The availability of new secure communication methods is of strategic importance in this emerging field of application. As history has amply demonstrated, from Caesar's cipher in Roman times to the German military's infamous Enigma machine cleverly deciphered by Polish mathematicians, having the ability to establish encrypted communication in hostile environments can make the difference between triumphing or succumbing. Although intrinsically safer than the use of electromagnetic waves, since it generates a signal that is difficult to intercept, even MoCo requires a minimum level of security from the outset to prevent possible attacks on the communication system. In order to allow for the effective and safe exchange of information between the transmitter and the receiver, an information carrier must be tolerated by the environment in which the transmitter emits it, and secondly, it must possess a property that allows for agile detection by the receiver, selectively revealing its presence relative to other components flowing in the transport channel.<sup>93</sup> It is clear that our strategy is now based on the use of carbon-based fluorescent nanoparticles as information carriers. The aim of this part of the work is to demonstrate that such information nanoparticles enable safe communication between implanted biodevices. Although many modulations have been theorised, it soon becomes apparent that the main limiting factor of MoCo is undoubtedly the low bandwidth due to the restrictions imposed by the transport speed of the information particles, which depends directly on the fluid-dynamic characteristics of the

transport medium. They cannot travel faster than the transport fluid, stochastic diffusion being a very slow process. The strategy addressed in chapter 7 to solve this problem consists in increasing the density of the information encoded within the single release of information particles. Evolved organisms encapsulate the entire message to be transmitted in a single release of the messenger in the biological transport fluid. This implies that the transfer of information does not involve the release of successive, appropriately modulated signals (e.g. using binary coding), but rather the release of a specific molecule, such as a hormone, that carries all the information needed to activate a specific biochemical response. In the work dealt with in the previous chapter, chemically different nanoparticles (despite being very similar carbon structures) with different emission spectra were used. The challenge to be faced in this work is to devise a modulation that allows us to vary the shape of the signal detected by the receiver by assigning a precise message to each shape. Compared to the previous one, the modulation proposed here is extremely simple to implement since it can be obtained by using a single type of "information particles" but adding a substance (also tolerated by the environment in which it travels) that locally alters a physical property of the carrier fluid, which is the viscosity.

## 8.1 Preliminary Results

To know the fate of the information nanoparticles from the transmitter to the receiver it is necessary to solve Eq. 2, albeit numerically. In the case under investigation, the reactivity is omitted and the channel is represented by a hypothetical cylinder vessel of micrometric diameter (of radius  $r$ ) and length ( $L$ ) of the order of tens of centimeters in which the laminar regime is in

force. The fluid, having viscosity  $\eta$ , is conducted through the straight and rigid channel, imposing a pressure difference ( $\Delta P$ ) between the two ends. Under these conditions, Poiseuille's law returns us the velocity profile, i.e. the velocities  $v(r)$  at different radial positions between the center ( $r = 0$ ) and the wall ( $r = R$ ), inside a capillary or a cylindrical channel, is given by:

---

$$v(r) = \frac{\Delta P}{4\eta L} (R^2 - r^2) \quad \text{eq.23}$$

---

Similar considerations can be made for channels that are more complex in geometry and in the case of non-perfectly laminar flows such as human blood. In this case, it will be necessary to solve the differential equations governing the motion to find the velocity field. From eq. 19 the Poiseuille velocity profile for ducts with very small  $R$  is parabolic, with the maximum velocity at the center of the duct. This will imply that the concentration profile of the information nanoparticles at the detector, and consequently the shape of the symbol signal received by the receiver, resulting from the solution of eq. 2 will not always be of Gaussian type. As far as the diffusion coefficient is concerned, the Stokes-Einstein equation is a good approximation for solving Eq. 2:

---

$$D_{IP} = \frac{k_B T}{6\pi\eta r_{IN}} \quad \text{eq.24}$$

---

where  $k_B$  is the Boltzmann constant,  $T$  is the temperature,  $r_{IN}$  is the hydrodynamic radius of the information nanoparticles. Figure 46 shows simulation results for a microfluidic channel having  $R = 0.1$  mm and  $L = R \cdot 100$ . Assuming that the value of the diffusion

## Fluorescent nanoparticles for secure communication among implantable medical devices

coefficient of the information nanoparticles is isotropic, it is possible to break it down into two contributions: axial and transverse (or radial) to the flow. Since there is advection along the flow direction, the axial contribution of diffusion can be considered negligible.

---

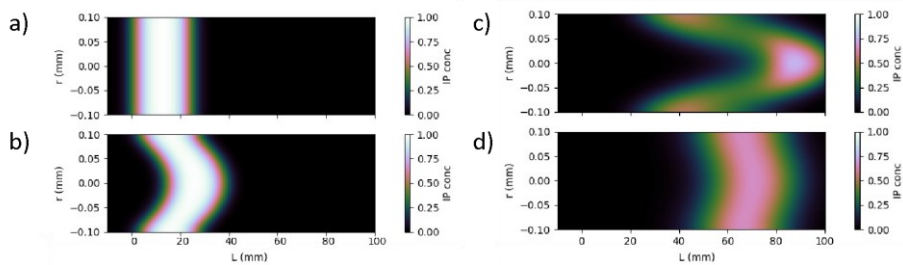


Figure 46 - False-color images resulting from the simulations; (a) concentration of information nanoparticles present in the tube at the initial simulation time ( $t=0$ ); (b) effect of flow velocity on the spatial distribution of information nanoparticles when subjected to laminar flow inside a narrow-diameter tube under zero-slip conditions at the walls; (c) spatial distribution of nanoparticles with low diffusion coefficient ( $3 \cdot 10^{-12} \text{ m}^2/\text{s}$ ) after traveling through the entire tube; (d) same simulation conditions but with diffusion coefficient 10 times higher.

---

Transversely, on the other hand, there is no movement of the carrier, so the only contribution to the movement of the information nanoparticles is attributable to diffusion stimulated by the transverse concentration gradient, if any. At the beginning of the process, when the plug of information nanoparticles has just been released and is extremely compact, no transverse gradient is present (Fig. 46a). As it continues along its path due to the velocity flow given by Eq. 19, the compact plug will assume a

shape that we can define as "arrow-shaped" (Fig. 46b) generating soon a transverse concentration gradient between the area where the carrier is pure and the two interfaces with the regions of high particle concentration, both the front (arrow head) and the back (arrow tails). If the diffusion coefficient is relatively low and the speed and length of the channel are such that the receiver can be reached quickly, then the transmitted signal will have a strongly asymmetrical shape. The receiver will detect in the first phase a concentration of information nanoparticles relative to the central part of the tube characterized by the highest transport speed. This will lead to the formation of an initial peak followed by a long tail relating to the arrival at the destination of the nanoparticles that have traveled in the areas closest to the walls, and therefore slower. The concentration profile of the nanoparticles is characterized by a faster part (front) in which the concentration is greater at the center of the channel than at the walls, and a later part (back) in which the concentration is greater at the walls of the channel than at the center. Relative to this, the total effect of transverse diffusion is to slow down the anterior interface and speed up the posterior interface, thus keeping the concentration distribution more symmetrical along the axial direction (Fig46c-d). This phenomenon is known as Taylor effect.<sup>193</sup> An increase in the diffusion coefficient or a decrease in the flow velocity affects the dispersion of the substance in a microfluidic channel, in the same way, i.e. they increase the Taylor effect. Figure 47a shows the signal detected by the receiver as the diffusion coefficient changes under the same conditions of velocity and channel size. The effect on the shape of the received signal is very clear. One could, therefore, exploit this variation to modulate the signal by assigning a different symbol to each shape. From an experimental point of view, to vary the diffusion coefficient, it is necessary to act, as shown by eq. 24, on the viscosity of the flow.

## Fluorescent nanoparticles for secure communication among implantable medical devices

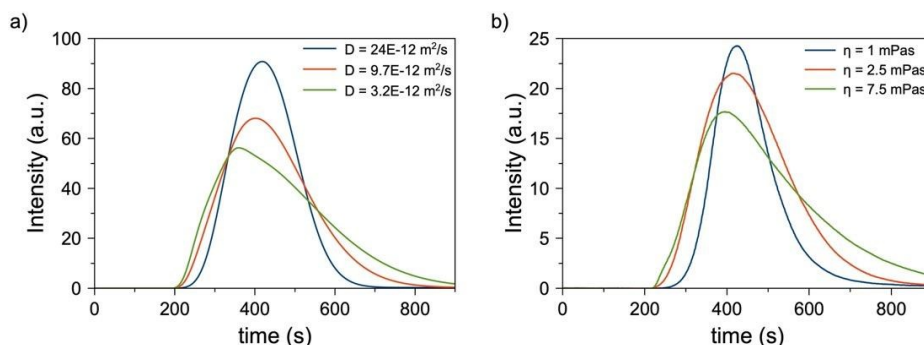


Figure 47 -(a) Signal detected by a receiver placed at a distance of 200 mm from the release point as obtained from simulations. Colors are associated with different values of diffusion coefficient; (b) Relevant fluorescence signal at 200 mm distance acquired during MoCo experiments. Colors are associated with different viscosity values.

Figure 47b shows the profile of the fluorescence signals detected by the receiver as the viscosity of the fluid changes when a single plug of information nanoparticles is released by the transmitter. The variation of the signal shape is in line with the theoretical predictions (Figure 47a) although less recognizable, compared to the simulation, because experimentally the diffusion coefficient was not significantly changed. To reach this condition, it would be necessary to have large differences in viscosity. However, this will cause limiting effects on the operating conditions, since the pressures necessary to guarantee constant flow velocity even at high viscosities become prohibitive and the solubility of the particles is not always guaranteed by varying this fluid property so much. However, the results obtained allow us to confirm the theoretical ones. Signal modulation by varying the viscosity affecting the diffusion coefficient of information nanoparticles has been conceptualized, described theoretically, and experimentally verified for the first time. We call this modulation *Viscosity Shift*

## Fluorescent nanoparticles for secure communication among implantable medical devices

*Keying* (VSK). This is a modulation unique to MoCo that has no equivalence in classical electromagnetic wave communication. Although practicable in this form, VSK modulation is difficult to apply "in operando" since it can be cumbersome to vary the viscosity of the whole flow of the channel in which information particles are transported. However, since VSK modulation is physically based on the ability to control the asymmetry of the signal at the detector will be sufficient to modify only the viscosity of the injected particles-plug, exploiting the instabilities of the interfaces between miscible liquids having different chemical-physical properties, such as the well-known Rayleigh-Taylor instability.<sup>196</sup> Therefore, the direction to follow for the development of viscosity-modulated MoCo will be to govern the shape of the fluorescence signal VS time by means of theoretical-experimental studies and exploit the viscosity value of the information particles solution, as a cryptographic key. Necessary to establish an encrypted connection between transmitter and receiver, in a context of MoCo between implanted biodevices.

## Chapter 9

### Final conclusions and future perspective

In this long project focused on our vision of molecular communication, several independent issues were addressed with a common goal: to optimize the process of transmitting a message through a biological channel, using carbon-based fluorescent nanoparticles as information particles, making it robust and efficient. The concept of MoCo is extremely wide and varied; therefore, it is crucial to understand on which area is the focus. We have chosen to focus the project on biotechnology, as it is a fast-growing field and a new frontier in cybernetics and cyber medicine. In this context, there are mainly three aspects to be addressed: i) nanodevices to be implanted in the biological system, acting as sensors, transmitters, or receivers; ii) connecting these devices by means of MoCo, exploiting already existing biological channels such as blood or lymphatic flow; iii) solving problems regarding the biocompatibility of nanodevices and information particles with the host biological system. Here, point ii) was mostly discussed, since the focus was mainly on the information particle, and then solutions to some critical aspects of transport in MoCo were proposed.

In chapter 2, an in-depth study of nanoparticles in the context of MoCo was addressed, giving an overview of how the scientific community has proposed their use, both in terms of molecular messengers and as an integral part of devices. Specifically, our proposal for a molecular messenger is based on fluorescent carbon nanoparticles. The reason for this is quickly stated: the synthesis techniques are simple and green, surface engineering is



possible to provide different chemical and physical properties, and optical properties can be modulated by doping or functionalization.

In chapter 3, a focus on the green economy was given by proposing the synthesis of carbon quantum dots from unsold lemon waste and how this allows to give value back to a product that otherwise would have been thrown away. Carbon quantum dots have proved to be efficient for applications in MoCo. In the following chapters we got to the heart of the research project, tackling particularly difficult problems arising from the natural physical phenomena involved in the transport of a substance in a flow.

In Chapter 4, we demonstrated that the use of self-assembling fluorescent nanoparticles makes it possible to reduce the phenomena of dispersion in microfluidic systems, thanks to the dynamism of supramolecular assemblies catalyzed by the presence of a cross-linking molecule (NDI). The results obtained show that fluorescent carbon nanoparticles, in the absence of the crosslinker, give a signal with lower intensity and much wider and more dispersed. The signal obtained in the presence of the crosslinker is narrow and intense, therefore more easily detectable and less subjected to ISI phenomena.

Chapter 5 deals with a different issue from the problem of dispersion, namely the problem of synchronization between transmitter and receiver. These two components of a MoCo system must be synchronized in order to communicate correctly using the common CSK and MoSK modulation methods. A new modulation method called Reaction Shift Keying (RSK) has been modelled and subsequently validated. It uses a modulant to

encode the message and allows information to be transmitted between transmitter and receiver without the need to synchronize the clock between them. This result is important for the biological field because the environments in which the information particles must propagate do not allow the speed of the flow to be controlled, and furthermore, it is not always predictable and depends on the physiological state of the individual.

In Chapter 6, a molecular-IoT prototype system using MoCo is presented. Three-sensor array measures certain physiological parameters: temperature, pH and electrical conductivity. A control center located upstream of the system reads the data obtained from the sensors and activates many actuators in order to adjust the physiological parameters. The actuation command does not use an electrical connection between the control center and the actuators. Instead, communication takes place via a microfluidic communication channel and the use of three different CQDs as information particles. A statistical model has been developed to optimize the baud rate of the communication channel without introducing reading errors caused by the ISI.

Chapter 7 proposes a solution to the slowness of MoCo. In fact, the transmission of a complex message takes a long time, even hours, since the transport speed of the information particles depends on the speed of the flow itself. As already mentioned, controlling the speed of the flow in a biological system is almost never possible and, moreover, it has been shown that excessive speeds cause greater dispersion of the pulse of information particles during transport. In this chapter we propose to increase the information content within the transmitted symbol by

exploiting three CQDs with different fluorescence spectra. In this way it is possible to insert three bits in each symbol instead of just one, or to build *ad hoc* coding systems for each communication system. The difficulty in this case is the correct detection of the signal, due to the presence of eight different symbols ( $2^3$ ). For this purpose, we installed a temporal scanner of the fluorescence wavelength in the receiver and by means of a light statistical method (consisting of a Fourier transform and a principal component analysis) the correct discrimination between one symbol and another is guaranteed.

Finally, in Chapter 8 a new and innovative modulation method is proposed, based on the fluid-dynamic properties of information particles, to achieve high-density MoCo. This is a remarkable achievement as it would allow a single type of information particle to be used to encode an innumerable number of symbols. Just by varying the viscosity of the carrier, it is possible to change the shape of the signal that the receiver picks up. This method of modulation is called Viscosity Shift Keying (VSK). This work is still at an early stage and still requires several studies and optimizations, especially for the application phase, which will be carried out in the years to come.

As MoCo is an open project and still in its infancy, the prospects for development and growth are high. Every aspect of it, even if already studied, requires refinement and optimization. It is a branch of communication science that requires interdisciplinary skills; therefore, collaboration between people with different skills is desirable for future projects.

### 9.1 Ongoing works

In order to focus on the aspect investigated in this work, namely MoCo in biological environments by means of fluid, and considering the experience gained, some aspects that are probably a priority to be explored in future works are proposed.

#### 9.1.1 Information particles

The key to success in MoCo is certainly the information particle. It represents the particle that contains the information that is to be written, transported and subsequently read. Although the use of fluorescent carbon nanoparticles is proposed here, given their physical and chemical properties, there are not many alternatives to them in the literature. A possible future perspective concerns the use of information particles of a different nature. In this connection, one could consider particles that allow the detection of several physical properties simultaneously and thus further increase in the density of information that can be written inside. Further ideas include the possibility of writing the message during transport, using photosensitive molecular messengers<sup>40,194</sup> and the use of a laser. The transport can be oriented and focused using magnetic particles and small electric fields, to greatly reduce scattering, especially over long distances.

### 9.1.2 Innovative receivers

To date, classic bench-top transducers such as mass spectrometers<sup>178</sup> or optical detection systems such as fluorimeters have been used as receivers for MoCo. One factor on which it is necessary to work is the detection and decoding of the information particles reaching the receiver. The use of bulky techniques with moving or shock-sensitive parts is not suitable for implantation as devices in biological systems, and the high-power consumption does not suit portability. The unreliability and probability of failure of essential components would be high; therefore, different detection solutions should be sought. By further exploiting the optical properties, it is possible to consider moving the actual receiver away from the detection zone, using the optical microfibers as a waveguide and then processing the signal in a different, less critical or even external zone of the biological system. Another innovative solution in this field would be to use electrolytic FETs, known as EGOFETs,<sup>195</sup> for electrical signal transduction. They behave like FETs in which the modulation of the gate depends on the electrolytic potential present in the dielectric. Working in liquid systems, if placed in a flow, they would ensure the detection of the information particle as it passes through if it had a charge.

### 9.1.3 New modulation methods

The choice of modulation method is complex and system-dependent, but it has a clear purpose: to increase the baud rate of the communication channel, without introducing errors or

noise. As explained in the other two points, the information particle and the detection system are critical in the optimization of the MoCo system. Unfortunately, it is not enough to have a very good detector and a very good information particle; the communication channel, especially if it is biological in nature, is difficult to control. In addition to the other components of the MoCo system, there must be an excellent modulation method as well, which enables the rapid and safe transfer of as many symbols as possible, and which is adapted to the chemical and physical characteristics of the communication channel, the information particles and the receiver. Only a balance between the logic and the hardware makes it possible to build a robust and functional system. The community of researchers with expertise in telecommunication is asked to help in this regard, since it is possible to draw on a great deal of information for the logical part and thus experiment with or adapt increasingly sophisticated and reliable modulation methods.

## References

1. Agyapong, P., Iwamura, M., Staehle, D., Kiess, W. & Benjebbour, A. Design considerations for a 5G network architecture. *IEEE Commun. Mag.* **52**, 65–75 (2014).
2. Gong, Y. Speech recognition in noisy environments: A survey. *Speech Commun.* **16**, 261–291 (1995).
3. Goel, P. & Chandra, M. FPGA Implementation of Adaptive Filtering Algorithms for Noise Cancellation—A Technical Survey. in *2015 International Conference on Advanced Computing and Communication Systems* 517–526 (IEEE, 2019). doi:10.1007/978-981-13-7091-5\_42.
4. Deb, A., Kar, A. & Chandra, M. Advanced linear adaptive filtering methods for active noise control: A technical survey. in *2015 International Conference on Advanced Computing and Communication Systems* 1–5 (IEEE, 2015). doi:10.1109/ICACCS.2015.7324088.
5. Shannon, C. E. A Mathematical Theory of Communication. *Bell Syst. Tech. J.* **27**, 379–423 (1948).
6. Holtz, J. Pulsewidth modulation—a survey. *IEEE Trans. Ind. Electron.* **39**, 410–420 (1992).
7. Oluseye, A. & Robert, O. MODULATION METHODS EMPLOYED IN DIGITAL COMMUNICATION : An Analysis. 85–93 (2012).
8. Jeevanandam, J., Barhoum, A., Chan, Y. S., Dufresne, A. & Danquah, M. K. Review on nanoparticles and nanostructured materials: History, sources, toxicity and regulations. *Beilstein J. Nanotechnol.* **9**, 1050–1074 (2018).
9. Dreyer, D. R., Ruoff, R. S. & Bielawski, C. W. From conception to realization: An historical account of graphene and some perspectives for its future. *Angew. Chemie - Int. Ed.* **49**, 9336–9344 (2010).
10. Thostenson, E. T., Ren, Z. & Chou, T.-W. Advances in the science and technology of carbon nanotubes and their composites: a review. *Compos. Sci. Technol.* **61**, 1899–1912 (2001).
11. Mohanraj, V. J. & Chen, Y. Nanoparticles - A review. *Trop. J. Pharm. Res.* **5**, 561–573 (2007).
12. Baig, N., Kammakam, I. & Falath, W. Nanomaterials: a review of synthesis methods, properties, recent progress, and challenges. *Mater. Adv.* **2**, 1821–1871 (2021).
13. Zhu, W., Bartos, P. J. M. & Porro, A. Application of nanotechnology in

- construction Summary of a state-of-the-art report. *Mater. Struct. Constr.* **37**, 649–658 (2004).
14. CHENG, M. *et al.* Nanotechnologies for biomolecular detection and medical diagnostics. *Curr. Opin. Chem. Biol.* **10**, 11–19 (2006).
  15. Savolainen, K. *et al.* Risk assessment of engineered nanomaterials and nanotechnologies—A review. *Toxicology* **269**, 92–104 (2010).
  16. Chaudhry, Q. *et al.* Applications and implications of nanotechnologies for the food sector. *Food Addit. Contam. Part A* **25**, 241–258 (2008).
  17. Joh, H. & Fan, D. E. Materials and Schemes of Multimodal Reconfigurable Micro/Nanomachines and Robots: Review and Perspective. *Adv. Mater.* **33**, 2101965 (2021).
  18. Hunkeler Urs, Hong Linh Truong, A. S.-C. MQTT-S—A publish/subscribe protocol for Wireless Sensor Networks. *IEEE* (2008).
  19. Shahin, F. *ZigBee wireless networks and transceivers*. Newnes. (2011).
  20. Al-Shamma'a, A. I., Shaw, A. & Saman, S. Propagation of Electromagnetic Waves at MHz Frequencies Through Seawater. *IEEE Trans. Antennas Propag.* **52**, 2843–2849 (2004).
  21. *Biological and Medical Aspects of Electromagnetic Fields*. (CRC Press, 2018). doi:10.1201/9781315221557.
  22. Kumar, M. R. A Compact Graphene Based Nano-Antenna for Communication in Nano-Network. *J. Inst. Electron. Comput.* **1**, 17–27 (2019).
  23. Jacquin-Joly, E. & Groot, A. T. Pheromones, Insects. in *Encyclopedia of Reproduction* 465–471 (Elsevier, 2018). doi:10.1016/B978-0-12-809633-8.20593-1.
  24. Alberts, B., Johnson, A., Lewis, J., Raff, M., Roberts, K., & Walter, P. Molecular biology of the cell. *Scand. J. Rheumatol.* **32(2)**, 125–125 (2003).
  25. Agosta, W. C. *Chemical communication: the language of pheromones*. (1992).
  26. Plante, Ianik, F. A. C., Plante, I., A., F. & Plante, Ianik, F. A. C. Monte-Carlo Simulation of Particle Diffusion in Various Geometries and Application to Chemistry and Biology. in *Theory and Applications of Monte Carlo Simulations* (InTech, 2013). doi:10.5772/53203.
  27. Roger, T. *Navier-Stokes equations: theory and numerical analysis*. (American Mathematical Soc., 2001).
  28. Pierobon, M. & Akyildiz, I. F. A Physical Channel Model for Molecular Communication in Nanonetworks. *IEEE J. Sel. Areas Commun.* **28**, 602–611 (2010).
  29. Pierobon, M. & Akyildiz, I. F. Capacity of a diffusion-based molecular communication system with channel memory and molecular noise.



- IEEE Trans. Inf. Theory* **59**, 942–954 (2013).
30. Nakano, T., Suda, T., Koujin, T., Haraguchi, T. & Hiraoka, Y. Molecular Communication through Gap Junction Channels. in 81–99 (2008). doi:10.1007/978-3-540-92273-5\_5.
  31. Albert P. Philipse. *Brownian Motion*. (2018).
  32. Yanagida, T., Ueda, M., Murata, T., Esaki, S. & Ishii, Y. Brownian motion, fluctuation and life. *Biosystems* **88**, 228–242 (2007).
  33. Kuran, M. S., Yilmaz, H. B. & Tugcu, T. A tunnel-based approach for signal shaping in molecular communication. in *2013 IEEE International Conference on Communications Workshops (ICC)* 776–781 (IEEE, 2013). doi:10.1109/ICCW.2013.6649338.
  34. Barros, M. T. Ca<sup>2+</sup>-signaling-based molecular communication systems: Design and future research directions. *Nano Commun. Netw.* **11**, 103–113 (2017).
  35. Unluturk, B. D. & Akyildiz, I. F. An End-to-End Model of Plant Pheromone Channel for Long Range Molecular Communication. *IEEE Trans. Nanobioscience* **16**, 11–20 (2017).
  36. Felicetti, L. *et al.* Modeling CD40-Based Molecular Communications in Blood Vessels. *IEEE Trans. Nanobioscience* **13**, 230–243 (2014).
  37. Xu, Z. *et al.* Manipulation of a neutral and nonpolar nanoparticle in water using a nonuniform electric field. *J. Chem. Phys.* **144**, (2016).
  38. Sharma, S., Katiyar, V. K. & Singh, U. Mathematical modelling for trajectories of magnetic nanoparticles in a blood vessel under magnetic field. *J. Magn. Magn. Mater.* **379**, 102–107 (2015).
  39. Kalambur, V. S., Han, B., Hammer, B. E., Shield, T. W. & Bischof, J. C. In vitro characterization of movement, heating and visualization of magnetic nanoparticles for biomedical applications. *Nanotechnology* **16**, 1221–1233 (2005).
  40. Baigl, D. Photo-actuation of liquids for light-driven microfluidics: State of the art and perspectives. *Lab Chip* **12**, 3637–3653 (2012).
  41. Lv, C., Varanakkottu, S. N., Baier, T. & Hardt, S. Controlling the Trajectories of Nano/Micro Particles Using Light-Actuated Marangoni Flow. *Nano Lett.* **18**, 6924–6930 (2018).
  42. Batson, P. E. *et al.* Plasmonic nanobilliards: Controlling nanoparticle movement using forces induced by swift electrons. *Nano Lett.* **11**, 3388–3393 (2011).
  43. Hiyama, S., Moritani, Y., Gojo, R., Takeuchi, S. & Sutoh, K. Biomolecular-motor-based autonomous delivery of lipid vesicles as nano- or microscale reactors on a chip. *Lab Chip* **10**, 2741 (2010).
  44. Enomoto, A., Moore, M. J., Suda, T. & Oiwa, K. Design of self-organizing microtubule networks for molecular communication. *Nano*

- Commun. Netw.* **2**, 16–24 (2011).
45. Gregori, M. & Akyildiz, I. A new nanonetwork architecture using flagellated bacteria and catalytic nanomotors. *IEEE J. Sel. Areas Commun.* **28**, 612–619 (2010).
  46. Cobo, L. C. & Akyildiz, I. F. Bacteria-based communication in nanonetworks. *Nano Commun. Netw.* **1**, 244–256 (2010).
  47. Solovev, A. A., Sanchez, S. & Schmidt, O. G. Collective behaviour of self-propelled catalytic micromotors. *Nanoscale* **5**, 1284–1293 (2013).
  48. Guix, M., Weiz, S. M., Schmidt, O. G. & Medina-Sánchez, M. Self-Propelled Micro/Nanoparticle Motors. *Part. Part. Syst. Charact.* **35**, 1–31 (2018).
  49. Löffler, R. J. G., Hanczyc, M. M. & Gorecki, J. A hybrid camphor-camphene wax material for studies on self-propelled motion. *Phys. Chem. Chem. Phys.* **21**, 24852–24856 (2019).
  50. Kuran, M. Ş., Yilmaz, H. B., Tugcu, T. & Akyildiz, I. F. Interference effects on modulation techniques in diffusion based nanonetworks. *Nano Commun. Netw.* **3**, 65–73 (2012).
  51. Koo, B.-H. B. H. *et al.* Molecular MIMO: From Theory to Prototype. *IEEE J. Sel. Areas Commun.* **34**, 600–614 (2016).
  52. Kuran, M. S., Yilmaz, H. B., Tugcu, T. & Akyildiz, I. F. Modulation techniques for communication via diffusion in nanonetworks. *IEEE Int. Conf. Commun.* (2011) doi:10.1109/icc.2011.5962989.
  53. ShahMohammadian, H., Messier, G. G. & Magierowski, S. Blind Synchronization in Diffusion-Based Molecular Communication Channels. *IEEE Commun. Lett.* **17**, 2156–2159 (2013).
  54. Mahfuz, M. U., Makrakis, D. & Mouftah, H. T. On the characterization of binary concentration-encoded molecular communication in nanonetworks. *Nano Commun. Netw.* **1**, 289–300 (2010).
  55. Ma, X. & Zhao, Y. Biomedical Applications of Supramolecular Systems Based on Host–Guest Interactions. *Chem. Rev.* **115**, 7794–7839 (2015).
  56. Terentyuk, G. S. *et al.* Laser-induced tissue hyperthermia mediated by gold nanoparticles: toward cancer phototherapy. *J. Biomed. Opt.* **14**, 021016 (2009).
  57. Baldwin, R. K., Pettigrew, K. A., Ratai, E., Augustine, M. P. & Kauzlarich, S. M. Solution reduction synthesis of surface stabilized silicon nanoparticles. *Chem. Commun.* **17**, 1822–1823 (2002).
  58. Jain, T. K., Reddy, M. K., Morales, M. A., Leslie-Pelecky, D. L. & Labhassetwar, V. Biodistribution, clearance, and biocompatibility of iron oxide magnetic nanoparticles in rats. *Mol. Pharm.* **5**, 316–327 (2008).

59. Suda, Y. *et al.* Preparation of carbon nanoparticles by plasma-assisted pulsed laser deposition method - Size and binding energy dependence on ambient gas pressure and plasma condition. *Thin Solid Films* **415**, 15–20 (2002).
60. Schatz, G. C. Using theory and computation to model nanoscale properties. *Proc. Natl. Acad. Sci.* **104**, 6885–6892 (2007).
61. Llopis-Lorente, A. *et al.* Interactive models of communication at the nanoscale using nanoparticles that talk to one another. *Nat. Commun.* **8**, 1–7 (2017).
62. Luis, B. *et al.* An Interactive Model of Communication between Abiotic Nanodevices and Microorganisms. *Angew. Chemie* **131**, 15128–15132 (2019).
63. Nakai, Y., Sugai, N., Kusano, H., Morita, Y. & Komatsu, T. Protein Microtube Motors with a Pt Nanoparticle Interior and Avidin Exterior for Self-Propelled Transportation, Separation, and Stirring. *ACS Appl. Nano Mater.* **2**, 4891–4899 (2019).
64. Großmann, R., Peruani, F. & Bär, M. A geometric approach to self-propelled motion in isotropic & anisotropic environments. *Eur. Phys. J. Spec. Top.* **224**, 1377–1394 (2015).
65. Großmann, R., Peruani, F. & Bär, M. Diffusion properties of active particles with directional reversal. *New J. Phys.* **18**, (2016).
66. Unterweger, H. *et al.* Experimental Molecular Communication Testbed Based on Magnetic Nanoparticles in Duct Flow. *IEEE Work. Signal Process. Adv. Wirel. Commun. SPAWC 2018-June*, (2018).
67. Xu, X. *et al.* Electrophoretic analysis and purification of fluorescent single-walled carbon nanotube fragments. *J. Am. Chem. Soc.* **126**, 12736–12737 (2004).
68. Qiao, Z.-A. Z. A. *et al.* Commercially activated carbon as the source for producing multicolor photoluminescent carbon dots by chemical oxidation. *Chem. Commun.* **46**, 8812–8814 (2010).
69. Tao, H. *et al.* In vivo NIR fluorescence imaging, biodistribution, and toxicology of photoluminescent carbon dots produced from carbon nanotubes and graphite. *Small* **8**, 281–290 (2012).
70. Cao, L. *et al.* Carbon Dots for Multiphoton Bioimaging. 11318–11319 (2007) doi:10.1021/ja073527l.
71. Yubin Song, S. Z. and B. Y. Bioimaging based on fluorescent carbon dots. *RSC Adv.* 27184–27200 (2014) doi:10.1039/c3ra47994c.
72. Xu, Y., Liu, J., Gao, C. & Wang, E. Applications of carbon quantum dots in electrochemiluminescence: A mini review. *Electrochem. commun.* **48**, 151–154 (2014).
73. Liu, H., Ye, T. & Mao, C. Fluorescent carbon nanoparticles derived

- from candle soot. *Angew. Chemie - Int. Ed.* **46**, 6473–6475 (2007).
74. Xu, H., Xie, L. & Hakkarainen, M. Coffee-Ground-Derived Quantum Dots for Aqueous Processable Nanoporous Graphene Membranes. *ACS Sustain. Chem. Eng.* **5**, 5360–5367 (2017).
  75. Wang, L. & Zhou, H. S. Green Synthesis of Luminescent Nitrogen-Doped Carbon Dots from Milk and Its Imaging Application. (2014) doi:10.1021/ac502646x.
  76. Sun, D. *et al.* Hair fiber as a precursor for synthesizing of sulfur- and nitrogen-co-doped carbon dots with tunable luminescence properties. *Carbon N. Y.* **64**, 424–434 (2013).
  77. Ye, R. *et al.* Coal as an abundant source of graphene quantum dots. *Nat. Commun.* **4**, 1–7 (2013).
  78. Das, R., Bandyopadhyay, R. & Pramanik, P. Carbon quantum dots from natural resource: A review. *Mater. Today Chem.* **8**, 96–109 (2018).
  79. Wang, J. *et al.* Dual-emission carbon dots achieved by luminescence center modulation within one-pot synthesis for a fluorescent ratiometric probe of pH, Hg<sup>2+</sup>, and glutathione. *Microchim. Acta* **187**, (2020).
  80. Prasannan, A. & Imae, T. One-pot synthesis of fluorescent carbon dots from orange waste peels. *Ind. Eng. Chem. Res.* **52**, 15673–15678 (2013).
  81. Emam, A. N., Loutfy, S. A., Mostafa, A. A., Awad, H. & Mohamed, M. B. Cyto-toxicity, biocompatibility and cellular response of carbon dots-plasmonic based nano-hybrids for bioimaging. *RSC Adv.* **7**, 23502–23514 (2017).
  82. Li, Y. *et al.* An electrochemical avenue to green-luminescent graphene quantum dots as potential electron-acceptors for photovoltaics. *Adv. Mater.* **23**, 776–780 (2011).
  83. Sheldon, R. A. Green chemistry and resource efficiency: Towards a green economy. *Green Chem.* **18**, 3180–3183 (2016).
  84. Wei, J. *et al.* Simple one-step synthesis of water-soluble fluorescent carbon dots from waste paper. *New J. Chem.* **38**, 906–909 (2014).
  85. Ramanan, V., Siddaiah, B., Raji, K. & Ramamurthy, P. Green Synthesis of Multifunctionalized, Nitrogen-Doped, Highly Fluorescent Carbon Dots from Waste Expanded Polystyrene and Its Application in the Fluorimetric Detection of Au<sup>3+</sup> Ions in Aqueous Media. *ACS Sustain. Chem. Eng.* **6**, 1627–1638 (2018).
  86. Zammataro, A. *et al.* Covalently functionalized carbon nanoparticles with a chiral Mn-Salen: A new nanocatalyst for enantioselective epoxidation of alkenes. *Chem. Commun.* **55**, 5255–5258 (2019).
  87. Havrdova, M. *et al.* Toxicity of carbon dots-Effect of surface

- functionalization on the cell viability, reactive oxygen species generation and cell cycle. *Carbon N. Y.* **99**, 238–248 (2016).
88. Wang, K. *et al.* Systematic safety evaluation on photoluminescent carbon dots. *Nanoscale Res. Lett.* **8**, 1–9 (2013).
  89. Mao, X. J. *et al.* Study on the fluorescence characteristics of carbon dots. *Spectrochim. Acta - Part A Mol. Biomol. Spectrosc.* **75**, 553–557 (2010).
  90. Liu, M. L., Chen, B. Bin, Li, C. M. & Huang, C. Z. Carbon dots: Synthesis, formation mechanism, fluorescence origin and sensing applications. *Green Chem.* **21**, 449–471 (2019).
  91. Hola, K. *et al.* Photoluminescence effects of graphitic core size and surface functional groups in carbon dots: COO<sup>-</sup> induced red-shift emission. *Carbon N. Y.* **70**, 279–286 (2014).
  92. Liu, W. *et al.* Carbon dots: Surface engineering and applications. *J. Mater. Chem. B* **4**, 5772–5788 (2016).
  93. Fichera, L., Li-Destri, G. & Tuccitto, N. Nanoparticles as suitable messengers for molecular communication. *Nanoscale* (2020) doi:10.1039/D0NR06999J.
  94. Kumar Thiyagarajan, S., Raghupathy, S., Palanivel, D., Raji, K. & Ramamurthy, P. Fluorescent carbon nano dots from lignite: unveiling the impeccable evidence for quantum confinement. *Phys. Chem. Chem. Phys.* **18**, 12065–12073 (2016).
  95. Chatzimitakos, T. G. & Stalikas, C. D. Carbon nanodots from natural (re)sources: a new perspective on analytical chemistry. in *Handbook of Nanomaterials in Analytical Chemistry* 3–28 (Elsevier, 2020). doi:10.1016/B978-0-12-816699-4.00001-3.
  96. Zhang, Z., Sun, W. & Wu, P. Highly Photoluminescent Carbon Dots Derived from Egg White: Facile and Green Synthesis, Photoluminescence Properties, and Multiple Applications. *ACS Sustain. Chem. Eng.* **3**, 1412–1418 (2015).
  97. Liang, Q., Ma, W., Shi, Y., Li, Z. & Yang, X. Easy synthesis of highly fluorescent carbon quantum dots from gelatin and their luminescent properties and applications. *Carbon N. Y.* **60**, 421–428 (2013).
  98. Liu, M., Xu, Y., Niu, F., Gooding, J. J. & Liu, J. Carbon quantum dots directly generated from electrochemical oxidation of graphite electrodes in alkaline alcohols and the applications for specific ferric ion detection and cell imaging. *Analyst* **141**, 2657–2664 (2016).
  99. Sahu, S., Behera, B., Maiti, T. K. & Mohapatra, S. Simple one-step synthesis of highly luminescent carbon dots from orange juice: Application as excellent bio-imaging agents. *Chem. Commun.* **48**, 8835–8837 (2012).

100. Singh, V. & Deverall, B. J. *Bacillus subtilis* as a control agent against fungal pathogens of citrus fruit. *Trans. Br. Mycol. Soc.* **83**, 487–490 (1984).
101. Food and Agriculture Organization of the United Nations (FAO). *Citrus: World Markets and Trade*. (2017).
102. Song, Y. *et al.* Investigation into the fluorescence quenching behaviors and applications of carbon dots. *Nanoscale* **6**, 4676–4682 (2014).
103. Wang, C., Xu, Z. & Zhang, C. Polyethyleneimine-Functionalized Fluorescent Carbon Dots: Water Stability, pH Sensing, and Cellular Imaging. *ChemNanoMat* **1**, 122–127 (2015).
104. Wu, X. *et al.* Nitrogen-doped carbon quantum dots for fluorescence detection of Cu<sup>2+</sup> and electrochemical monitoring of bisphenol A. *RSC Adv.* **8**, 20000–20006 (2018).
105. Park, Y., Yoo, J., Lim, B., Kwon, W. & Rhee, S.-W. Improving the functionality of carbon nanodots: doping and surface functionalization. *J. Mater. Chem. A* **4**, 11582–11603 (2016).
106. Zhu, X. *et al.* Synthesis of polyethylenimine-impregnated Al-fumarate metal-organic framework and its CO<sub>2</sub> adsorption characteristics. *Chinese Sci. Bull.* **64**, 2441–2449 (2019).
107. Quang, D. V. *et al.* Impregnation of Amines Onto Porous Precipitated Silica for CO<sub>2</sub> capture. *Energy Procedia* **63**, 2122–2128 (2014).
108. Manioudakis, J. *et al.* Effects of nitrogen-doping on the photophysical properties of carbon dots. *J. Mater. Chem. C* **7**, 853–862 (2019).
109. Barman, M. K., Jana, B., Bhattacharyya, S. & Patra, A. Photophysical Properties of Doped Carbon Dots (N, P, and B) and Their Influence on Electron/Hole Transfer in Carbon Dots–Nickel (II) Phthalocyanine Conjugates. *J. Phys. Chem. C* **118**, 20034–20041 (2014).
110. Liu, C. *et al.* Nano-carrier for gene delivery and bioimaging based on carbon dots with PEI-passivation enhanced fluorescence. *Biomaterials* **33**, 3604–3613 (2012).
111. Yang, Y. *et al.* Fluorescent N-Doped Carbon Dots as in Vitro and in Vivo Nanothermometer. *ACS Appl. Mater. Interfaces* **7**, 27324–27330 (2015).
112. Ma, X. *et al.* Synthesis of N-doped carbon dots via a microplasma process. *Chem. Eng. Sci.* **220**, 115648 (2020).
113. Liu, X. *et al.* N-Doped carbon dots: green and efficient synthesis on a large-scale and their application in fluorescent pH sensing. *New J. Chem.* **41**, 10607–10612 (2017).
114. Lu, S. *et al.* Hydrothermal synthesis of nitrogen-doped carbon dots with real-time live-cell imaging and blood–brain barrier

- penetration capabilities. *Int. J. Nanomedicine* **Volume 11**, 6325–6336 (2016).
115. Stefanakis, D. *et al.* Synthesis of fluorescent carbon dots by a microwave heating process: structural characterization and cell imaging applications. *J. Nanoparticle Res.* **16**, 2646 (2014).
  116. Zhang, W. *et al.* Supramolecular interactions via hydrogen bonding contributing to citric-acid derived carbon dots with high quantum yield and sensitive photoluminescence. *RSC Adv.* **7**, 20345–20353 (2017).
  117. Li, L., Liu, D., Mao, H. & You, T. Multifunctional solid-state electrochemiluminescence sensing platform based on poly(ethylenimine) capped N-doped carbon dots as novel co-reactant. *Biosens. Bioelectron.* **89**, 489–495 (2017).
  118. Dong, X. *et al.* Fast one-step synthesis of N-doped carbon dots by pyrolyzing ethanolamine. *J. Mater. Chem. C* **2**, 7477–7481 (2014).
  119. Xu, M. *et al.* A green heterogeneous synthesis of N-doped carbon dots and their photoluminescence applications in solid and aqueous states. *Nanoscale* **6**, 10307–10315 (2014).
  120. Tuccitto, N., Li-Destri, G., Messina, G. M. L. & Marletta, G. Reactive messengers for digital molecular communication with variable transmitter-receiver distance. *Phys. Chem. Chem. Phys.* **20**, 30312–30320 (2018).
  121. Brannon, J. H. & Magde, D. Absolute quantum yield determination by thermal blooming. Fluorescein. *J. Phys. Chem.* **82**, 705–709 (1978).
  122. Thakur, M. S. & Bhatia, V. Performance Analysis of Flow Assisted Diffusion Based Molecular Communication for D-MoS<sub>K</sub>. in *2018 IEEE 87th Vehicular Technology Conference (VTC Spring)* 1–6 (IEEE, 2018). doi:10.1109/VTCspring.2018.8417797.
  123. Pierobon, M. & Akyildiz, I. F. Noise Analysis in Ligand-Binding Reception for Molecular Communication in Nanonetworks. *IEEE Trans. Signal Process.* **59**, 4168–4182 (2011).
  124. Kadloor, S., Adve, R. S. & Eckford, A. W. Molecular Communication Using Brownian Motion With Drift. *IEEE Trans. Nanobioscience* **11**, 89–99 (2012).
  125. Chude-Okonkwo, U. A. K., Malekian, R., Maharaj, B. T. & Vasilakos, A. V. Molecular Communication and Nanonetwork for Targeted Drug Delivery: A Survey. *IEEE Commun. Surv. Tutorials* **19**, 3046–3096 (2017).
  126. Jamali, V., Ahmadzadeh, A., Wicke, W., Noel, A. & Schober, R. Channel Modeling for Diffusive Molecular Communication—A Tutorial Review. *Proc. IEEE* **107**, 1256–1301 (2019).

127. Berman, A. S. Laminar Flow in Channels with Porous Walls. *J. Appl. Phys.* **24**, 1232–1235 (1953).
128. Bicen, A. O. & Akyildiz, I. F. System-Theoretic Analysis and Least-Squares Design of Microfluidic Channels for Flow-Induced Molecular Communication. *IEEE Trans. Signal Process.* **61**, 5000–5013 (2013).
129. Arjmandi, H., Ahmadzadeh, A., Schober, R. & Nasiri Kenari, M. Ion Channel Based Bio-Synthetic Modulator for Diffusive Molecular Communication. *IEEE Trans. Nanobioscience* **15**, 418–432 (2016).
130. Li-Destri, G., Fichera, L., Zammataro, A., Trusso Sfrassetto, G. & Tuccitto, N. Self-assembled carbon nanoparticles as messengers for artificial chemical communication. *Nanoscale* **11**, 14203–14209 (2019).
131. Zhao, F. *et al.* Supramolecular quantum dots as biodegradable nano-probes for upconversion-enabled bioimaging. *Chem. Commun.* **51**, 13201–13204 (2015).
132. Ghosh, A., Parasar, B., Bhattacharyya, T. & Dash, J. Chiral carbon dots derived from guanosine 5'-monophosphate form supramolecular hydrogels. *Chem. Commun.* **52**, 11159–11162 (2016).
133. Xie, Y.-J. *et al.* An Elaborate Supramolecular Assembly for a Smart Nanodevice for Ratiometric Molecular Recognition and Logic Gates. *Chem. - A Eur. J.* **22**, 8339–8345 (2016).
134. Cadranel, A. *et al.* Screening Supramolecular Interactions between Carbon Nanodots and Porphyrins. *J. Am. Chem. Soc.* **140**, 904–907 (2018).
135. Sun, S., Zhang, L., Jiang, K., Wu, A. & Lin, H. Toward High-Efficient Red Emissive Carbon Dots: Facile Preparation, Unique Properties, and Applications as Multifunctional Theranostic Agents. *Chem. Mater.* **28**, 8659–8668 (2016).
136. Thalacker, C., Miura, A., De Feyter, S., De Schryver, F. C. & Würthner, F. Hydrogen bond directed self-assembly of core-substituted naphthalene bisimides with melamines in solution and at the graphite interface. *Org. Biomol. Chem.* **3**, 414–422 (2005).
137. Cohen, Y., Avram, L. & Frish, L. Diffusion NMR spectroscopy in supramolecular and combinatorial chemistry: An old parameter - New insights. *Angew. Chemie - Int. Ed.* **44**, 520–554 (2005).
138. Avram, L. & Cohen, Y. Diffusion NMR of molecular cages and capsules. *Chem. Soc. Rev.* **44**, 586–602 (2015).
139. Evans, R. *et al.* Quantitative interpretation of diffusion-ordered NMR spectra: Can we rationalize small molecule diffusion coefficients? *Angew. Chemie - Int. Ed.* **52**, 3199–3202 (2013).
140. Giuffrida, M. L., Rizzarelli, E., Tomaselli, G. A., Satriano, C. &



- Sfrazzetto, G. T. A novel fully water-soluble Cu(i) probe for fluorescence live cell imaging. *Chem. Commun.* **50**, 9835–9838 (2014).
141. Tuccitto, N. *et al.* The memory-driven order-disorder transition of a 3D-supramolecular architecture based on calix[5]arene and porphyrin derivatives. *Chem. Commun.* **52**, 11681–11684 (2016).
142. Pappalardo, A. *et al.* Supramolecular polymer networks based on calix[5]arene tethered poly(p-phenyleneethynylene). *Macromolecules* **45**, 7549–7556 (2012).
143. Islam, M. A. Einstein-Smoluchowski diffusion equation: A discussion. *Phys. Scr.* **70**, 120–125 (2004).
144. Zhu, S. *et al.* The photoluminescence mechanism in carbon dots (graphene quantum dots, carbon nanodots, and polymer dots): current state and future perspective. *Nano Res.* **8**, 355–381 (2015).
145. Guyer, J. E., Wheeler, D. & Warren, J. A. FiPy: Partial Differential Equations with Python. *Comput. Sci. Eng.* **11**, 6–15 (2009).
146. Kuran, M. S., Yilmaz, H. B., Tugcu, T. & Akyildiz, I. F. No Title. *2011 IEEE Int. Conf. Commun. (ICC), IEEE.*
147. Tuccitto, N., Li-Destri, G., Messina, G. M. L. L. & Marletta, G. Fluorescent Quantum Dots Make Feasible Long-Range Transmission of Molecular Bits. *J. Phys. Chem. Lett.* **8**, 3861–3866 (2017).
148. Wang, F., Hao, Q., Zhang, Y., Xu, Y. & Lei, W. Fluorescence quenchometric method for determination of ferric ion using boron-doped carbon dots. *Microchim. Acta* **183**, 273–279 (2016).
149. Chou, C. T. A markovian approach to the optimal demodulation of diffusion-based molecular communication networks. *IEEE Trans. Commun.* **63**, 3728–3743 (2015).
150. Awan, H. & Chou, C. T. Generalized Solution for the Demodulation of Reaction Shift Keying Signals in Molecular Communication Networks. *IEEE Trans. Commun.* **65**, 715–727 (2017).
151. Calì, F. *et al.* Carbon Quantum Dots from Lemon Waste Enable Communication among Biodevices. *Chemosensors* **9**, 202 (2021).
152. Gedda, G., Lee, C. Y., Lin, Y. C. & Wu, H. F. Green synthesis of carbon dots from prawn shells for highly selective and sensitive detection of copper ions. *Sensors Actuators, B Chem.* **224**, 396–403 (2016).
153. Giambianco, N., Zhavnerko, G., Tuccitto, N., Licciardello, A. & Marletta, G. Coadsorption-dependent orientation of fibronectin epitopes at hydrophilic gold surfaces. *Soft Matter* **8**, 8370–8378 (2012).
154. Giambianco, N. *et al.* Chelating Surfaces for Native State Proteins Patterning: The Human Serum Albumin Case. *ACS Appl. Mater. Interfaces* **7**, 23353–23363 (2015).

155. Salinas-Castillo, A. *et al.* Carbon dots for copper detection with down and upconversion fluorescent properties as excitation sources. *Chem. Commun.* **49**, 1103–1105 (2013).
156. Wang, F. *et al.* Graphene quantum dots as a fluorescent sensing platform for highly efficient detection of copper(II) ions. *Sensors Actuators, B Chem.* **190**, 516–522 (2014).
157. DENG, X. Y. *et al.* Synthesis of Functionalized Carbon Quantum Dots as Fluorescent Probes for Detection of Cu<sup>2+</sup>. *Chinese J. Anal. Chem.* **48**, e20126–e20133 (2020).
158. Wu, J. *et al.* Continuous flow synthesis of ketones from carbon dioxide and organolithium or grignard reagents. *Angew. Chemie - Int. Ed.* **53**, 8416–8420 (2014).
159. Fichera, L., Li Destri, G., Tuccitto, N., Li-Destri, G. & Tuccitto, N. Fluorescent Nanoparticle-based Internet of Things. *Nanoscale* **12**, 9817–9823 (2020).
160. Saetear, P. *et al.* Taylor Dispersion Analysis of Polysaccharides Using Backscattering Interferometry. *Anal. Chem.* **89**, 6710–6718 (2017).
161. Chamieh, J. *et al.* Limits in Size of Taylor Dispersion Analysis: Representation of the Different Hydrodynamic Regimes and Application to the Size-Characterization of Cubosomes. *Anal. Chem.* **89**, 13487–13493 (2017).
162. Taylor, G. I. & A, P. R. S. L. Dispersion of soluble matter in solvent flowing slowly through a tube. *Proc. R. Soc. London. Ser. A. Math. Phys. Sci.* **219**, 186–203 (1953).
163. Jacobs, C. B., Peairs, M. J. & Venton, B. J. Review: Carbon nanotube based electrochemical sensors for biomolecules. *Anal. Chim. Acta* **662**, 105–127 (2010).
164. Torsi, L., Magliulo, M., Manoli, K. & Palazzo, G. Organic field-effect transistor sensors: A tutorial review. *Chem. Soc. Rev.* **42**, 8612–8628 (2013).
165. Soto, R. J., Hall, J. R., Brown, M. D., Taylor, J. B. & Schoenfisch, M. H. In Vivo Chemical Sensors: Role of Biocompatibility on Performance and Utility. *Anal. Chem.* **89**, 276–299 (2017).
166. Kisseleff, S., Schober, R. & Gerstacker, W. H. Magnetic nanoparticle based interface for molecular communication systems. *IEEE Commun. Lett.* **21**, 258–261 (2017).
167. Wicke, W. *et al.* Molecular communication using magnetic nanoparticles. in *IEEE Wireless Communications and Networking Conference, WCNC* vols 2018-April 1–6 (2018).
168. Grebenstein, L. *et al.* Biological Optical-to-Chemical Signal Conversion Interface: A Small-Scale Modulator for Molecular Communications.

- IEEE Trans. Nanobioscience* **18**, 31–42 (2019).
169. Wu, D. *et al.* Fluorescent chemosensors: The past, present and future. *Chem. Soc. Rev.* **46**, 7105–7123 (2017).
170. Wang, L. *et al.* Common origin of green luminescence in carbon nanodots and graphene quantum dots. *ACS Nano* **8**, 2541–2547 (2014).
171. Jornet, J. M. & Akyildiz, I. F. Graphene-based Plasmonic Nano-Antenna for Terahertz Band Communication in Nanonetworks. *IEEE J. Sel. Areas Commun.* **31**, 685–694 (2013).
172. Schüll, N. D. Data for life: Wearable technology and the design of self-care. *Biosocieties* **11**, 317–333 (2016).
173. Jakicic, J. M. *et al.* Effect of wearable technology combined with a lifestyle intervention on long-term weight loss: The IDEA randomized clinical trial. *JAMA - J. Am. Med. Assoc.* **316**, 1161–1171 (2016).
174. Awolusi, I., Marks, E. & Hallowell, M. Wearable technology for personalized construction safety monitoring and trending: Review of applicable devices. *Autom. Constr.* **85**, 96–106 (2018).
175. Tang, L. & Eaton, J. W. Inflammatory Responses to Biomaterials. *Am. J. Clin. Pathol.* **103**, 466–471 (1995).
176. Glyn-Jones, S. *et al.* Risk factors for inflammatory pseudotumour formation following hip resurfacing. *J. Bone Joint Surg. Br.* **91-B**, 1566–1574 (2009).
177. Farsad, N., Yilmaz, H. B., Eckford, A., Chae, C.-B. C. B. & Guo, W. A comprehensive survey of recent advancements in molecular communication. *IEEE Commun. Surv. Tutorials* **18**, 1887–1919 (2016).
178. Giannoukos, S., McGuinness, D. T., Marshall, A., Smith, J. & Taylor, S. A Chemical Alphabet for Macromolecular Communications. *Anal. Chem.* **90**, 7739–7746 (2018).
179. Lee, B., Roh, S. & Park, J. Current status of micro- and nano-structured optical fiber sensors. *Opt. Fiber Technol.* **15**, 209–221 (2009).
180. Dehghan, M. Numerical solution of the three-dimensional advection–diffusion equation. *Appl. Math. Comput.* **150**, 5–19 (2004).
181. Fichera, L., Li-Destri, G., Ruffino, R., Messina, G. M. L. & Tuccitto, N. Reactive nanomessengers for artificial chemical communication. *Phys. Chem. Chem. Phys.* **21**, 16223–16229 (2019).
182. Sharma, A., Gadyly, T., Neogy, S., Ghosh, S. K. & Kumbhakar, M. Molecular Origin and Self-Assembly of Fluorescent Carbon Nanodots in Polar Solvents. *J. Phys. Chem. Lett.* **8**, 1044–1052 (2017).
183. Wold, S., Esbensen, K. & Geladi, P. Principal component analysis. *Chemom. Intell. Lab. Syst.* **2**, 37–52 (1987).
184. Li, C. *et al.* Real-Time Temperature Measurements of HMEC-1 Cells

- during Inflammation Production and Repair Detected by Wireless Thermometry. *IEEE Trans. Biomed. Eng.* **66**, 1898–1904 (2019).
185. Rushanan, M., Rubin, A. D., Kune, D. F. & Swanson, C. M. SoK: Security and Privacy in Implantable Medical Devices and Body Area Networks. in *2014 IEEE Symposium on Security and Privacy* 524–539 (IEEE, 2014). doi:10.1109/SP.2014.40.
  186. Humayed, A., Lin, J., Li, F. & Luo, B. Cyber-Physical Systems Security—A Survey. *IEEE Internet Things J.* **4**, 1802–1831 (2017).
  187. Centers for Disease Control and Prevention. National Diabetes Statistics Report, 2020. <https://www.cdc.gov/diabetes/data/statistics-report/index.html> (2020).
  188. Hovorka, R. Closed-loop insulin delivery: from bench to clinical practice. *Nat. Rev. Endocrinol.* **7**, 385–395 (2011).
  189. Ramchandani, N., Arya, S., Ten, S. & Bhandari, S. Real-Life Utilization of Real-Time Continuous Glucose Monitoring: The Complete Picture. *J. Diabetes Sci. Technol.* **5**, 860–870 (2011).
  190. Steil, G. Closed-loop insulin delivery—the path to physiological glucose control. *Adv. Drug Deliv. Rev.* **56**, 125–144 (2004).
  191. Castle, J. R. *et al.* Novel Use of Glucagon in a Closed-Loop System for Prevention of Hypoglycemia in Type 1 Diabetes. *Diabetes Care* **33**, 1282–1287 (2010).
  192. Hei, X., Du, X., Lin, S., Lee, I. & Sokolsky, O. Patient Infusion Pattern based Access Control Schemes for Wireless Insulin Pump System. *IEEE Trans. Parallel Distrib. Syst.* **26**, 3108–3121 (2015).
  193. Kirby, B. *Micro- and Nanoscale Fluid Mechanics*. (Cambridge University Press, 2010). doi:10.1017/CBO9780511760723.
  194. Santer, S. Remote control of soft nano-objects by light using azobenzene containing surfactants. *J. Phys. D: Appl. Phys.* **51**, aa95ca (2018).
  195. Parmeggiani, M. *et al.* P3HT Processing Study for In-Liquid EGO-FET Biosensors: Effects of the Solvent and the Surface. *Proceedings* **15**, 39 (2019).
  196. Sharp, D. H. An overview of Rayleigh-Taylor instability. *Phys. D Nonlinear Phenom.* **12**, 3–18 (1984).